DEVELOPMENT AND TESTING OF A FLEXIBLE PLASTIC HYDROGEN ION-SELECTIVE ELECTRODE FOR IN VIVO pH MEASUREMENTS OF AIRWAY SURFACE LIQUID

A Thesis Submitted to the
College of Graduate and Postdoctoral Studies
In Partial Fulfillment of the Requirements
For the Degree of Master of Science
In the Department of Large Animal Clinical Sciences
University of Saskatchewan
Saskatoon

By

RONALDO AVELLA LAVADO

PERMISSION TO USE

In presenting this thesis/dissertation in partial fulfillment of the requirements for a Postgraduate degree from the University of Saskatchewan, I agree that the Libraries of this University may make it freely available for inspection. I further agree that permission for copying of this thesis/dissertation in any manner, in whole or in part, for scholarly purposes may be granted by the professor or professors who supervised my thesis/dissertation work or, in their absence, by the Head of the Department or the Dean of the College in which my thesis work was done. It is understood that any copying or publication or use of this thesis/dissertation or parts thereof for financial gain shall not be allowed without my written permission. It is also understood that due recognition shall be given to me and to the University of Saskatchewan in any scholarly use which may be made of any material in my thesis/dissertation.

DISCLAIMER

Reference in this thesis/dissertation to any specific commercial products, process, or service by trade name, trademark, manufacturer, or otherwise, does not constitute or imply its endorsement, recommendation, or favoring by the University of Saskatchewan. The views and opinions of the author expressed herein do not state or reflect those of the University of Saskatchewan, and shall not be used for advertising or product endorsement purposes.

Requests for permission to copy or to make other uses of materials in this thesis/dissertation in whole or part should be addressed to:

Head of the Department of Large Animal Clinical Sciences
University of Saskatchewan
52 Campus Drive
Saskatoon, Saskatchewan, S7N 5B4, Canada

OR

Dean
College of Graduate and Postdoctoral Studies
University of Saskatchewan
116 Thorvaldson Building, 110 Science Place
Saskatoon, Saskatchewan, S7N 5C9, Canada

ABSTRACT

Cystic fibrosis (CF) is the most common fatal autosomal recessive genetic disorder among people of Caucasian ancestry. It is caused by mutations in the cystic fibrosis transmembrane conductance regulator (CFTR) gene, which encodes a transepithelial transporter responsible for ion transport and maintaining fluid homeostasis. These mutations impair chloride and bicarbonate transport to the airway lumen, leading to mucus thickening and acidification of the airway surface liquid (ASL). These alterations impair host-defence, making CF patients more prone to recurrent microbial infections in the respiratory tract.

This project aimed to develop a pH meter capable of measuring ASL pH in vivo through bronchoscopy, which involved optimizing the construction of long plastic H^+-selective electrodes using polyethylene (PE) tubing, assessing their usability, and testing their effectiveness in a tracheostomized piglet model. These advancements are critical for future research on pH levels and fluctuations in the lungs of CF pigs and human patients, enhancing our understanding of pH imbalances in CF patients' ASL.

Using PE tubing is effective for the manufacturing of long and flexible ion-selective electrodes (ISEs), with a success rate between 85% and 90%. Their mean Nernstian slope, adjusted R^2 and response time were comparable with similar devices previously reported, maintaining their usability stable for up to two days after manufacture. Shielding the electrodes with a custom-built grounded stainless-steel braid reinforced tubing significantly reduced the noise amplitude in the recordings ($p<.001$), enabling their introduction and use through an endoscope working channel. The plastic ISE were able to record ASL pH fluctuations in the tracheostomized piglet (mean=0.07 pH units), although the ΔpH and $\Delta[CO_2]$ were smaller than the ones reported in previous works. ΔpH and the electrodes response time were negatively linearly corelated ($p=.003$), and the adjusted R^2 and minimum and maximum pH were positively linearly corelated ($p=.01$ and .008, respectively). These results suggest that electrodes with low response times and high adjusted R^2 should be used in future assays. The novel plastic ISE design demonstrated satisfactory performance and usability during the tests, making it a promising tool for future in vivo bronchoscopy assays in CF pigs and human subjects.

ACKNOWLEDGEMENTS

First, I would like to show my gratitude to every Canada resident for their financial support of numerous research projects through their contributions to the tax system.

I would also like to thank my family and friends, both resident in Saskatoon and São Paulo for sharing a part of their lives with me, in special to my mom, Tania, who has always done everything in her power to allow me to have options and trail my own path, to my everyday partner and fiancée Claudia, who has never left my hand and chose to write a story with me, and to our cat Mina, who has always kept my lap warm during long studying sessions.

Finally, I would like to thank all professionals that helped me achieving this project's goals, especially Dr. Montgomery, my supervisor, and Dr. Ianowski, my co-supervisor, for the opportunity and the trust put on me. I would like to thank my committee members, Dr. Tyan and Dr. Tam for their brilliant insights during our project discussions, to Dr. Luan for his priceless contributions to all development steps of this project, to Mr. Nicolas Romero and Mr. Jim Boire, and to all staff from USask, from the cleaners to the decision makers for keeping this great University running. A special thanks to Dr. Seddon and Dr. Jelinski for their contributions as Graduate Chairs and all staff from the LACS department. I would like to thank CIHR for granting financial support for the development of this project.

DEDICATION

This dissertation is dedicated to Claudia, who began this journey as my girlfriend, is now my fiancée, and will soon be my wife. Thank you for your unwavering support, patience, and partnership during the most challenging moments.

TABLE OF CONTENTS

LIST OF TABLES

LIST OF FIGURES

LIST OF EQUATIONS

LIST OF ABBREVIATIONS

Adj	Adjusted
ASL	Airway Surface Liquid
BFS	Backfilling Solution
bpm	Breaths per minute
CF	Cystic Fibrosis
CFTR	Cystic Fibrosis Transmembrane Conductance Regulator
CIHR	Canadian Institutes of Health Research
Elect	Electrode
EMI	Electromagnetic Interference
END	Endoscope
GEEs	Generalized estimating equations
IQR	Interquartile range
ISE	Ion-Selective Electrode
Max	Maximum
Min	Minimum
NS	Nernstian slope
PE	Polyethylene
PVC	Polyvinyl Chloride
r	Pearson's correlation coefficient
RE	Referencing Electrode
RR	Respiratory rate
RS	Referencing Solution
RT	Response time
SD	Standard deviation
SE	Standard error

CHAPTER 1 - INTRODUCTION

1.1. Introduction

This dissertation presents advancements in the development of plastic H^+-selective electrodes for in vivo pH measurements of airway surface liquid (ASL). It is part of a larger multidisciplinary project funded by the Canadian Institutes of Health Research (CIHR). Among its various objectives, this research framework aims to assess pH levels and potential fluctuations in the lungs of cystic fibrosis (CF) pigs, comparing diseased and healthy regions within the same lung. Additionally, by applying bicarbonate to the ASL in CF-altered tissues and measuring the pH in real-time, the study will test the hypothesis that impaired pH fluctuations in the ASL are partly due to defective bicarbonate secretion. Following successful investigations in the porcine model, similar studies will be conducted with human CF volunteers. The development and evaluation of this innovative device, as detailed in this thesis, are crucial for achieving these goals and improving our understanding of pH imbalances in the ASL of CF patients.

1.2. Background and motivation

Cystic fibrosis (CF) is the most prevalent fatal autosomal recessive genetic disorder among people of Caucasian ancestry (Cutting, 2005). In 2022, approximately 33,000 people in the United States and over 4,400 people in Canada lived with the disease (Cystic Fibrosis Foundation, 2023; Cystic Fibrosis Canada, 2023). In Canada, CF represents 1 in 3,848 live births. It is characterized by mutations in the cystic fibrosis transmembrane conductance regulator (CFTR), a transepithelial transporter involved in ion transport and fluid homeostasis (Bergeron & Cantin, 2019). Although important alterations are found in different systems, cystic fibrosis-related lung disease is the main factor responsible for the mortality and morbidity associated with CF (Conese & Di Gioia, 2021). Impaired Cl^- and HCO_3^- transport to the airway's lumen results in the accumulation of abnormally viscous mucus and acidification of the ASL (Bergeron & Cantin, 2019; Gustafsson et al., 2012). These alterations contribute to host-defence disbalances, predisposing CF patients to recurring bacterial

infections that, in more severe cases, may lead to inflammation and tissue remodelling of the airways (Berkebile & McCray, 2014; Conese & Di Gioia, 2021).

Different animal models to study CF's development are currently available. Among them, swine systems are often used in studies aiming to elucidate dynamic processes related to CF due to their genetic, phenotypic, and anatomical similarities with human patients (Keiser & Engelhardt, 2011; Liu et al., 2017; Rogers et al., 2008). The porcine model is of special importance for the test of novel devices that, after validation, can be successfully used to study human CF patients.

The development of an accurate, reliable, user-friendly, and cost-effective pH measurement method is essential for studying ASL acid-base disturbances. Creating a pH meter that can assess pH in the lower airways of live patients presents several challenges. The device must be long and flexible to reach target areas via bronchoscopy while being non-invasive to ensure patient safety and comfort. Additionally, the pH meter should provide stable readings despite patient breathing movements and external disturbances such as electromagnetic interference (EMI). H^+-selective electrodes offer a promising solution for this objective. Unlike pH-selective fluorescent indicators, ion-selective electrodes (ISEs) measure ion concentrations continuously and in real-time, which makes them well-suited for assessing dynamic physiological processes such as ASL pH oscillations during breathing.

Plastic H^+-selective electrodes are particularly advantageous for this task. Their flexible nature and the potential to manufacture them in extended lengths compared to glass-based devices allow plastic ISEs to be inserted through a bronchoscope's working channel. O'Donnell (1992) has described the manufacturing process of plastic ISEs using polyethylene syringes, which has been successfully employed by Kim and colleagues (2021) to measure nasal pH fluctuations in human CF and non-CF volunteers. However, this design has limitations. Building plastic ISEs requires the manual pulling of heat-softened plastic polyethylene syringes, demanding the practice of manual skills. For this reason, the devices' characteristics can often be inconsistent, with electrode tips ranging from 150 to 550 micrometres (Kim et al., 2021). Furthermore, the total length of electrodes built with this technique is insufficient for the passage through a bronchoscope's working channel, ranging from 50 cm (O'Donnell, 1992) to 1 meter (Kim et al., 2021).

This dissertation proposes optimized building techniques for manufacturing user-friendly, uniform plastic H^+-selective electrodes that are long enough to be used via the

working channel of a bronchoscope. Strategies to mitigate EMI and maintain these electrodes' performance over time are also discussed. Additionally, a proof-of-concept assay was conducted to assess the prototype's effectiveness in measuring ASL pH in vivo using a tracheostomized one-week-old healthy piglet. A new design using polyethylene tubing with an outer thickness of 0.61 mm allows a thin, flexible, and uniform plastic H^+-selective electrode capable of fitting through the bronchoscope's working channel, contributing to the collection of previously inaccessible data. This assembly enables real-time visualization and measurement of pH at various airway sites, facilitating comparisons between diseased and healthy lung portions in the same subject.

Future in vivo investigations using the innovative plastic H^+-selective electrode characterized and validated in this dissertation will offer the first dynamic description of the ASL pH profile in the lower respiratory tract of CF patients. Discoveries made using this device will aid in developing effective patient management strategies and novel therapies, potentially enhancing the well-being and life expectancy of individuals living with the disease.

1.3. Objectives and Scope

To achieve the thesis' overall objective of developing a pH meter suitable for in vivo pH measurements of airway surface liquid, the following specific objectives were identified:

Objective 1: To optimize building techniques of long plastic H^+-selective electrodes. Design considerations included: (1) electrode length and flexibility, (2) ease and time of building, (3) success rate and uniformity, (4) adequate Nernstian slope, adjusted R^2, and response time, (5) resistance to drift and loss of slope, (6) effectiveness of EMI shielding, and (7) compatibility with an endoscope. Prototype tests were performed in a controlled experimental setup using calibration solutions of known pH.

Objective 2: To assess the effectiveness of the novel plastic H^+-selective electrodes in measuring ASL pH in vivo. Success parameters included: (1) ease of assembly and synergic work with peripheral equipment, (2) ability to accurately detect ASL pH oscillations between inspiration and expiration, (3) identification of environmental and subject-derived interferences, and (4) variability between different electrodes. In vivo assays were carried out on a tracheostomized one-week-old healthy piglet.

The scope of this dissertation was to determine optimized manufacturing techniques of long plastic H^+-selective electrodes that can be used for assessing ASL pH fluctuations in live subjects in real-time.

1.4. Organization of dissertation

This dissertation consists of five chapters:

Chapter 1 introduces the research presented in this thesis, outlining its role within a larger multidisciplinary project. It provides background and motivation for the studies conducted and clearly states the two main objectives and scope of the thesis.

Chapter 2 provides a comprehensive literature review essential for understanding the need to develop a long, flexible plastic H^+-selective electrode for in vivo pH measurements of ASL, which supports both experimental chapters (Chapters 3 and 4). It begins with an overview of cystic fibrosis-related lung disease, highlighting significant research advancements, epidemiology, etiology, and pathophysiology. It emphasizes the alterations in ASL observed in CF, including increased mucus viscosity and lowered pH, and discusses impaired host defence mechanisms. The review then shifts focus to the use of in vivo porcine models in CF studies, detailing the advantages of animal models over in vitro systems, specifically the benefits and challenges associated with swine models. Lastly, it analyzes various methods for in vivo ASL pH measurements, with a particular focus on ISEs. The discussion on ISEs covers aspects such as manufacturing, calibration, response time, and issues such as drift, loss of slope and electromagnetic interference, concluding with an appraisal of plastic ISEs for in vivo pH measurements. This review provides the foundation for the subsequent chapters by contextualizing the need for and potential impact of the innovative electrode developed in the thesis.

Chapter 3 details the process of testing various manufacturing approaches for a novel plastic H^+-selective electrode. It outlines the modifications made to O'Donnell's design (1992) based on polyethylene syringes and their effects on usability, accuracy, and maintenance of performance over time. The chapter provides a complete characterization of the optimized plastic electrode, highlighting key features such as success rate, uniformity, Nernstian slope, response time, and resistance to drift and loss of slope. Additionally, chapter 3 explores strategies for EMI shielding and evaluates the compatibility of the novel plastic electrode with a working veterinary endoscope.

Chapter 4 begins by evaluating the performance in vivo of the plastic H^+-selective electrode, developed and characterized in Chapter 3, by conducting an experiment using a tracheostomized one-week-old healthy piglet. This section details the methods used to measure pH dynamically while simultaneously recording respiratory gas profile analysis, electrocardiogram, and breathing movements. The chapter also presents results from the analysis of ASL pH and CO_2 concentration fluctuations, demonstrating the effectiveness of the novel plastic H^+-selective electrode for in vivo pH measurements.

Chapter 5 closes the dissertation with a general discussion, summarizing the results from the two previous research chapters, including an evaluation of the advancements introduced by the new plastic H^+-selective electrode and its in vivo usability. It highlights and discusses the advantages of this new design compared to existing technologies, as well as its limitations. Additionally, it proposes points for improvement in both the device itself and the experimental setup for future investigations in vivo. The chapter concludes with a reflection on the challenges to be addressed in forthcoming studies using this device to investigate ASL pH fluctuations in both swine and human CF patients.

CHAPTER 2 - LITERATURE REVIEW

2.1. Overview of cystic fibrosis-related lung disease

2.1.1. Important research advancements

Cystic Fibrosis (CF) is a multisystemic disease that affects the lungs, pancreas, gastrointestinal and reproductive track, marked by the accumulation of unusually viscous mucus (Zuelzer & Newton, 1949). This feature contributed to the use of the term "mucoviscidosis", how CF was referred to in the first research on the topic (Farber et al., 1943). The first description of CF was performed with pancreatic symptoms in view, differentiating CF of the pancreas from celiac disease (Andersen, 1938). The abnormally viscous mucus observed in various systems explains some CF-related clinical signs. However, it does not account for the unusually high salt levels found in the sweat of individuals with CF. (Bergeron & Cantin, 2019). Thirteen years after Andersen's first work with the disease, Kessler and Andersen linked CF with transepithelial salt transportation malfunction by observing 12 dehydrated children presented to a pediatric hospital during a heat wave. It was observed that the infants had low serum Cl^- and high HCO_3^- concentrations, which were reversed with electrolyte therapy (Kessler & Andersen, 1951).

Further studies observed high concentrations of K^+, and especially Na^+ and Cl^- in the sweat of CF patients (di Sant'Agnese et al., 1953). These results suggested that dehydration, a common clinical sign in these patients, was secondary to a marked salt loss from sweat glands. Further, this discovery supported the development of the first sweat test for CF diagnostic (Gibson & Cooke, 1959). During the 1980s, research focused on the pathophysiology of the sweat glands in CF patients showed that the disease provoked intense alteration in anion transportation. More precisely, it was found that these glands exhibit reduced chloride permeability due to insufficient sodium chloride reabsorption, and reduced Cl^- secretion when stimulated by adrenergic signals (Bijman & Fromter, 1986; Quinton & Bijman, 1983). Furthermore, research on CF pancreas showed that the deficiency in HCO_3^- secretion is partially due to decreased Cl^- secretion (Kopelman et al., 1988). It was observed that CF patients had more electronegative nasal epithelia when compared to controls

(Knowles et al., 1981), being also impermeable to chloride (Knowles et al., 1983). Altogether, the early research on its pathogenesis points that Cl^- permeability dysfunction is a major cause of the alterations observed in CF (Kreindler, 2010).

Canadian research has been fundamental for a deeper understanding of CF. Studies conducted in Toronto by Tsui and collaborators identified the most common CF mutation (Riordan et al., 1989); the deletion of three base pairs in the region q 31 of the human chromosome 7 results in the in-frame deletion of a phenylalanine residue at amino acid position 508 (legacy name F508del) (Riordan et al., 1989). Later, the polypeptide encoded by this gene was identified and named cystic fibrosis transmembrane conductance regulator (CFTR) (Riordan et al., 1989). This discovery paved the way for further genetic studies to understand the various CF mutations, explain their pathophysiological implications, and develop specific gene therapies currently available.

2.1.2. Epidemiology

Cystic fibrosis incidence varies greatly according to region and ancestry, being the most prevalent fatal autosomal recessive genetic disorder among people of Caucasian ancestry (Cutting, 2005; O'Sullivan & Freedman, 2009). Guo and collaborators (2022) conducted an epidemiological assessment of the CF prevalence in 158 countries, analyzing 2875 published research articles and national registries, as well as developing online surveys with CF experts and patient organizations. According to this study, around 105,000 people have been reported to be diagnosed with cystic fibrosis in 94 different countries in 2022. However, estimations of undiagnosed patients suggest that up to 162,000 people live with the disease, given that no information was available for 64 countries (Guo et al., 2022). In North America, it has been estimated that 37,000 people are positive for CF, with most patients residing in the US and Canada, representing a mean prevalence of 0.347±0.46 in the region (Guo et al., 2022).

The Cystic Fibrosis Foundation reported more than 33,000 people on its 2022 patient registry in the United States alone (Cystic Fibrosis Foundation, 2023). Further, the 2022 Cystic Fibrosis Canada's annual data report described that over 4,400 Canadians live with CF, corresponding to 1 in 3,848 live births. In 2002, 3,396 patients have been diagnosed with CF in Canada, representing an increase of 30% in a decade (Cystic Fibrosis Canada, 2023). Among other factors, the increased life expectancy from 28.1 years in 2003 to 38.4 years in 2022 is one of the main responsible for the rise in prevalence in the country since people are living longer. In Canada, more than 66% of the CF patients are adults, whereas this group

accounted for less than half of the CF population 20 years ago (Cystic Fibrosis Canada, 2023).

Considering only the previously mentioned Canadian and American registries, there are approximately 44,400 CF patients on the continent. This suggests that Guo and colleagues may have underestimated the prevalence of the disease in North America. Guo and coworkers (2022) also exposed that the lack of proper means to report CF diagnoses, mainly in developing countries, makes worldwide estimates less precise and with a high variance of mean prevalence between global regions. Thus, the development and maintenance of organized and specific registries for CF epidemiological data is fundamental for an adequate global overview of the disease, aiding in monitoring and decision-making.

2.1.3. Etiology and pathophysiology

Physiological alterations in cystic fibrosis occur in epithelial cells of different systems, with insufficient Cl^- and HCO_3^- permeability as a common underlying cause (Kreindler, 2010). In cystic fibrosis, important alterations are found in the respiratory, pancreatic, gastrointestinal and reproductive tracts, but the main cause of mortality and morbidity associated with the disorder is cystic fibrosis-related lung disease (Conese & Di Gioia, 2021). In advanced stages, CF patients suffer from recurring bacterial airway infection, intense neutrophilic-driven inflammation, mucus-obstructed airways due to increased mucus viscosity, and advancing bronchiectasis (Stoltz et al., 2015).

CFTR is a cAMP-dependent glycoprotein from the ATP-binding cassette family of transporters (ABC) (Kreindler, 2010). It is situated in the lumen-facing of epithelial cells, and is involved in ion transport and fluid homeostasis (Bergeron & Cantin, 2019). CFTR is expressed in different cell types, including ciliated epithelial cells, submucosal glands, and ionocytes. Ionocytes are a rare and just recently described cell type present mainly in the human trachea and proximal bronchi, being the main CFTR-producing cells (Montoro et al., 2018; Plasschaert et al., 2018; Scudieri et al., 2020; Zajac et al., 2021). This protein is responsible for transepithelial bicarbonate transport through its channel, which is determinant for the maintenance of physiological pH in the apical membrane and mucus (Gustafsson et al., 2012). Furthermore, CFTR promotes a strong inhibition of ENaCs (Gentzsch et al., 2010), channels responsible for sodium reabsorption into the epithelial cells, and it has a regulatory effect on HCO_3^-/Cl^- exchangers (Riordan, 2008). Malfunctions or decreased levels of CFTR promote, therefore, an increased sodium concentration in these cells' cytoplasm and alters the

airway epithelia electrophysiological properties, increasing the negative transepithelial potential difference (Stoltz et al., 2015). Lacking in CFTR function increases the transepithelial Cl^- transport to the interstice via non-CFTR channels, resulting in NaCl and water transport from the airway surface liquid (ASL) to the epithelial cells through osmosis (Bergeron & Cantin, 2019). This process dehydrates the mucus layer of the ASL, hampering the optimal mucociliary clearance (Zajac et al., 2021). Concurrently, insufficient HCO_3^- secretion to the airways and impairment of HCO_3^-/Cl^- exchangers result in a lowered ASL pH, reducing the antimicrobial capacity of peptides (Abou Alaiwa et al., 2014; Johansson et al., 1998). These two main alterations in the airway physiology contribute synergically to impair the host-defence in CF patients, predisposing them to chronic bacterial infections and inflammation, as further discussed in the next topic (Bergeron & Cantin, 2019; Gustafsson et al., 2012; Pezzulo et al., 2012; Shah et al., 2016).

CF is an autosomal recessive disease, marked by mutations in the CFTR gene (Conese & Di Gioia, 2021). To date, more than 2000 variants of the gene have been identified, which are categorized into six classes according to the outcome of the gene translation and function of the CFTR protein (Marson et al., 2016). Class I mutations provoke the most severe clinical cases, in which the CFTR protein synthesis is affected either due to the absence of mRNA transcription (class IA) or degradation of truncated mRNA as a consequence of stop-codon mutations (class IB) (Conese & Di Gioia, 2021). The most common mutations are categorized into Class II, in which mutant CFTR proteins are destroyed in the proteasome due to folding defects. Class III mutations are related to impaired gating, reducing its open probability, and Class IV comprises mutations leading to inadequate chloride and bicarbonate ion conductance. Alternative splicing decreases the amount of CFTR transcription, defining mutations class V, while mutations class VI cause the weakening of the protein. Both classes V and VI are considered less severe, since the CFTR function is present, although in less extension (Conese & Di Gioia, 2021).

2.1.4. Airway surface liquid alterations in cystic fibrosis

Pulmonary cystic fibrosis is a condition marked by mucus accumulation, inflammation and tissue remodelling (Kunzelmann et al., 2017). These features are closely linked to changes in the airway surface liquid (ASL) viscosity and pH, which disbalances the host defence capacities and predisposes CF patients to chronic microbial infections (Berkebile & McCray, 2014). Further, these two pathophysiological alterations are closely related to each other, given that a lower ASL pH contributes to the ASL's mucous layer thickening (Bansil &

Turner, 2006; Berkebile & McCray, 2014; Bhaskar et al., 1991). Microorganisms' contamination is the initial cause of inflammation and tissue remodelling in the airways, representing the main morbidity and mortality cause in cystic fibrosis-related lung disease (Conese & Di Gioia, 2021). Thus, it is necessary to understand the relationship between these two important ASL disbalances and the predisposition to airway infection in CF patients.

The airway epithelium is the lower airway's line of defence against inhaled microorganisms, representing both a physical and chemical barrier. It is coated by the ASL, a microbicide-rich medium in which pathogens are degraded (Tam et al., 2011). Lactoferrin, lysozyme, LL-37, β-defensins, secretory leukocyte peptidase inhibitor (SLPI), SP-A and SP-D are some of the many antimicrobial proteins present in the ASL (Meyerholz et al., 2010). Further, this protective fluid also contains cells from the innate immune system such as macrophages and neutrophils that are responsible for the phagocytosis of microbial debris (Berkebile & McCray, 2014).

The ASL is a physiological fluid mainly produced by submucosal glands in the larger airways, coating the epithelium with a thin layer of ~10 μm (Zajac et al., 2021). This fluid comprises two distinct layers: the periciliary liquid (PCL), which is an aqueous solution that directly covers epithelial cells and cilia, and the mucus layer (MCL), a heterogeneous viscous liquid sitting on top of the PCL, composed mainly of cellular debris and mucins, glycosylated proteins of high molecular weight (Berkebile & McCray, 2014; Williams et al., 2006). This double-layer composition allows the ciliated cells to beat with their cilia right in the interface between the PCL and MCL. Thus, disturbances in the PCL/MCL ratio can be detrimental to mucociliary clearance and, consequently, predispose CF patients to bacterial infections (Zajac et al., 2021).

The pH of ASL in healthy patients is slightly lower than the interstitium (Zajac et al., 2021). In vivo ASL pH measurements in healthy adults range from 5.6 to 6.7 in the nasal epithelia, being slightly more acidic than in the distal airway, with a pH close to 7.0 in the bronchi (Zajac et al., 2021). Alterations in this finely tuned acid-basic balance have been proven to dramatically impair the ASL antimicrobial capacity (Pezzulo et al., 2012; Stoltz et al., 2015), as discussed in the next topics.

Increased mucus viscosity

In CFTR absence or reduced function, an increased sodium reabsorption to epithelial cells occurs, leading to a decrease in the transepithelial potential difference (Stoltz et al.,

2015). An increase of Cl^- transport via non-CFTR channels to the interstice results in NaCl and water absorption through osmosis from the ASL to the epithelial cells (Bergeron & Cantin, 2019). The loss of moisture from the PCL portion of the ASL decreases the PCL/MCL ratio, resulting in a more viscous ASL (Hoegger et al., 2014).

It has also been observed that a lower ASL pH contributes to worsen mucus viscosity alterations. The mucus in acidic ASL recovered from newborn CF piglets was more viscous compared to non-CF subjects' ASL (Tang et al., 2016). After the application of hypertonic saline or heparin, the viscosity of CF ASL has been largely corrected and became similar to the ASL from wild-type animals (Tang et al., 2016). Results from this study suggest that ASL pH influences mucus viscosity, likely by affecting noncovalent interactions, specifically the electrostatic bonds, which are highly sensitive to pH fluctuations (Tang et al., 2016). In short, the lower ASL pH found in CF patients exacerbates the altered mucus viscosity caused by ASL dehydration.

As a consequence of ASL mucus thickening, CF patients are more prone to airway obstruction and microbial infections than non-CF subjects, mainly secondarily to improper mucociliary clearance (Berkebile & McCray, 2014). The inflammatory stimuli from bacterial infections and epithelial tissue remodelling further stimulate the production of mucins, perpetuating the increase in mucus viscosity and sustaining bacterial infections in a cause-consequence loop (Bansil & Turner, 2006).

Mucous layer disbalances can affect the function of microbicide molecules in the ASL. Mucins directly interact with LL-37, an important antimicrobial peptide, decreasing its microbicides activities by reducing the molecule's ability to interact with pathogens (Bucki et al., 2007; Felgentreff et al., 2006). Thus, it is suggested that increasing the amount and viscosity of mucins in the ASL of CF subjects compromises the airway host defence capacity by simultaneously reducing the cilial clearance and diminishing the microbicide effect of protective peptides (Berkebile & McCray, 2014).

Lowered pH

The primary function of the CFTR channel is to transport chloride and bicarbonate from the apical membrane of the airway's epithelial cells toward the ASL (Smith & Welsh, 1992). Bicarbonate acts as a buffer in the ASL, meaning its secretion is crucial for regulating the ASL pH (Berkebile & McCray, 2014). In CF patients who have absent, lower or

inadequate CFTR function, the deficient bicarbonate transport to the ASL results in a significant acidification of the ASL (Coakley et al., 2003).

Several in vivo studies have aimed to compare ASL pH in CF and non-CF subjects. Experiments using different animal models showed conflicting results when comparing the ASL pH of CF and non-CF subjects. Jayaraman and collaborators (2001) used a non-invasive BCECF-dextran pH indicator to assess the ASL pH in the trachea of anesthetized mice. The authors observed a mean pH of 6.95 ± 0.05 in wild-type mice and a mean pH of 6.84 ± 0.07 in CF animals, both groups being statistically similar (Jayaraman et al., 2001). Contrarily, a study using a porcine model and a pH-sensitive planar optical probe detected a significantly lower mean pH in the tracheal ASL of CFTR -/- swine (~6.9 pH units) compared to non-CF subjects (~7.2 pH units; precise values not provided) (Pezzulo et al., 2012).

The literature on human subjects is also inconsistent. Although most publications comparing the ASL pH in CF and non-CF human patients reported a more acidic pH in the CF groups, a few studies showed no differences between them. These conflicting results must be evaluated carefully in terms of the number of subjects observed, the portion of the airway assessed, and the technique used to measure the ASL pH (Schultz et al., 2017).

McShane and coworkers (2003) measured the nasal pH from the edge of the nares to up to 6 cm inward using a monocrystalline antimony catheter in healthy and CF adult patients. At the tip of the nares, both groups had similar ASL pHs (CF pH 5.6±0.1; non-CF pH 5.5±0.1). Contrarily, at 4-5 cm distal from the nares the CF group had significantly more acidic ASL compared to the control group (CF 6.2±0.1; non-CF 6.7±0.13). By using a gold electrode, the same authors observed a higher mean pH in the distal airways of both groups compared to measurements on the nose. However, no significant ASL pH differences between CF and non-CF children were observed in the lower respiratory tract (CF 7.1±0.2; non-CF 7.1±0.1) (McShane et al., 2003). This study had important detection limitations, such as the inclusion of only 5 CF and 6 non-CF children. The low n-value potentially reduced its capacity to detect significant differences between the groups, requiring further studies in this demographic cohort.

In contradiction to the results observed in the first experiment of McShane and coworkers (2003), a study employing an oesophageal pH mobidium probe in neonates found that CF infants had a lower nasal ASL (pH 5.2 ± 0.3) compared to non-CF neonates (pH 6.4 ± 0.2) (Abou Alaiwa et al., 2014). Interestingly, the same study found no significant differences

when comparing the nasal pH in CF adults and older infants to non-CF subjects (Abou Alaiwa et al., 2014). These conflicting results might be due to the technique employed. It has been suggested that the use of mobidium oesophageal pH probes is not ideal given their relatively large tip diameters (up to 2.5 mm). Since the ASL layer is a few micrometres thick, it is expected that a large portion of the probe was not in contact with the fluid, potentially interfering with the results (Schultz et al., 2017).

Further, Schultz and coworkers (2017) reported no pH differences between the ASL in the lower airway of CF and non-CF children. The mean ASL pH in the right middle lobe bronchi of CF subjects was 6.98 ± 0.15, similar to 7.00 ± 0.12 observed in control infants ($p = 0.62$). The inclusion of 37 CF and 30 non-CF children provided the study with an 87% power to detect differences as little as 0.1 pH units between groups, with a confidence interval of 95% (Schultz et al., 2017). This study is the strongest evidence in favour that CF infants do not suffer from ASL acid-basic imbalances early in life. However, it contradicts the results from investigations using in vivo and in vitro swine models (Pezzulo et al., 2012; Tang et al., 2016). The differing outcomes can be attributed to intrinsic physiological differences that influence CF progression in the two species (Schultz et al., 2017). This species-specific disease development must be taken into consideration to translate findings made using porcine animal models to human medicine.

Song and colleagues (2006) measured the pH in freshly collected submucosal gland fluid droplets through fluorescence by submerging the samples in oil stained with BCECF-dextran. They observed a statistically significant more acidic gland fluid in CF patients (6.57 ± 0.09) compared to samples from healthy subjects (7.18 ± 0.06) (Song et al., 2006). It is important to note that the subject's age and the severity of the disease also significantly influence the ASL pH alterations observed in CF patients (Berkebile & McCray, 2014).

Carbon dioxide concentrations vary greatly in the airways, from 0.03% during inhalation up to approximately 5.6% during expiration (Kim et al., 2021). Such oscillation can change the nasal ASL pH in healthy patients, going from pH 9 during inspiration to down to 7.5 in the expiration, representing a more than 10-fold change in proton concentration in a single breathing cycle (Kim et al., 2021). However, significantly lower nasal pH fluctuations are seen in CF patients, ranging from a pH of 7.7 during inspiration to 7 during expiration. CF patients not only had lower nasal pH throughout the breathing cycle but also had significantly lower pH fluctuations compared to healthy patients (Kim et al., 2021). After a local

application of bicarbonate solution in the ASL of CF patients, the maximum pH during exhalation was increased by >1 pH unit and the minimum pH during inspiration by >0.5 pH unit, promoting a nasal pH fluctuation of ~1 pH unit, similar to observations in non-CF subjects (Kim et al., 2021).

The ASL acts as a pH buffer in the airways, and it is the initial protection force against pathogens found in the air (Kim et al., 2021). Peptides, proteins and lipids with bacteria-killing capacities are present in the ASL, protecting the lower airways from inhaled microorganisms (Travis et al., 2001). These important microbicides are not reduced in quantity in CF patients, but their antimicrobial capacities may be reduced secondarily due to physiological changes in the disease such as impaired acid-basic balance (Pezzulo et al., 2012; Stoltz et al., 2015). Of note, the peptide LL-37 changes its tridimensional structure in lower pH solutions, resulting in a reduced microbicide capacity (Johansson et al., 1998). Further, the synthesis of β-defensin 1 by epithelial cells in the airways is significantly lower in acidic substrate (Nakayama et al., 2002). An in vitro study showed that an ASL pH reduction of 1.2 pH units, from 8 to 6.8, significantly decreased the microbicide capacities of the human β-defensin-3 (hBD-3) and LL-37 peptides against *S. aureus* (Abou Alaiwa et al., 2014). The LL-37's bacteria-killing effect against *P. aeruginosa* was also reduced. Moreover, this study showed that lowering the ASL pH in vitro reduced the antimicrobial synergistic capacities between LL-37 and hBD-3, as well as between LL-37 and lysozyme (Abou Alaiwa et al., 2014).

2.1.5. Impaired host defence

The reduced antimicrobial potential of peptides and impaired mucociliary clearance in the airways of CF subjects both contribute to decreased protection against inhaled microorganisms and an increased susceptibility to bacterial infections, as shown by research in both humans and animal models.

No signal of inflammation was observed in the early hours after birth in piglets with CF, suggesting that the inflammation and tissue remodelling observed in more severe cases of the disease are secondary to inadequate bacteria-killing capacities (Pezzulo et al., 2012; Stoltz et al., 2010). In infants, several different bacteria colonize the lungs, but mainly *S. aureus* and *H. influenzae* (Goetz & Ren, 2019). Later, with an age from 6 to 10 years, the infection becomes more restricted to *P. aeruginosa* and a few other species (Gangell et al., 2011, Foundation CF, 2012). The result of a cascade initiated by a chronic *P. aeruginosa* infection

and the formation of a biofilm in the airways may lead to inflammation and, further, remodelling of the respiratory tract tissue (Goetz & Ren, 2019; Stoltz et al., 2015).

Pezzulo and collaborators (2012) tested the hypothesis that the ASL pH affects the antimicrobial capacity of CF pigs by assessing their response to the placement of grids coated with *S. aureus* or *P. aeruginosa* on their airway. The authors observed a significantly lower bacteria-killing capacity in the CF subjects compared to non-CF animals. This difference was reduced when pH in the airways was increased by the addition of sodium bicarbonate, enhancing the antimicrobial efficacy in CF pigs. On the other hand, the bactericide capacity of wild-type pigs was decreased when exposed to high carbon dioxide concentrations, which lowered the pH in the airways (Pezzulo et al., 2012). These results suggest that airway host defence is highly dependent on pH, with improved function in more alkaline environments.

Kim and coworkers (2021) observed that the protective capacities against *P. aeruginosa* in fluid from Calu-3 cultures were inhibited in higher PCO_2, resulting in a lowered pH. Interestingly, no bacterial growth was observed when cultures were maintained at a constant PCO_2 of 2.5% but marked bacteria-killing occurred in cells under fluctuating PCO^2 but at the same time-averaged PCO_2 of 2.5% (Kim et al., 2021). Therefore, the authors suggested that not only the average ASL pH is relevant for antimicrobial capacities, but also the physiologic pH fluctuation resulting from the breathing cycle has a strong bacterial killing effect. ASL pH oscillations are generally expected in older infants and adult CF subjects, but the patients' genotype may influence the acid-basic balance in the airways, although the specific mechanisms behind this observation are yet not fully understood (Stoltz et al., 2015).

2.2. Methods for in vivo ASL pH measurements in the lower respiratory tract

Alterations in ASL pH are crucial in CF morbidity and mortality, mainly due to their role in increasing susceptibility to bacterial infections (Berkebile & McCray, 2014). Research has established that the inadequate transepithelial bicarbonate secretion in the airways of CF patients leads to an acidic ASL pH (Coakley et al., 2003). This acid-base imbalance is detrimental to the airways' protection against inhaled microorganisms, disrupting mucociliary clearance by increasing the mucus viscosity and decreasing the antimicrobial activity of ASL peptides (Berkebile & McCray, 2014; Johansson et al., 1998; Tang et al., 2016). Therefore, a deeper understanding of the mechanisms and consequences of ASL pH imbalances in the early stages of CF in vivo is paramount for the development of effective management strategies and therapies. These advancements have the potential to positively impact the CF

patients' welfare, improving their quality of life and life expectancy. Although available, most of the studies in this field assessed the pH in the upper airways. The lack of knowledge on ASL acidification in the lower respiratory tract, where CF alterations are more pronounced, highlights a critical gap in our understanding. Addressing this gap is essential for developing comprehensive management strategies and therapies that target the full extent of ASL pH imbalances and their impact on CF pathology.

The development and validation of accurate, reliable, user-friendly and inexpensive pH measuring methods is paramount for the study of ASL acid-basic disturbances. The development of a novel pH meter capable to measure pH in the lower airways of live human patients faces several challenges. First, the equipment must be long and flexible enough to achieve the site of interest in the lower respiratory tract through bronchoscopy. Simultaneously, it should be as non-invasive as possible, increasing the safety of the method and the acceptability of study subjects, permitting also sequenced assessments in the same patient. The device must provide a constant reading regardless of the patient's breathing movement. The thin width of the ASL layer further complicates maintaining a consistent interface between the fluid and the sensor. Finally, the pH meter should accurately and consistently sense the pH, safe from external disturbances such as electromagnetic interferences.

Various approaches to assess ASL pH in vivo are currently available. Each method has its advantages and significant limitations, which must be considered in light of the specific research question being addressed. Further, the technique employed must be compatible with the study subjects, considering if they are either human patients, small or large animal models. In the next topics, the published ASL pH measuring methods are discussed, including reflections regarding their advantages and limitations.

2.2.1. pH test strip

The use of test strips is probably the simplest pH measurement method. It is a semi-quantitative technique to measure acidity in fluids according to colour change in the strip; at every 0.5 pH units increment, the pH-sensitive reagent embedded on the paper changes colour from orange (more acid, pH ≈ 5) to light green (neutral, pH ≈ 7) and, finally, to blue (more alkaline, pH ≈ 8.5) (Siemens Healthcare Limited, 2024). Besides pH, this type of test strip is also commonly used to detect and measure the concentration of various substances on biological tissues such as urine, cerebrospinal liquid and pleural effusions (Mise et al., 2010).

Vukovac and coworkers (2019) used a test strip (Multistix 10 SG; Bayer-Diagnostics, Leverkusen, Germany) to assess the airway pH in patients suffering from chronic obstructive pulmonary disease. Researchers attached a piece of a test strip to a bronchoscope using a forceps that was inserted into its working channel. The test strip was, then, placed into a peripheral branch for 15 to 20 seconds, before being retracted inwards to the working channel to avoid contamination from other airway regions (Vukovac et al., 2019).

Although widely used in clinical settings, the application of this technique in research studies has several disadvantages. Firstly, the strip changes colour in 0.5 pH unit intervals, representing an important precision limitation. Another accuracy issue is due to its observer-dependent nature, since it relies on the investigator's colour perception to compare the test strip to a reference scale. Vukovac and coworkers (2019) employed multiple researchers to define the pH based on the stripe colour. Nevertheless, this technique's results are significantly more subjective than alternative methods available. Given the use of physical test papers, this technique only allows a single pH measurement at a time. This limitation restricts the ability to compare different airway sites and extends the duration of the trial, leading to safety and welfare concerns for the study subjects. Finally, the use of a test strip piece held on the outer side of a bronchoscope raises significant safety concerns, risking the introduction of a foreign object deep in the airways if the paper accidentally detaches from the forceps.

2.2.2. BCECF-dextran

2′,7′-Bis-(2-carboxyethyl)-5-(and-6-)carboxyfluorescein (BCECF) is a dye whose absorbance is highly pH sensitive. This molecule redshifts from pH 3.6 to 9.2, proportionally to the hydrogen ion concentration on the media (Han & Burgess, 2010). To measure pH in a sample embedded with BCECF, researchers measure the resulting fluorescence intensity after delivering excitation light at 440 and 490 nm wavelengths (Thiagarajah et al., 2004). The ratio of these excitations is then correlated to the sample's pH using the Thomas' method of ex-vivo calibration (Thomas et al., 1979).

This dye is permeable through cell membranes, allowing the application into cells without further damaging them. Also, the extracellular leakage rate of BCECF is small compared to other molecules, comprising approximately 10% after 10 to 20 minutes at 25 °C. This characteristic is adequate for intracellular studies, especially for cytosolic pHs in a normal range of 6.8-7.4 pH units (Han & Burgess, 2010). Conjugating BCECF with dextran

improves its cellular retention and largely diminishes its cytotoxicity. However, the dye photo bleaches quickly, which can lead to inaccurate pH measurements and cell damage. (Weiner & Hamm, 1989). These downsides strongly reduce the use of BCECF-dextran for in vivo pH measurements in humans, risking strong adverse effects.

Jayaraman and colleagues (2001) measured the tracheal ASL pH in vivo by directly applying BCECF-dextran in the upper airway lumen of mice. The dye was delivered using a small feeding needle passed through the mouth. Then, the trachea was exposed by an incision in the neck's midline, allowing fluorescence detection through the tracheal wall (Jayaraman et al., 2001). The experimental subjects were euthanized by pentobarbital injection. Although this technique is possible in animal models, the need to surgically expose the tissue of interest to perform the fluorescence measurements makes it impractical in larger models and impossible in human patients.

2.2.3. Planar optodes

The use of planar optodes to measure pH is based on the fluorescence decay time of pH-sensitive indicator dyes embedded in a polymer matrix, which is measured by a 10 mm thick sensor foil (Blossfeld & Gansert, 2007). In the early uses of this technique, the very fast decay time (in the range of nanoseconds) of these dyes made necessary the use of intricated and costly sensors. A novel measuring method called dual lifetime referencing (DLR) uses a mixture of luminophores, organic molecules that have varying decay times resulting from similar excitation spectra (around 470 nm). This method detects fluorescence intensity through light phase shifts, where the phase angle reflects the analyte concentration, making it more practical for sensor applications (Blossfeld & Gansert, 2007). Research on pH assessment in submerged soil reports excellent stability of planar optodes in periods over 8 weeks, especially for measurements between 6.5 and 8 pH units (Blossfeld & Gansert, 2007).

This equipment was used by Pezzulo and coworkers (2012) to measure the ASL pH in CF KO pigs. A 3 x 3 mm planar optode (PreSens GmbH) was placed in the tracheal lumen, creating a direct interface with the tracheal mucosa. The optode was calibrated using flat filters containing buffer solutions with known pHs before each measurement. In this study, the CO_2 concentration in the inhaled air was maintained at 5% to avoid interferences in the pH reading. As a consequence, the authors expected that the ASL concentration of CO_2 during expiration was above the physiological concentration of 5% (Kim et al., 2021; Pezzulo et al., 2012). This study limitation may have led to a lowered ASL pH compared to the

physiologically expected during the inspiration and expiration phases of breathing (Pezzulo et al., 2012).

2.2.4. pH-sensitive luminescent dye-based fibre-optic probes

The device developed by Schultz and colleagues (2017) used BF2-chelated hydroxy-tetraarylazadipyrromethane as a pH-sensitive compound. This molecule is more fluorescent in acidic environments and less fluorescent in alkaline environments. This material was dissolved in a 0.4% polyurethane hydrogel D4 and Egyptian blue microparticles were added in a 1.3:1 proportion in weight of Egyptian blue/D4. The resultant mixture allows dual lifetime referencing readout, increasing the accuracy and facilitating the usability of the method (Schultz et al., 2017). A 1 mm thick and 120 cm long PMMA [poly(methylmethacrylates) fibre (Ratioplast, Germany)] had one of its tips reduced in diameter to around 250 μm using heat, followed by the opening of a small indentation in its centre by a hot needle. This cavity created in the PMMA fibre enhanced the uptake of the pH-sensitive solution previously described.

A phase fluorometer (Firesting, PyroScience, Aachen, Germany) transmitted an excitatory light with a wavelength of 624 nm to the fibre-optic probe which emitted back to the photodetector a 700–1,000 nm long emission light. Then, the cotangent of the phase angle resultant from the luminescence phase shift was calculated, which is proportional to the concentration of the pH indicator in its fluorescent form. The probe was calibrated before each use using pH 4.5, 7.6 and 10.5 buffers (Schultz et al., 2017).

To measure the ASL pH in the lower airways, the fibre-optic probe was placed inside the 1.2 mm working channel of a pediatric bronchoscope (Olympus BF type 3C160, Olympus, Tokyo, Japan), protruding its tip from the equipment (Schultz et al., 2017). Through direct visualization, the apparatus was directed to the right middle lobe bronchus, where the tip of the sensor came into contact with the ASL. The use of the bronchoscope allowed a finer placement of the probe against the airway epithelia, minimizing a non-desired ion flux across the airway lumen due to excessive mechanical pressure (Schultz et al., 2017). Measurements were conducted within a 10-minute timeframe, before subsequent bronchoalveolar lavages.

One of the most relevant advantages of this method is the lower potential for measurement interference, possible by the incorporation of the pH-sensitive solution in the hydrogel matrix. This configuration limits the interaction of the pH-sensitive dye with the proteins found in the ASL, providing a more accurate and stable reading (Schultz et al., 2017),

which is an important limitation of the BCECF-dextran technique. Further, the flexible characteristic of the probe allows its use alongside direct visualization of the airways through the bronchoscope. As aforementioned, this feature represents an improvement in maneuverability and accuracy in terms of measurement location compared to non-visual techniques.

On the other hand, the use of fibre-optic probes in direct contact with the airway epithelia may trigger glandular secretion, interfering then with the ASL pH measurements (Armstrong et al., 1997). This limitation was, at least in part, addressed by the authors through the careful and precise placement of the probe on the site of interest (Schultz et al., 2017). Further, the 250 μm probe used was significantly smaller than the 3mm× 3 mm-sized planar optical probe used by Pezzulo and collaborators (2012) in swine models, supposedly promoting a less intense mechanical disruption of the airways. Although it provides a more reliable reading, this technique requires the acquisition of costly materials, namely the fibre-optic, besides a phase fluorometer. Further, the intricate manufacturing process and pH-sensitive dye mixture might be prohibitive in certain laboratory setups.

2.2.5. Monocrystalline antimony catheter

Monocrystalline antimony catheters are capable of measuring pH through an electrochemical process. This type of probe is composed of a metal/metal oxide electrode that, when into contact with a solution, undergoes a pH-sensitive oxidation-reduction reaction (Ask et al., 1982). The potential difference between the antimony electrode and the reference electrode created by this electrochemical reaction is proportional to the pH of the solution, which is then converted into a pH value using calibration data. Some of the advantages of this technique compared to conventional glass ion-selective electrodes (further discussed) include improved accuracy, faster response time, longer lifespan and miniaturized size (Ask et al., 1982).

Although most commonly used in gastro-oesophageal studies, McShane and collaborators (2003) used commercially available monocrystalline antimony catheters (Synectics Medical Digitrapper Mark III, Synectics Medical Ltd, Middlesex, UK) to measure nasal ASL pH in CF and healthy human patients (study 1). After calibration, they initially placed the probe in the nasal mucosa at the tip of the nose, followed by measurements going 1 cm more distal until the further placement at 4 cm from the nostrils. The use of an oesophageal probe on the nasal floor provided useful results, but the authors reported

important technical limitations. First, the contact of the probe with the mucosa may lead to exacerbated alkaline nasal secretion release, resulting in a higher pH measurement that interfered with the readings (McShane et al., 2003). Furthermore, the catheter was mistakenly placed into a mucus plug in three circumstances, which led to data removal from these subjects.

2.2.6. Gold probes

Gold probes function through the same electrochemical principles as monocrystalline antimony catheters, sharing the same advantages and limitations. In the previously mentioned publication, McShane and collaborators (2003) also used a commercially available gold sensor (Synectics Medical Digitrapper Mark II, Synectics Medical Ltd, Middlesex, UK) to measure the ASL pH in the nasal floor of CF and non-CF human subjects (studies 2 and 3). Interestingly, the authors only observed statistically significant differences in readings made with the antimony probe, while the golden sensor measured similar nasal pHs between the two groups. Although the reason for this discrepancy has not been fully elucidated, it has been proposed that the altered nasal potential difference observed in CF patients may result in an inaccurate pH reading by the antimony probe. Thus, the authors suggested that only gold probes be used to study ASL pH in CF subjects (McShane et al., 2003).

McShane and coworkers (2003) also used a gold pH probe to measure ASL pH in the lower airways of CF and non-CF infants (study 5). The subjects were maintained under inhaled general anesthesia to allow the passage of a 2.8- or 3.6-mm thick bronchoscope, depending on the patient. A sterile tape was used to secure the gold probe to the exterior of the bronchoscope, extending 0.5 cm beyond its tip. The technique was successfully employed in 11 infants, although complications due to difficulties in the handling of the bronchoscope and pH sensor hampered the assessment of one subject (McShane et al., 2003). Fixing the gold probe to the outer side of the bronchoscope increased significantly the total cross-sectional diameter of the equipment, limiting its use depending on the study subject's airway size (McShane et al., 2003).

2.2.7. Mobidium pH probe

Abou Alaiwa and colleagues used a so-called "mobidium pH probe" to perform in vivo ASL pH measurements in CF and non-CF patients in three opportunities (Abou Alaiwa et al., 2014, 2016, 2018). Their experiments were conducted using impedance and pH probes from the ZepHr® Reflux Monitoring System (former Sandhill Scientific, currently Diversatek

Healthcare, Highlands Ranch, CO, USA). Initially developed to perform esophagus reflux examinations, these probes are composed of polyurethane and are available in different lengths to allow assessment of patients of different sizes. Unfortunately, no information regarding this pH probe working mechanism was provided in Abou Alaiwa and coworkers' publications, nor was it available on Diversatek Healthcare's website. Furthermore, the only additional reference to such a "mobidium pH probe" found in research databases was in a review by Zajac and colleagues (2021). However, the review did not provide further details on the equipment, limiting the discussion of this method.

2.2.8. Ion-selective electrodes

Ion-selective electrodes (ISEs) are tubular investigational devices capable of measuring the concentration of a specific ion in a targeted region of biological tissue in real time (Lee et al., 2013). Different approaches for manufacturing such devices are described in the literature. The choice of an ISE's design should take into consideration the ion of interest, the profile of interfering ions on the sample, the expected dynamic of ion concentration change, and the nature of the sample (in vitro or in vivo; the site of interest in an in vivo subject).

The first ion-selective microelectrodes were described by Thomas (1978). These devices were composed of regular glass microtubes with a small piece of ion-selective glass sealing its tip, which works as a semi-permeable membrane. An electrochemical potential is formed in the interface between the ion-selective glass and the sample fluid by the passage of hydrogen ions toward the glass, at the pace at which sodium ions are transferred to the solution (Voipio et al., 1994). These ion-selective glass electrodes suffer considerably less interference from confounding ions compared to liquid membrane electrodes. This high specificity is the main advantage of its use against more modern electrodes, but glass electrodes are only capable of measuring the concentration of a few ions (H^+, Na^+, and K^+). Other important limitations of ion-selective glass electrodes are the undesirably large tip diameter that limited their use in vitro, their slow responsiveness, and complicated fabrication (Voipio et al., 1994). Currently, this type of pH probe is less commonly used in experimental setups, being largely substituted for more modern designs using ion-selective ionophore cocktails.

Advancements in ISE manufacturing techniques introduced the incorporation of ion-selective liquid membranes (ionophore cocktails) into glass microtubes, allowing for a significantly smaller tip diameter (<1 μm) and a shorter response time compared to ion-

selective glass electrodes (Lee et al., 2013). Modern self-referencing H^+-selective cells (or pH probes) work with a pair of electrodes: an ISE and a reference microelectrode (RM) (Reid & Zhao, 2011). Both microelectrodes can be manufactured through very similar techniques using the same cylindric material, as further described. Common material options are heat-pulled thin-walled borosilicate glass capillaries (Luan et al., 2020) and polyethylene syringes (Kim et al., 2021; O'Donnell, 1992).

ISE manufacture and setup

Previous reports of ISE manufacture describe this process in four to five main steps, depending on the material of choice and the laboratory's preferences. Plastic ISE building techniques using polyethylene syringes are explained in detail by O'Donnell (1992), summarized below.

1. Pulling

Long, flexible plastic electrodes can be manufactured using disposable 1 mL polyethylene syringes. After the plunge removal, a 1-2 cm section of the syringe barrel must be softened using a low flame, constantly rotating it horizontally. Then, the sections before and after the softened area are slowly pulled apart by hand, creating a conic tube with a thin tip (~0.1 mm in diameter). While the tube is cooling down, it can be continuously pulled to reduce the diameter even further. Then, the tube can be cut with a razor blade close to the syringe hub, at the opposite end of the flange where the plunger fits (it will be important in the filling step). This technique allows the manufacture of flexible microtubes as long as 50 cm and with a tip diameter as small as 40 micrometres, according to the researcher's practice and manual skills.

2. Tip bevelling

The goal of bevelling is to create tips resembling hypodermic needles, which results in a larger tip opening while increasing sharpness. This process is especially necessary for intracellular assays. Given its softer nature compared to glass microtubes, plastic microtube tips can easily be cut to an angle using a sharp razor blade. Under a dissection microscope, the researcher can manually define the microtube length and angle of bevelling.

3. Silanization

Differently from glass micropipettes, microtubes made from polyethylene syringes are intrinsically hydrophobic. This inherent characteristic makes the process of silanization

unnecessary for manufacturing plastic ISE. After being pulled, polyethylene microtubes can be filled as described below.

4. Filling

Approximately 0.2 ml of BFS is injected into the back of the syringe and the plunger is reinserted. By carefully pressing the plunger, the BFS is pushed to the tip of the thinned tube until it completely fills the syringe. With the help of a dissecting microscope, the tip is then inserted into a glass capillary tube containing about 1 µl of ionophore cocktail. No air must be present in the entire length of the microtube, including its tip. By gently pulling the plunger or simply by capillarity, a column of about 1-2 mm of ionophore cocktail is drawn into the tip of the plastic microtube. The tubing can then be withdrawn from the glass tube, completing the microtube filling process. To manufacture plastic REs, the RS (3M KCl solution for H^+-selective electrodes) is combined with agar at a 3% concentration, being used to fill the REs in a similar manner as the ISE. Mixing agar with the RS prevents liquid leakage from the plastic tubes, thereby eliminating the need for a sealing step.

5. Sealing

Plastic electrodes often require one more step in the manufacturing process. Mainly due to large hydrostatic pressures, the ionophore cocktail can easily leak out of the microtube. The same problem was observed upon unintentional contact between the tip and hydrophobic surfaces such as acrylic and polyvinyl chloride dishes. To address this problem, the tip of the ISE plastic microtube can be filled with a mixture of one-part ionophore cocktail to two-parts polyvinyl chloride (PVC) solution in tetrahydrofuran at a concentration of 15% (w/v). After curing, a thick gel-like membrane seals the electrode, avoiding liquid leakage. This process does not impact the ISE resistance and response time, allowing normal ion concentration measurements and prolonging the ISEs' lifespan. There is no need to seal the plastic REs, since filling them with the RS and agar mixture, as described in step 4, is sufficient to avoid leakages.

Although the manufacturing processes of glass and plastic ISE cells are relatively similar, each design has impactful advantages and limitations. Therefore, these factors must be taken into account to decide the optimal approach to answer a determined research question.

Glass ISEs are sharper and have thinner bevelled tips, as small as 1µm in diameter, being capable of impaling a single cell (Lee et al., 2013). H^+-selective glass electrodes have a response time of around 30 msec (Johansson et al., 1975). Although O'Donnell (1992) reported response times between 2 and 4 seconds for polyethylene ISE, devices manufactured by Kim and collaborators (2021) using the same technique demonstrated faster response times, achieving less than 1 second with 1-meter-long plastic electrodes. The considerably thinner and sharper tip and the faster response promoted by glass ISE cells compared to its plastic counterpart make it a better option for intracellular ion flux measurements (Voipio et al., 1994). However, the manufacturing process and usability of plastic ISE might be advantageous in some cases.

The pulling process using glass micropipettes requires the use of specialized equipment. It is reasonable to assume that all laboratories conducting ion activity measurements already have a glass micropipette puller. However, for research groups new to this field or those expecting to use ISEs infrequently, the costs of purchasing and maintaining this equipment can be prohibitive. Also, given its hydrophilic characteristics, glass microtubes must pass through an additional step. Although straightforward, the silanization process demands the acquisition and handling of TMSDMA, a toxic substance. Further, baking and silanizing the glass micropipettes under a fume hood introduce complexity to glass ISE manufacture and prolong the process. These devices are inherently short, rigid and fragile. Such characteristics limit the usability of glass ISE cells for applications other than in vitro. Although more suitable for intracellular ion concentration assays, the use of glass ISE cells reduces the accessibility of the equipment during in vivo experiments.

Unlike glass micropipettes, manufacturing plastic ISEs does not require specialized equipment. This method enables the production of flexible microelectrodes up to 1 meter in length (Kim et al., 2021), which facilitates in vivo assays at challenging sites unreachable for glass ISEs. Plastic ISEs are better suited for applications involving delicate mucosal tissues, such as gills, lower airways, esophagus, and even blood vessels, as they reduce the risk of damaging these tissues during experimentation (O'Donnell, 1992). Additionally, the flexibility of these electrodes minimizes the risk of breakage during preparation and use, making them a more user-friendly option (O'Donnell, 1992).

Although this manufacturing technique represents a low-cost and uncomplicated method to build flexible ISEs, it has limitations. The tips of plastic electrodes manufactured

by Kim and coworkers (2021) had considerably uneven diameters, ranging from 150 to 550 micrometres. These inconsistencies may affect the responsiveness of the electrodes and could introduce challenges when using the pH probe alongside other investigative equipment. For example, it is paramount that a long and flexible ISE be as smooth and uniform as possible to ensure its effective insertion in the working channel of bronchoscopes. The manual component of the electrode manufacturing process allows inconsistent outcomes since it relies directly on the researcher's ability and consistency while pulling up the softened plastic. Therefore, practice might be necessary to manufacture viable and uniform plastic ISE made from polyethylene syringes.

Once the optimal material for constructing the ISEs has been selected, attention must be given to choosing the appropriate ionophore cocktail. There are different hydrogen ion ionophore cocktails commercially available, consisting of three main components: the ionophore, a solvent, and an additive (Voipio et al., 1994). As previously mentioned, this cocktail needs to be combined with a backfilling solution to form the ISE. A commonly used cocktail for pH measurements, including in this experiment, is the H^+-selective ionophore I cocktail B (Sigma cat. no. 95293). The composition of this cocktail and combined BFS are described in Table 2.1 (adapted from Lee et al., 2013). The use of the hydrogen ionophore I cocktail B allows pH measurements in the 5.5-9.0 range, covering most physiological processes (Lee et al., 2013). This range includes the nasal ASL pH fluctuations during the breathing cycle in healthy human volunteers as described by Kim and coworkers (2021), going from pH 9 during inspiration down to 7.5 in the expiration.

Table 2.1. Composition and components of H^+-selective ionophore I cocktail B (Sigma Cat. No. 95293) and associated backfill solution.

Component		Composition	Characteristics
Cocktail	Ionophore	10% (w/w) tridodecylamine (TDDA; CAS no. 102-87-4)	TDDA is a lipophilic amine that is predominantly uncharged in an organic solution equilibrated with a neutral aqueous solution, making it a neutral proton carrier (Ammann et al., 1981).
	Solvent	89.3% 2-nitrophenyl octyl ether (o-NPOE; CAS no. 37682-29-4)	
	Additive	0.7% potassium tetrakis(4-chlorophenyl) borate (KTCPB; CAS no. 14680-77-4)	Reduces anion interference and electrical resistance without compromising ion-selectivity (Ammann et al., 1985, 1981)
Backfilling solution		0.1 mol l-1 NaCl and 0.1 mol l-1 sodium citrate, adjusted to pH 6 (Thomas, 1978)	Buffered electrolyte solution

Note. Adapted from "Monitoring ion activities in and around cells using ion-selective liquid-membrane microelectrodes", by S. K. Lee, W. F. Boron, and M. D. Parker, 2013, Sensors, 13(1), p. 991 (https://www.mdpi.com/1424-8220/13/1/984). CC BY-NC.

After being manufactured, the back opening of ISE and RE can then be inserted by silver chloride-coated silver wires (Ag/AgCl wires) interfacing with the BFS and RS, respectively (Lee et al., 2013). These Ag/AgCl wires are part of connector jacks (or microelectrode holders) that are plugged into a pair of probe headstages connected to a dual-channel electrometer through copper wires. This equipment amplifies the electrodes' signal and interfaces to a computer that collects and records the data (Reid & Zhao, 2011). To perform ion concentration assays using self-referencing microelectrodes, both microelectrodes must be positioned with their tips close together and be in direct contact with the solution or tissue of interest (Luan et al., 2020).

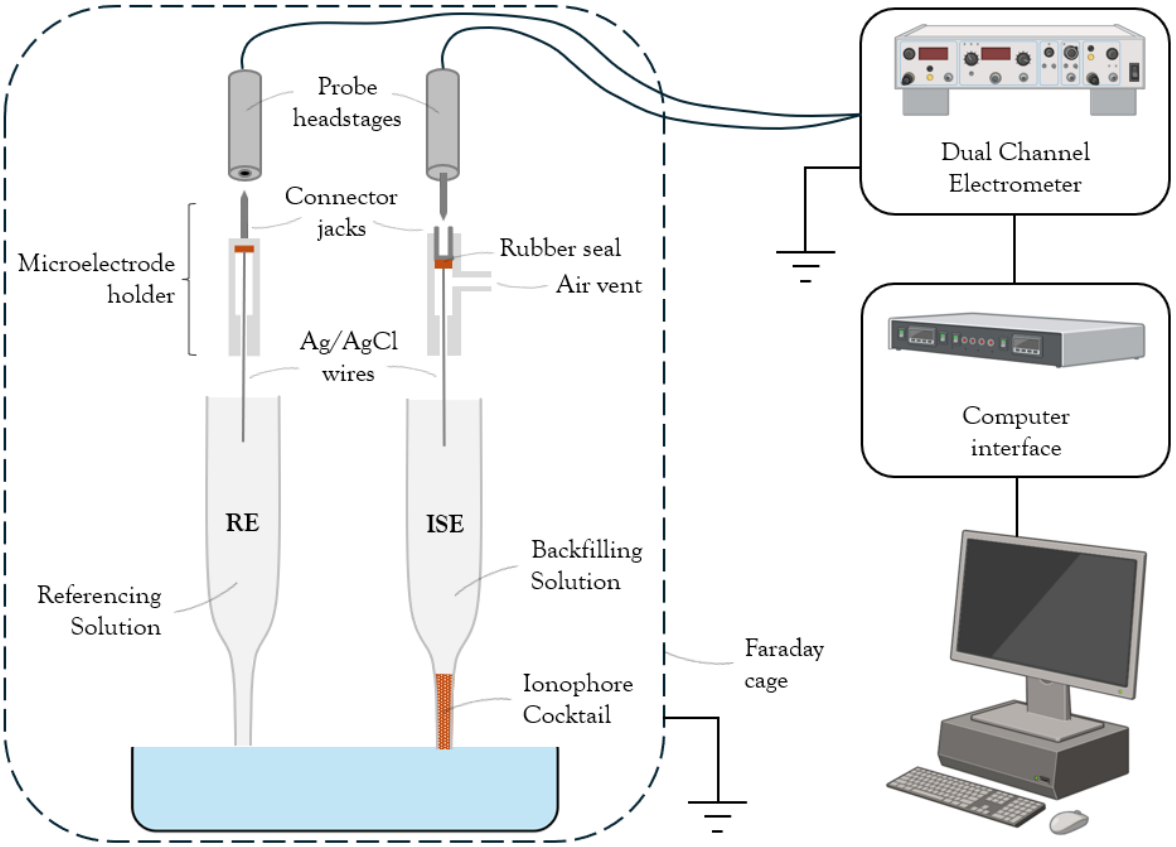

Figure 2.1. Diagram of the assembly of an H^+-selective electrode and referencing electrode including peripheral equipment. Created with BioRender.com.

Nernstian response and ISE calibration

Lee and colleagues (2013) provide a complete review of the electrochemical theories involved in ISE usefulness. Briefly, ISEs sense differences in a specific ion's concentration (in this case, H^+), between two solutions: solution 1, the fluid of interest (the ASL, for example), whose H^+ concentration is unknown; and solution 2, the BFS in the ISE, whose H^+ concentration is known. These two solutions are separated by an ion-specific permeable membrane, the ionophore cocktail. When the H^+ concentration in the sample is the same as in the BFS, the net ion movement through the cocktail is zero, since both fluids are at equilibrium. However, if the fluid of interest has a different ion activity compared to the BFS, hydrogen ions will begin to diffuse through the ionophore cocktail membrane. The movement of these ions and, consequently, of electrical charge, immediately generates an electrical potential difference across the selective membrane. More precisely, if an ISE is moved from a

solution at equilibrium to a sample containing 10 times more hydrogen ions than the BFS, a 58 mV electrochemical potential difference will be detected at room temperature, as described in (2.1) (Voipio et al., 1994). In other words, moving the ISE from a solution of pH 7 to a second solution of pH 6 (therefore, a ten-fold H^+ concentration increase), will create a potential difference of 58 mV. Contrarily, if the ISE is first submerged in a sample of pH 7 and then in another of pH 8 (therefore, a ten-fold H^+ concentration decrease), the reading will be -58 mV. The proportionality between ion concentrations and electrical potential difference is the principle behind the ISM effectiveness, known as a Nernstian response (Lee et al., 2013). This response is ruled by the diverse factors included in the Nernstian equation as demonstrated by Lee and collaborators (2013): Ψ is the electrostatic potential of the system, 1 and 2 refer to the two solutions to be assessed, R is the universal gas constant (8.314 J·mol−1·K−1), T is the absolute temperature in Kelvin, z is the charge number of the ion (valence), F is the Faraday constant (96,485 C·mol^{-1}), and [X] is the concentration of the cation of interest:

$$\Delta\Psi_{2-1} = \frac{RT}{zF} \ln \frac{[X^{Z+}]_1}{[X^{Z+}]_2} \tag{2.1}$$

Since RT / (F × log e) = 0.058 at room temperature (20 °C), (2.1) can be simplified (Lee et al., 2013):

$$\Delta\Psi_{2-1} = \frac{0.058}{z} \log \frac{[X^{Z+}]_1}{[X^{Z+}]_2} \tag{2.2}$$

Equation 2.2 assumes that the electrical potentials of solutions 1 and 2 are the same, which may not be true in practice since different assay compartments (cytoplasm vs extracellular, for example) may have different electrical potentials. For this reason, using a RE concomitantly to an ISE is essential, as the RE signal is subtracted from the ISE signal by the dual-channel electrometer, resulting in an accurate true ion-selective signal. Therefore, the RE and ISE must interface with the same assay compartment/solution (Lee et al., 2013).

After manufacture and before its use, the ISE cells must be calibrated (Voipio et al., 1994). This process has the objectives of asses the ISEs functionality and creating data to be used to calculate the unknown ion concentration. There are two main calibration methods. The dipping method (determining the static response time, discussed below) consists of sequentially immersing the ISE cell in a series of buffered solutions of known H^+ concentrations, also called standard solutions, while continuously recording (Maccà, 2004). It is suggested the use of standard solutions with lower and higher ion concentrations compared to the expected composition of the sample (Lee et al., 2013). Thus, if a researcher expects to find a pH close to neutral, it would be ideal to use solutions with pH below and above 7. Alternatively, in the injection method (determining the dynamic response time), the ISE cell is kept immersed in a solution of known ion concentration before a concentrated aliquot containing the ion of interest is added, rapidly increasing its concentration (Maccà, 2004).

The voltage detected during the calibration process can then be plotted, drawing a calibration curve with $\log[H^+]$ as the independent variable (x-axis) and the voltage (mV) as the dependent variable (y-axis) (figure 2.2). After performing a linear regression using the calibration points, the equation of the fitted line (2.3) can be used to calculate the log of a given ion's concentration (2.4) (Baucke et al., 1993). By substituting y for the voltage detected and solving for x, it is possible to calculate the $\log [H^+]$, which can then be converted to pH. The precision depends mainly on two factors: the regression line slope (Nernstian slope) and the R^2 value. To be considered an accurate electrode, the Nernstian slope at room temperature should be close to 58 mV/decade, and the R^2 value of the linear regression should be higher than 0.9 (Luxardi et al., 2015).

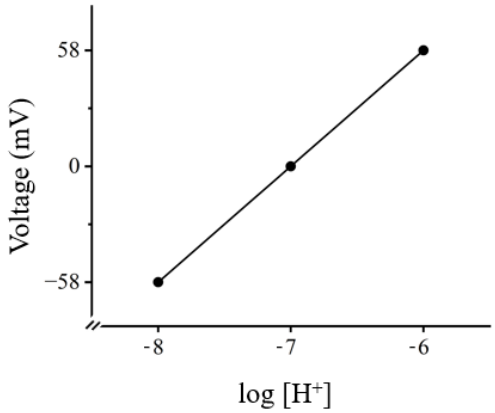

Figure 2.2. Calibration curve of an H^+-selective electrode exhibiting a perfect Nernstian response. Nernstian slope = 58; adjusted $R^2 = 1$.

$$Voltage\ (mV) = 58 \times \log [H^+] + 406 \quad (2.3)$$

If a voltage of 29 mV is detected in a given sample, by substituting y by 29 in (2.3) we have:

$$29 = 58 \times \log [H^+] + 406 \quad (2.4)$$

Now, reorganizing (2.4) and solving for log $[H^+]$, we are left with:

$$\log [H^+] = \frac{29 - 406}{58} \quad (2.5)$$

As a result, log $[H^+]$ = -6.5. Given that pH = -log $[H^+]$, it is concluded that the solution of interest has a pH = 6.5.

Response time

Response time is a crucial factor in the use of ISEs in clinical and experimental settings (Ammann, 1986). When studying dynamic phenomena, such as ASL pH oscillations during breathing, a fast ISE responsiveness is vital. The electrode must detect changes in ion concentration faster than the rate of change itself. If the pH fluctuates more quickly than the

ISE can measure, the electrode may fail to accurately capture extreme values. As a result, the amplitude of the readings may not fully reflect the actual range of ion concentration in the sample. A slow-response ISE can significantly affect the outcomes of an investigation, limiting the understanding of dynamic processes.

Since 1976, different response time measurements have been proposed by official standardizing organizations and reported in the literature. The first definition of "practical response time" available on "Recommendations for Nomenclature of Ion-Selective Electrodes" (1976) is described as follows:

> The length of time which elapses between the instant at which an ion-selective electrode and a reference electrode are brought into contact with a sample solution (or at which the concentration of the ion of interest in a solution in contact with an ion-selective electrode and a reference electrode is changed) and the first instant at which the potential of the cell becomes equal to its steady-state value within 1 mV. (Recommendations for Nomenclature of Ion-Selective Electrodes, 1976, p. 130)

Complementing the above-quoted definition, these recommendations also include reporting the experimental conditions of the measurements, including the stirring rate, composition of the test solution, temperature, among others. The response time established in 1976 was referred to as t^* in later works (Maccà, 2004).

Just three years later, in "Recommendations for Publishing Manuscripts on Ion-Selective Electrodes", the concept of practical response time was defined with additional detail (Guilbault, 1979, p.141). Instead of stating that the measurement endpoint is "the first instant at which the potential of the cell becomes equal to its steady-state value within 1 mV," the new recommendation defined it as "the first instant when the potential of the cell has reached 90% of the final value." (Guilbault, 1979, p.141). To differentiate between these two recommendations, the symbol adopted for the 1979 definition is t_{90} (Maccà, 2004). Interestingly, a newer homonymous recommendation document published in 1981 restored the first definition made in 1976 (Guilbault, 1981).

The most recent definition of response time, published in 1994 by IUPAC, does not rely solely on the observation of the steady-state value at a solution of a new concentration. Instead, it proposes the use of a slope calculated by dividing the voltage difference (ΔE) by the time elapsed until the threshold is achieved (Δt), as described below:

> The time which elapses between the instant when an ion-selective electrode and a reference electrode (ISE cell) are brought into contact with a sample solution (or at which the activity of the ion of interest in a solution is changed) and the first instant

> at which the emf/time slope (ΔE/Δt) becomes equal to a limiting value selected on the basis of the experimental conditions and/or requirements concerning the accuracy (e.g. 0.6 mV/min.). (Buck & Lindner, 1994, p. 2533)

For example, if an ISE experiences a voltage change (ΔE) of 50 mV over a period (Δt) of 5 seconds, the rate of change is 10 mV per second. This helps in determining how responsive the ISE is and in comparing it with other electrodes or technologies. As aforementioned, this definition also requires the choice of a limiting value, which can be modified according to the clinical application and experimental setup (Buck & Lindner, 1994).

The use of these three different response time definitions complicates the comparison of the quality of various ISEs reported in the literature. The ΔE/Δt definition can theoretically be related mathematically to the previous definitions (t^* and t_{90}). However, this linkage requires knowledge of the final electrode potential (Buck & Lindner, 1994), which is often not reported by authors, hampering therefore the comparison between different response time measurements (Maccà, 2004). The use of t^* response time definition has several limitations, including the introduction of a significant error in the reading. A 1 mV difference from the equilibrium corresponds to 4% of the total ΔE of a monovalent ion. Further, research showed that this measurement is highly dependent on the experimental parameters, suggesting that it is not the most reliable option to quantify the response time (Maccà, 2004). Similarly, given the logarithmic relation between voltage and ion concentration, the error introduced by using the t_{90} definition can be as large as -37% if assuming a perfect Nernstian response (Maccà, 2004).

Drift and loss of slope

After the manufacture of ISEs, two main intrinsic forms of instability may be observed in the readings over time. The first one, drift, is understood as a down-shift of the calibration curve along the voltage axis (y-axis), lowering the y-intercept while maintaining the original slope (Tsien & Rink, 1980) (figure 2.3). This graphical observation results from the loss of voltage detection over time in a solution of constant ion concentration. The main cause of drift seems to be the loss of water from the ISEs due to evaporation, which leads to changes in the ionic profile of the reference solutions (Voipio et al., 1994). Sealing the upper tip of the ISEs where it interfaces with the Ag/AgCl wire partially prevents this issue.

Drift is observed on a larger scale immediately after ISE fabrication and during the initial calibration steps, decreasing considerably after 10 to 30 minutes (Tsien & Rink, 1980).

Therefore, it is recommended to keep freshly manufactured ISEs in a solution with ionic activity similar to the sample of interest for at least one hour to allow for equilibration before calibration and use. If a drift greater than 1 mV/min is observed after this period, it indicates that the ISE is not functioning properly and should be discarded for experimentation (Tsien & Rink, 1980).

The second form of instability is the loss of slope. In ISEs with a loss of slope, the difference in voltage observed between two calibration solutions decreases over time. Therefore, this phenomenon is seen as a progressive decrease in the angle of the calibration curve, flattening it over time (Tsien & Rink, 1980) (figure 2.3 B). Although observed to some extent in all ISEs, including those sealed with polyvinyl chloride, the rate of this instability varies greatly depending on factors such as the quality of the microtube silanization, presence of aqueous solutions inside the electrode, and ionophore leaching into the sample or calibration solution (Tsien & Rink, 1980).

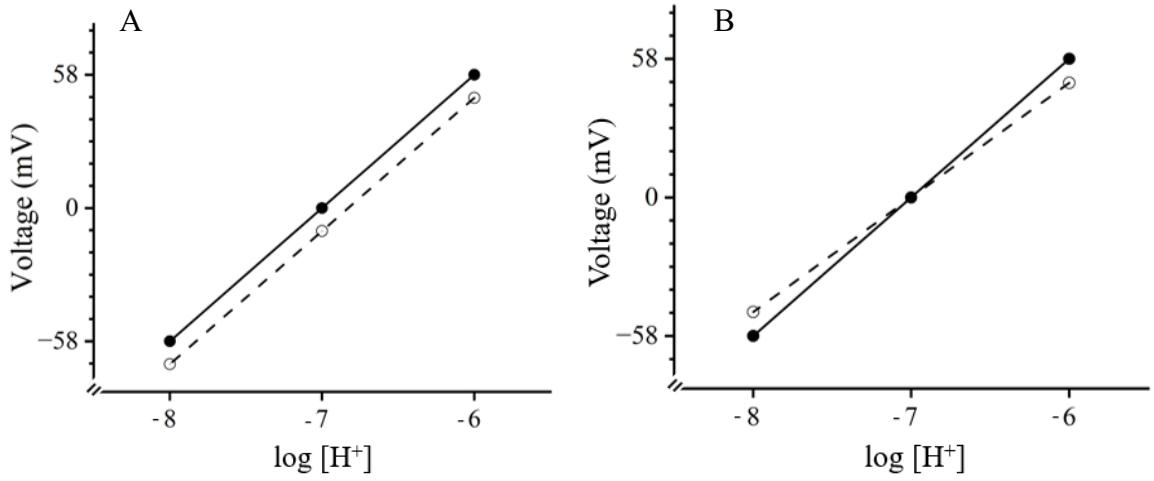

Figure 2.3. Graphical examples of two instability forms in an H^+-selective electrode. Initial calibration data points are represented by solid circles and resulting regression line by solid lines, while secondary measurements are represented by open circles and dotted lines. Drift (figure A, left) is observed as the down-shift of the calibration curve along the voltage axis. The slope of 58 is maintained, but a 10 mV decrease in each recording reduces the intercept of the equation of the line. Loss of slope (figure B, right) is marked by a shorter voltage difference between calibration solutions, resulting in a smaller slope angle.

Drifting and loss of slope are significant factors to consider when using ISEs. If not addressed, these issues can skew ion concentration measurements, as the calibration curve's accuracy may be compromised by changes in voltage over time. Therefore, it is essential to calibrate all ISEs before starting an assay to ensure their accuracy and to perform a second calibration immediately after measurements (Voipio et al., 1994). The second calibration is crucial for comparing results with the initial calibration, providing insights into any drifting that occurred during the experiment. Additionally, it ensures that a more recent and accurate calibration curve is used to calculate the unknown ion concentration in the sample.

Electromagnetic interference

In addition to experiencing drifting and loss of slope over time, which are inherent issues in ISE use, they are also affected by environmental instabilities. The strength of electrical signals from ISE readings is relatively weak, in the order of millivolts. Unwanted capacitances from laboratory equipment—such as refrigerators, light sources, heat plates, and computers—can be detected by the electrodes and Ag/AgCl wires (Voipio et al., 1994). Besides equipment, the constant electrical alternating current (AC) present in every laboratory is itself a strong source of electromagnetic interference (EMI) (Glasscott et al., 2022). This EMI is noticed as noise in the recordings, resulting from voltage signals generated by these electrical currents as they pass through the high-resistance ionophore cocktail. This phenomenon reduces the signal-to-noise ratio, reducing accuracy and complicating data analysis.

To mitigate this issue, it is a common practice to perform ion concentration measurements inside a Faraday cage to shield the microelectrodes and Ag/AgCl wires from EMI, providing cleaner, more accurate readings (Lee et al., 2013). A Faraday cage works by producing electric charges on its metal mesh surface because of incoming electromagnetic waves. Grounding the cage eliminates the electrical charge on its surface, which cancels the electric field at the cage's surface and effectively reduces the electric field inside of it (Pula et al., 2019).

Postprocessing techniques can further reduce ambient noise. Researchers can use dedicated software to digitally filter signals above a certain frequency. For example, a low-pass filter with a top-cut of 50 Hz can remove all signals with frequencies higher than 50 Hz, including the AC that is delivered at 60 Hz in North America, dramatically reducing its EMI impact (Glasscott et al., 2022; Rodrigo & Chapman, 1990).

Effect of temperature

As exposed in (2.1), the Nernstian response is directly affected by the temperature at which the ion concentration measurement is performed (Lee et al., 2013). For practical purposes, an ideal Nernstian response is often approximated as 58 mV per decade of concentration change (Voipio et al., 1994). However, this assumption is only true at room temperature (20 °C), as demonstrated in (2.2). Since this value has a multiplying effect as noted in (2.1), experiments conducted at higher temperatures will result in greater electrostatic potential differences and, therefore, in calibration curves with larger slopes. When a slope higher than 58 mV per decade is calculated, it is considered that the ISE had a super-Nernstian response (Madeira et al., 2021). For this reason, it is recommended that the ISE calibration be performed at the same temperature as the sample (Voipio et al., 1994). Alternatively, a sophisticated ISE temperature self-calibration method has been described (Saha et al., 2022). This technique involves a real-time correction of voltage using temperature data from the sample solution. The authors reported pH and nitrate measurements as close as 0.3% and 5% to the true value, respectively (Saha et al., 2022).

2.2.9. Appraisal of plastic ISEs use for in vivo ASL pH measurements

The use extracellular of ISE has several advantages when compared to other widely used pH sensors, such as pH-sensitive fluorescent indicators. ISEs can continuously measure ion concentrations, allowing for real-time assessment of dynamic physiological processes including the ASL pH during the breathing cycle. Dynamic measurements are not as straightforward when using fluorescent indicators. These methods have important limitations such as bleaching over time, seeing as a reduction in light emission. This phenomenon complicates, therefore, continuous recording of ion activity (Voipio et al., 1994). Also, the equipment and material necessary to build ISE and to record its readings are inexpensive and easily accessible. Fluorometers, on the other hand, can be cost-prohibitive. Finally, since it directly measures the concentration of an ion in a sample without the previous addition of any reagents, the use of ISEs is more suitable for in vivo experiments, especially in humans. The use of BCECF as a pH-sensitive dye demands a more labour-intensive sample preparation and has an important cytotoxicity effect (Weiner & Hamm, 1989).

Plastic ion-selective electrodes ISEs offer another significant advantage for in vivo ASL pH measurements in the lower respiratory tract. Their long and flexible design allows them to be used in conjunction with an endoscope, which facilitates the handling of the pH

probe and provides real-time visualization and measurement of pH at various sites along the airways. This capability enables comparisons between different regions of the respiratory tract, such as the upper and lower airways. Further, measurements of healthy and diseased lung areas can be performed in sequence, an approach that is not feasible with pH-sensitive dyes as previously mentioned.

The endoscope helps to avoid regions with high mucus concentration that might interfere with readings. McShane and collaborators (2003) demonstrated a method where a gold probe was taped to the outer side of a bronchoscope. However, this design had limitations, primarily due to the increased diameter of the apparatus, making it difficult to use in the airways of smaller patients. In contrast, plastic electrodes can be manufactured to be thin, flexible, and uniform enough to fit through the working channel of an endoscope. This innovation would enable data collection that was previously inaccessible. Consequently, developing and validating a user-friendly, reliable device for measuring ASL pH in the lower respiratory tract across patients of varying sizes has the potential to transform research in this area.

ISEs also have limitations. Confounders such as the electrode's depth of immersion in the fluid of interest, inadequate placement of the RM, CO_2 concentration, and temperature changes can occur in the ISE use (Voipio et al., 1994; Zajac et al., 2021). Moreover, ionophore cocktails are imperfectly ion-selective (Lee et al., 2013). Ions other than the one of interest may contribute to creating interference in the readings of ISE, limiting the detection of the probe (Voipio et al., 1994). Finally, ISEs are highly sensitive to EMI (Voipio et al., 1994). This sensitivity demands that the microelectrodes and samples be shielded from the environment, reducing the noise and providing a cleaner reading (Glasscott et al., 2022). This limitation complicates the use of ISEs in live macroscopic organisms, such as during in vivo experiments in larger mammals, due to the challenge of simultaneously shielding both the subject and the ISE.

The principles underlying the usefulness of ISEs and the availability of materials for their manufacture enable researchers to test and refine different probe prototypes to meet specific research objectives. Moreover, innovations in ISE technology designed for a particular experiment can have broad positive impacts on research in other areas due to the versatile nature of these devices. For example, new shielding techniques developed to measure ASL pH in cystic fibrosis patients, a very specific challenge, can be adapted for use

in ISEs designed to study other tissues and diseases. By simply adjusting the ionophore cocktail according to the ion of interest, researchers can modify and enhance ISE prototypes to address diverse research questions. This capacity for advancement and adaptation facilitates collaboration among research groups, promoting the development of improved ISE technologies and more accurate result interpretation.

The use of plastic H^+-selective electrodes in vivo has been reported. In a study aiming to measure the nasal ASL pH in CF and non-CF human patients, Kim and collaborators (2021) used the technique described by O'Donnell (1992) and summarized above to manufacture plastic H^+-selective microelectrodes. The authors built approximately 1-meter-long electrodes and used phosphate-buffered solutions with pHs from 6.5 to 9.5 in their calibration process. The electrodes' quality was satisfactory, showing a mean Nernstian slope of -51.1 ± 3.0 mV and a R^2 value of 0.9851 ± 0.0027. Although the paper reported successful use of this electrode design in the nasal wall, there are no available examples in the literature of H^+-selective electrodes being used in the lower airways in vivo.

2.3. In vivo porcine model for studying cystic fibrosis

Animal models aid to elucidate pathophysiological mechanisms involved in a variety of diseases. Many different CF in vitro and in vivo models are currently available. Therefore, understanding each model's advantages and limitations is fundamental for selecting the most suitable option to answer a specific research question.

2.3.1. Advantages of in vivo animal models over in vitro models

Given its accessibility in terms of ease of maintenance and inexpensiveness when compared to in vivo models, in vitro systems allow the speedy development of studies with a large n-value (McCarron et al., 2021). These models can depict a single tissue or organ at a time, being especially suitable for studies focusing on one or a few aspects of a physiological or pathophysiological phenomenon. Consequently, in vitro models are less capable of simultaneously replicating several mechanisms present in the development of a multisystemic disease such as CF (McCarron et al., 2021). Although initial research whose results helped to elucidate CFTR's mechanisms used cell-cultured samples, the simplicity of these in vitro models limits the understanding of broader, interrelated phenomena (Semaniakou et al., 2019). For example, the use of in vivo models allows the observation of dynamic processes such as the ASL pH oscillations during inspiration and expiration, as demonstrated by the work performed by Kim and colleagues (2021). In vitro systems would not be able to imitate

the breathing dynamics of a live animal, being less interesting to be used to answer this specific research question.

The different pathophysiological mechanisms responsible for the clinical signs observed in CF are complex, rapidly worsening as the patient ages and the disorder gets more severe. Using animal models allows researchers to study the initial phenomena that trigger the physiological disturbances responsible for the morbidity and mortality associated with the disease. Elucidating pathogenesis mechanisms is fundamental for the development of novel diagnostic and therapies. People living with CF are directly impacted by discovers from studies using animal models, since this type of study allows pre-clinical trials of different therapeutical approaches that, if successful in animal models, can be tested and employed in human patients (McCarron et al., 2021).

2.3.2. Animal models to study cystic fibrosis

The first in vivo CF animal model was described only three years after the discovery of the CFTR gene in 1989 (Snouwaert et al., 1992). Since then, several new models have been developed and extensively studied. Currently, a large variety of animal models are available for exploring different aspects of CF pathogenesis and development (Semaniakou et al., 2019). Most published studies used murine models of CF, mainly due to its lower costs to maintain in regular research bioterium, fast reproduction cycle and a large number of newborns per litter (McCarron et al., 2018, 2021). In fact, a systematic review of 636 papers describing 751 animal models used in CF research found that, until December 2015, 691 murine models were mentioned, representing 92% of all animal models reported (Leenaars et al., 2020). The porcine model was the second most frequent, being used in only 46 studies (6%), followed by ferrets (8 times, 1%), rats and zebrafish (3 times each, 0.4%) (Leenaars et al., 2020). Since this review was published, research using sheep (Fan et al., 2018), rabbits (Xu et al., 2021) and Drosophila (Kim et al., 2020) has also been performed.

A large share of what we now know about CF is due to discoveries in the past two and a half decades using murine models (Lavelle et al., 2016). Despite the previously exposed factors in favour of using mice in CF studies, research has shown that the CF development in this model has intrinsic differences compared to the disease progression in humans. CF in mice does not naturally evolve into lung disease as it occurs in humans (Semaniakou et al., 2019), which hampers further discoveries especially when the airways are the main interest of study. Furthermore, relevant differences in the anatomy and physiology between murine

models and humans led researchers to seek alternative in vivo models such as pigs (Wang et al., 2014).

2.3.3. Advantages of using swine animal models

Contrarily to murine models, both pigs and ferrets show a more similar CF progress to humans, showing no signs of inflammatory response at birth and being susceptible to continuous bacterial infection early in life (Ostedgaard et al., 2011; Rogers et al., 2008; Stoltz et al., 2010; Sun et al., 2010; Wine, 2010). These models, mainly the porcine, have been recently more used in research given their similarity to the human CF phenotype (Keiser & Engelhardt, 2011). This characteristic allows a closer and specific examination of the very first pathophysiological mechanisms notable in CF before the onset of microbial infections and tissue remodelling, avoiding confounders from these phenomena seen in later stages of the disease.

The first CFTR-ΔF508 heterozygous porcine model was developed in 2008 by Rogers and Stoltz. A few years later, in 2011, Ostedgaard and coworkers used these heterozygous subjects to create CFTR-ΔF508 homozygous pigs. Neonate CFTR knock-out (KO) pigs show no signs of pulmonary disease, similar to findings in CF children (Rogers et al., 2008). However, these animals develop more severe and earlier lung infections than infants (Stoltz et al., 2010; Sun et al., 2010). CF in pigs is not only similar to humans in terms of clinical presentation but also genetically; the amino acid sequence of CFTR is 92% identical to the human protein (Liu et al., 2017). Besides the similarity in terms of genetics, physiology and CF pathogenesis, the macroscopical resemblances with the human body make the pig an interesting option for studying CF (Rogers et al., 2008). It has lung and airway characteristics close to those observed in humans, including comparable airway size, lung dimensions and structure (Donnelley et al., 2019; Rogers et al., 2008). Pigs have larger airways compared to smaller animal models, facilitating in vivo studies involving the dynamic measurements of ASL pH, for example.

This set of features facilitates the translation of discoveries made in the swine model to impactful novel diagnostic tools and therapies focused on improving the quality of life and extending the life expectancy of patients living with CF. The porcine model has also been used to study other pulmonary diseases such as chronic bronchitis (Cao et al., 2015).

A comprehensive and accurate characterization of a disease is the most expensive and time-consuming phase in the validation of a new in vivo model (McCarron et al., 2021). Since

the first trials using CF swine models, our understanding of the main aspects of the disease in pigs has been elucidated. The establishment of this foundational knowledge and validation of the CF swine model enables experiments focusing on discoveries that can be effectively translated into human medicine.

In the last decade, the porcine CF model has been used more frequently in studies aiming to understand the early mechanisms present in the disease. The CF swine model has been studied to characterize their airway bacterial infection profile and to test their protective capacities against it (Stoltz et al., 2010). Pezzulo and collaborators (2012) used CFTR KO piglets to determine the relationship between the inadequate bicarbonate secretion to the ASL and the lower pH observed in the airways. Immunologic and inflammatory aspects of CF have been examined in the porcine model. Paemka and coworkers (2017) observed malfunctioning macrophages at the early stages of CF in CFTR KO newborn piglets, identifying this as a significant factor in the heightened inflammatory response characteristic of the disease. A novel X-ray-computed tomographic-based method designed to assess the mechanisms involved in mucociliary clearance, a key component of CF pathogenesis, was first tested in wild-type newborn piglets (Hoegger et al., 2014). By observing the movement of individual and grouped particles in the proximal airways of these healthy porcine subjects, researchers hypothesized that flawed mucus detachment from submucosal glands occurs from the early stages of CF (Hoegger et al., 2014). This finding was particularly useful in enhancing our understanding of the early mechanisms responsible for CF's morbidity.

Results from the growing body of research in genetically modified CF swine were fundamental to the development of a more comprehensive understanding of the disease. The use of this model has also facilitated the application of discoveries in meaningful disease management strategies in humans. Although many studies have been successfully conducted, the maintenance of genetically modified CF pigs requires significant attention and resources.

2.3.4. Challenges of using CF swine animal models

Meconium ileus (MI) is one of the most common disorders affecting the gastrointestinal tract (GIT) of human CF patients within the first hours of life, being present in between 13 and 17% of cases (Van Der Doef et al., 2011). It usually demands surgical procedures to correct the accumulation of abnormally viscous mucus in the distal ileum and proximal colon (Murshed et al., 1997; Rescorla & Grosfeld, 1993). With an incidence of 100%, this disorder

is lethal in CFTR KO newborn piglets (Stoltz et al., 2013). This complication is the main responsible for the difficulties involving the use of the porcine animal model in CF research.

Surgical correction of MI immediately after birth through ileostomy is a possibility in pigs, but the method often results in high morbidity and mortality (Semaniakou et al., 2019; Stoltz et al., 2013). Seeking an alternative to overcome this challenge and enable the use of the swine CF model, Stoltz and colleagues (2013) developed gut-corrected CFTR KO pigs. This was accomplished by promoting wild-type CFTR mRNA expression in the intestine using the rat intestinal fatty-acid-binding protein promoter (iFABP). The experiment was a success, and the authors concluded that only approximately 20% of the wild-type CFTR mRNA was sufficient to prevent the occurrence of MI. This outcome was possible even in the absence of pancreatic or hepatic correction, extending the subjects' lifespan and allowing their use in research involving CF (Stoltz et al., 2013).

Regardless of recent advancements in the development of a CF swine model, most experiments count on a small number of animals. The inclusion of a larger cohort is often limited by the expensive, time-consuming and labour-intensive management (McCarron et al., 2018). In most cases, research using this model only examines newborn piglets given their tendency to develop life-threatening complications at an early age (Semaniakou et al., 2019). This phenomenon limits the number of research on adult CF pigs and, therefore, our understanding of the later stages of CF in this model (Semaniakou et al., 2019).

Despite the challenges, researchers successfully used CF porcine subjects in numerous important studies, which have significantly advanced our understanding of the disease. Recent groundbreaking discoveries were only possible due to the anatomical and physiological similarities shared between the swine and human organisms. The use of swine models and the development of novel research tools that allow precise measurements in vivo have the potential to contribute even further to the CF research field.

2.4. Conclusion

In conclusion, developing and validating a precise plastic hydrogen-selective electrode capable of recording the lower airway's ASL pH in real-time through bronchoscopy could significantly enhance our understanding of the acid-basic disbalance during the early stages of cystic fibrosis. Elucidating these key contributors to the disease's mortality and morbidity would enable more efficient patient management and therapies, significantly enhancing the quality of life of CF patients. While hydrogen-selective electrodes made with polyethylene

syringes have been effective for in vivo use, their design currently restricts their application to the upper airways. To overcome this limitation, this thesis proposes a modification to the plastic ion-selective electrode (ISE) manufacturing technique outlined by O'Donnell (1992) by using polyethylene tubing with an outer diameter of 0.61 mm. This modification will create a more user-friendly, uniform, and longer electrode that can fit through the working channel of a veterinary endoscope, enabling the collection of previously inaccessible data.

CHAPTER 3 - DEVELOPMENT AND CHARACTERIZATION OF A LONG, FLEXIBLE PLASTIC H^+-SELECTIVE ELECTRODE

3.1. Introduction

One hallmark of cystic fibrosis (CF) is the acidification of the airway surface liquid (ASL) due to insufficient bicarbonate transepithelial transport (Coakley et al., 2003). This alteration is known to contribute to host defence impairment through decreasing peptides' microbicide effects and impairing mucociliary clearance (Abou Alaiwa et al., 2014; Berkebile & McCray, 2014; Johansson et al., 1998; Pezzulo et al., 2012). Lower ASL pH predisposes CF patients to recurring bacterial infections in the respiratory tract, contributing to chronic inflammation, airways obstruction and, advancing bronchiectasis (Stoltz et al., 2015). Although it is a multisystemic disease, cystic fibrosis-related lung disease represents the main cause of the morbidity and mortality in CF (Conese & Di Gioia, 2021). Therefore, deepening our knowledge of ASL pH disbalances' role in the initial phases of the disease is essential for clarifying the underlying mechanisms of CF pathogenesis. Advances in this area could contribute to the development of novel therapies, potentially extending and improving the quality of life for CF patients.

For this purpose, developing a method that can continuously record ASL pH in live CF subjects would allow researchers to compare the acid-base profiles across different sections of the airway and between diseased and healthy regions of the same lung. Additionally, it would enable accurate measurement of pH oscillations in the lower airways relative to the patient's breathing phase. Unfortunately, no investigational device has yet demonstrated the ability to achieve these results, to the authors' knowledge.

Ion-selective electrodes (ISEs) are devices designed to measure the concentration of specific ions in targeted areas of biological tissue in real-time (Lee et al., 2013). The most common material used to build ISEs are glass micropipettes. Still, their relatively short, fragile and rigid characteristics limit their use for in vivo ion measurements in tissues less accessible such as the lower airways. Alternatively, O'Donnell (1992) described the

manufacturing process of plastic ISE, built by pulling heated polyethylene (PE) syringes. One-meter-long plastic H^+-selective electrodes built using this technique were used by Kim and colleagues (2021) to measure ASL pH oscillations on the nasal wall of CF and non-CF human patients. Compared to glass electrodes, using plastic electrodes for in vivo assays in the airways has several advantages. First, plastic electrodes can be manufactured longer than glass devices, enabling them to reach more distal portions of the airways. Additionally, their flexibility facilitates the handling of the device in such constrained space. Finaly, plastic electrodes are less fragile, reducing the risks of breaking during handling and while an experiment is carried out. Although it represents an interesting alternative to rigid glass electrodes, manufacturing plastic electrodes using melted syringes also has important limitations. The pulling step on its fabrication demands training and manual abilities, complicating the uniformity of devices. Moreover, using PE syringes as a raw material limits the final device length, ranging from 50 cm to 1 meter (Kim et al., 2021; O'Donnell, 1992). Developing longer, uniform plastic H^+-selective electrodes would represent a significant advancement in ISEs build techniques. Such a device would allow researchers to use it concomitantly with an endoscope by feeding the ISE cells through the working channel. This assembly would enable the visualization of sites of interest while performing ASL pH measurements, facilitating the data collection at different regions of the airways.

To develop an ISE suitable for use with endoscopy, several design parameters need to be considered. First, the electrode must be long enough to fit through the entire length of the endoscope working channel. Also, it should be flexible and sturdy to allow manoeuvrability without compromising its integrity. Finally, the ISE must be able to continuously measure H^+ concentration in vivo safe from electromagnetic interference (EMI). The biggest cause of noise seen on ion-selective electrode measurements is due to the EMI. Common sources of EMI in the laboratory environment are electrical equipment and the electrical alternating current that powers the devices itself, such as the endoscope (Glasscott et al., 2022). For this reason, ion concentration assays are usually carried out inside Faraday cages that isolates its contents from environmental EMI. Investigations using ISEs within a Faraday cage are common in vitro or in small animal in vivo experiments. Although research using larger individuals can be performed inside Faraday cages, the animal's heartbeat and skeletal muscle contractions may interfere on the readings by creating EMI. Therefore, an electromagnetic shielding system that can enclose the ISEs and fit through an endoscope working channel must be developed.

This chapter introduces a novel design for plastic H^+-selective electrodes with enhanced versatility for use in the lower airways through bronchoscopy. To achieve this goal, the chapter outlines two general objectives and several specific objectives, which are addressed through a series of experiments using pH calibration solutions with known H^+ concentrations. These objectives are crucial for evaluating the basic functionality of this H^+-selective electrode prototype before proceeding to in vivo tests described in Chapter IV.

General objective 1: To develop and describe an optimized approach for building plastic H^+-selective electrodes.

1.1. To provide a detailed description of each step involved in the manufacture of the plastic H^+-selective and referencing electrodes using polyethylene tubing.

1.2. To provide a detailed description of the electromagnetic shielding developed using a grounded stainless steel braid reinforced tubing.

1.3. To describe the advantages and disadvantages of this novel building technique compared to previously published plastic electrodes, including parameters such as electrode length and flexibility, ease and time of building, success rate and uniformity.

General objective 2: To characterize the new prototype's usability through a series of tests using pH calibration solutions.

2.1. To assess the electrodes' performance over time by comparing their Nernstian slope, adjusted R^2, and response time over 4 days after manufacturing.

2.2. To compare the electromagnetic interference recorded by the electrodes without shielding, with shielding, and with shielding inside of a working channel of a veterinary endoscope.

2.3. To assess the electromagnetic interference recorded by the electrodes over 4 days after manufacturing.

2.4. To compare the effects of temperature on the noise recorded by the electrodes using pH calibration solutions at three different temperatures.

2.5. To assess the effects of temperature on the electrodes' Nernstian slope using pH calibration solutions at three different temperatures.

3.2. Material and methods

3.2.1. Plastic H^+-selective electrode and referencing electrode building technique

The following steps outline the optimized techniques for constructing, quality controlling, and storing long plastic H^+-selective and referencing electrodes made with PE tubing. The discussion section of this chapter also compares these techniques with previously published methods, highlighting the advancements and limitations that result from the novel approach described.

1. Tubing preparation

Both the ion-selective electrodes (ISEs) and referencing electrodes (REs) were built using PE tubing (BD Intramedic™, Cat. No. 14-170-12P, Waltham, MA, USA) of 0.28 mm of inner diameter and 0.61 mm of outer diameter. Using a razor blade, the PE tubing was perpendicularly cut at a 1.7-meter length. The electrodes length was set by convenience since the stainless-steel braid reinforced tubing (see "electromagnetic shielding") is manufactured at 1.5 meters in length.

2. Electrode construction

ISEs: The tubing was saturated with backfilling solution (BFS) using a 1 mL plastic disposable syringe connected to a 31-gauge blunt tip needle (Hamilton Company, Cat. No. 91031, Reno, NV, USA) (Figure 3.1.A). A small aliquot of Hydrogen ionophore I - cocktail B (Sigma Aldrich, Cat. No. 95293, St. Louis, MO, USA) was collected by capillarity into a 10µl micropipette tip. The micropipette tip's back end was then fixed to a Petri dish lid using plasticine modeling clay leaving its tip containing the cocktail easily accessible. Under a dissecting microscope at 6.3 magnification, the tip of the tubing saturated with BFS was carefully positioned making contact with the micropipette tip (Figure 3.1.B). After ensuring that no air bubble was present in the BFS-ionophore cocktail interface, a 2-3 mm tall cocktail column was drawn into the tubing by gently pulling the syringe's plunger (Figure 3.1.C).

REs: Following the same process of ISE filling, the PE tubing was saturated with the RS (3M KCl) (Figure 3.2.A).

3. Sealing

ISEs: A 15% (w/v) solution of polyvinyl chloride (PVC) (Sigma Aldrich, Cat. No. 81392, St. Louis, MO, USA) in tetrahydrofuran (Sigma Aldrich, Cat. No. 401757, St. Louis,

MO, USA) was prepared into a 10 ml slim glass specimen tube. After closing the tube with a lid to avoid solvent evaporation, the solution was homogenized using a vortex mixer for 10 seconds. Then, it was either left overnight at room temperature or kept in a warm bath at 37 °C for two hours to ensure that the PVC was completely dissolved. The ISE tip was vertically dipped 1 cm into the PVC solution for a couple of seconds, removed from it and kept pointing downwards for 30 seconds until the solvent evaporated (Figure 3.1.D). This process was repeated 3 times to ensure proper sealing of the ISE, confirmed by the build-up of a gel-like semi-translucent layer involving the distal portion of the electrode and sealing its opening (Figure 3.1.E). In some circumstances, air bubbles were trapped between the ionophore cocktail and the PVC solution. To avoid that, it was ensured that the cocktail column was flush to the tubing orifice while dipping it into the PVC solution by keeping a constant pressure in the syringe's plunger just strong enough to avoid the filling to be further drawn into the tubing by capillarity. This process can be challenging since further pushing the plunger can lead to cocktail leakage.

REs: In a 40 mL beaker, 10 mL of the RS was combined with 0.3 g of agar (Sigma Aldrich, Cat. No. A1296, St. Louis, MO, USA), resulting in a RS/agar mixture at a 3% concentration (w/v). This solution was heated in a microwave for 5 seconds at a time, gently homogenizing between cycles. It is crucial to avoid boiling the mixture to prevent air bubbles from forming inside of the electrode. The heating process was repeated 4 to 6 times until the agar was completely dissolved in the RS. After the mixture cooled for about 2 minutes and while still in a liquid state, the open end of the tubing filled with RS was submerged into the beaker (Figure 3.2.B). By slowly pulling the syringe's plunger, a 1 cm tall RS/agar solution column was drawn into the tubing (Figure 3.2.C).

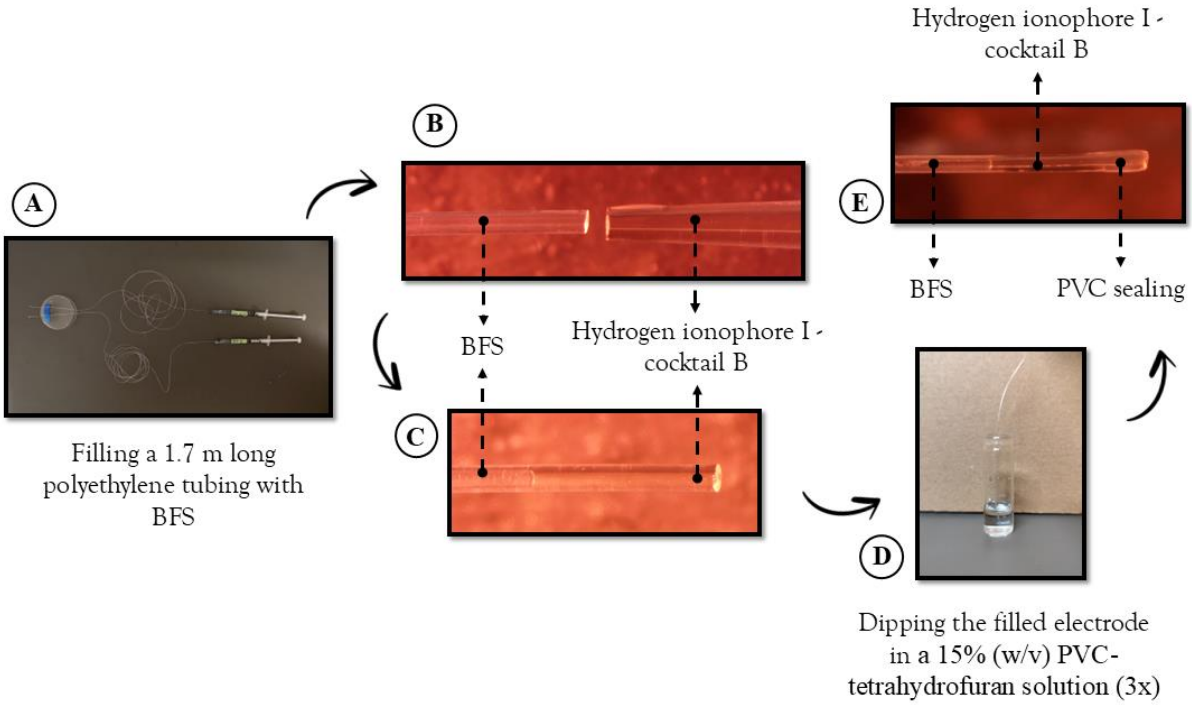

Figure 3.1. Manufacturing processes of H^+-selective electrodes using polyethylene tubing. Abbreviations: BFL, Backfilling solution.

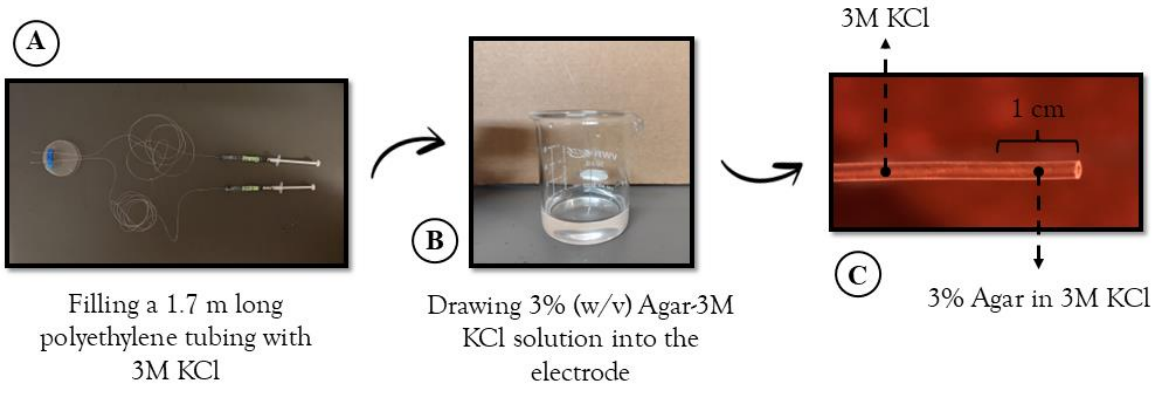

Figure 3.2. Manufacturing processes of referencing electrodes using polyethylene tubing.

4. Visual quality control

About 5 minutes after the sealing process, the PVC solution and the RS/agar mixture hardened and were fully cured. By following two simple steps, the electrodes quality was assessed before calibrating and using them in experimentation. First, the totality of the

electrodes was observed under a dissecting microscope to confirm that the tubing was completely and homogenously filled, free of air bubbles. Additionally, the electrodes sealing was tested by gently pressing the syringe plunger and observing if any fluid leakage occurred.

5. Storing

The electrodes internal fluids interfaces were allowed to stabilize overnight before the assays, aiding in decreasing the effects of drift. ISEs were kept in 50 mL plastic Falcon™ tubes (Thermo Fisher Scientific Inc., Cat. No. 14-432-22, Waltham, MA, USA) containing 5 mL of phosphate buffered saline (PBS) solution (Cytiva, Cat. No. SH30256.FS, Marlborough, MA, USA) corrected to a pH 7. A small hole was made in the lid, through which the sealed end of the ISEs was inserted and submerged in the PBS solution. Plasticine modelling clay on the outer side of the tube was used to secure the electrode in place, being rolled around the tube (Figure 3.3.A). Finally, a simple knot on the opened end of the electrode avoided fluid evaporation. This system allowed several electrodes to be coherently stored in a single Falcon tube, and different tuber could be organized into a rack to facilitate storing and transportation (Figure 3.3.B). The same storing method was used for REs, except that they were submerged into RS (3M KCl). All electrodes were stored in the Falcon™ tubes immediately after each test.

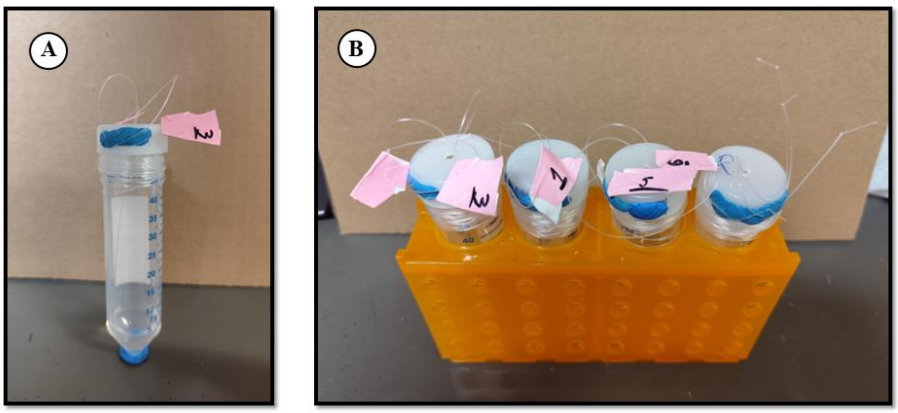

Figure 3.3. Storage system developed using Falcon™ tubes to hold plastic electrodes maintaining their tips submerged.

3.2.2. Electromagnetic shielding

A 1.5 m long stainless-steel braid reinforced tubing of an inner and outer diameter of approximately 1.45 mm and 1.93 mm, respectively (New England Tubing Technologies, Cat. No. NETT01218-C1, Lisbon, NH, USA) was used to shield the electrode cells against EMI. The braid is conductive and, by connecting it to the grounding plug of an electric outlet, it works as a flexible Faraday cage. This braid is revested by natural PEBAX (Figure 3.4.A), an isolating elastomer polymer that must be removed to prepare the braid for grounding.

Under a dissecting microscope, a razor blade was used to carefully remove the external polymer layer to expose the stainless-steel braid in a section of 1.5 cm at one of its ends (Figure 3.4.B). Special care was taken not to damage the thin and fragile wires that compose the braid during this process. Then, a coat of silver conductive paint (MG Chemicals, Cat. No. 842AR-P, Burlington, ON, Canada) was applied directly on the braid to increase the area of contact (Figure 3.4.C). After the paint dried out, this tubing section was revested using a 5 mm width copper conductive tape (SparkFun Electronics, Cat. No. 13827, Niwot, CO, USA) (Figure 3.4.D), on which a 0.6 mm thick tin-lead solder stipe (Yoshida Welding, Cat. No. 55, Mito, Japan) was soldered in a spiralled shape (Figure 3.4.E). This spiral reinforced the tubing end, allowing the braid tubing to be held by an alligator clip connected to the grounding system of the laboratory building (Figure 3.5.A). After these steps, the stainless-steel braid reinforced tubing was ready to be used to shield the electrodes against the environmental EMI, allowing its use outside of a conventional Faraday cage.

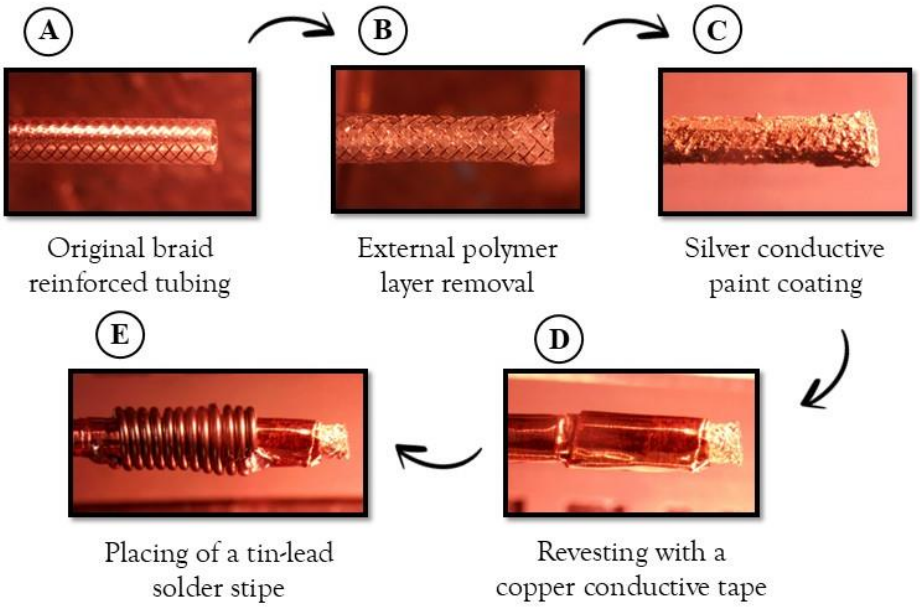

Figure 3.4. Preparation of a stainless-steel braid reinforced tubing for grounding.

3.2.3. H^+-selective electrode cells assembly and data collection

After manufacturing the ISE and RE and preparing the grounded stainless-steel braid reinforced tubing, the H^+-selective electrode cell can be assembled and begin recording. After being removed from the storage tubes, the tied ends of the electrodes were cut using a razor blade, reopening its orifice. The Ag/AgCl wires from a female (World Precision Instruments, Cat. No. MEH2SFW, Sarasota, FL, USA) and a male microelectrode holder (World Precision Instruments, Cat. No. EBH1, Sarasota, FL, USA) were inserted 5 mm into the ISE and RE, respectively, interfacing with the BFS and RS (Figure 3.5.B). This pair of microelectrode holders were secured on a tripod by a pair of micromanipulators (Narishige, Cat. No. MM-3, London, UK) (Figure 3.5.A). Two probe head stages connected the microelectrode holders to a dual channel differential electrometer (World Precision Instruments, Cat. No. FD223a, Sarasota, FL, USA), which was connected to a data acquisition hardware device (ADInstruments, PowerLab 8/35, Sydney, Australia). Finally, this interface equipment was connected to a computer via a USB cable, which collected recording data using the software LabChart (Version 7.3.8; ADInstruments, 2016, Sydney, Australia).

The tripod securing the microelectrode holders and probe head stages was kept inside a grounded 1m x 1m x 1m Faraday cage (Kinetic Systems, Inc, Pleasanton, CA, USA) to reduce the EMI's effects on the upper end of the apparatus. A small 3 cm wide circle opening

was made on the mesh on the side of the cage for the passage of the probe head stages cables. A second tripod, also inside the Faraday cage, was used to secure an alligator clip 5 cm below the microelectrode holders that held the braid reinforced tubing in a vertical position (Figure 3.5.A). This alligator clip was connected to the grounding system of the building using an insulated 2.5 mm thick stranded copper wire and a male cord connector. The alligator clip grounding cable and the braid tubing exited the cage through the same opening as the probe head stages cables. The ISE and RE were fed through the braid tubing, protruding 2 mm from its end (Figure 3.5.C). This assembly protected the electrode cell against EMI on the outer side of the cage, where the performance assays were conducted.

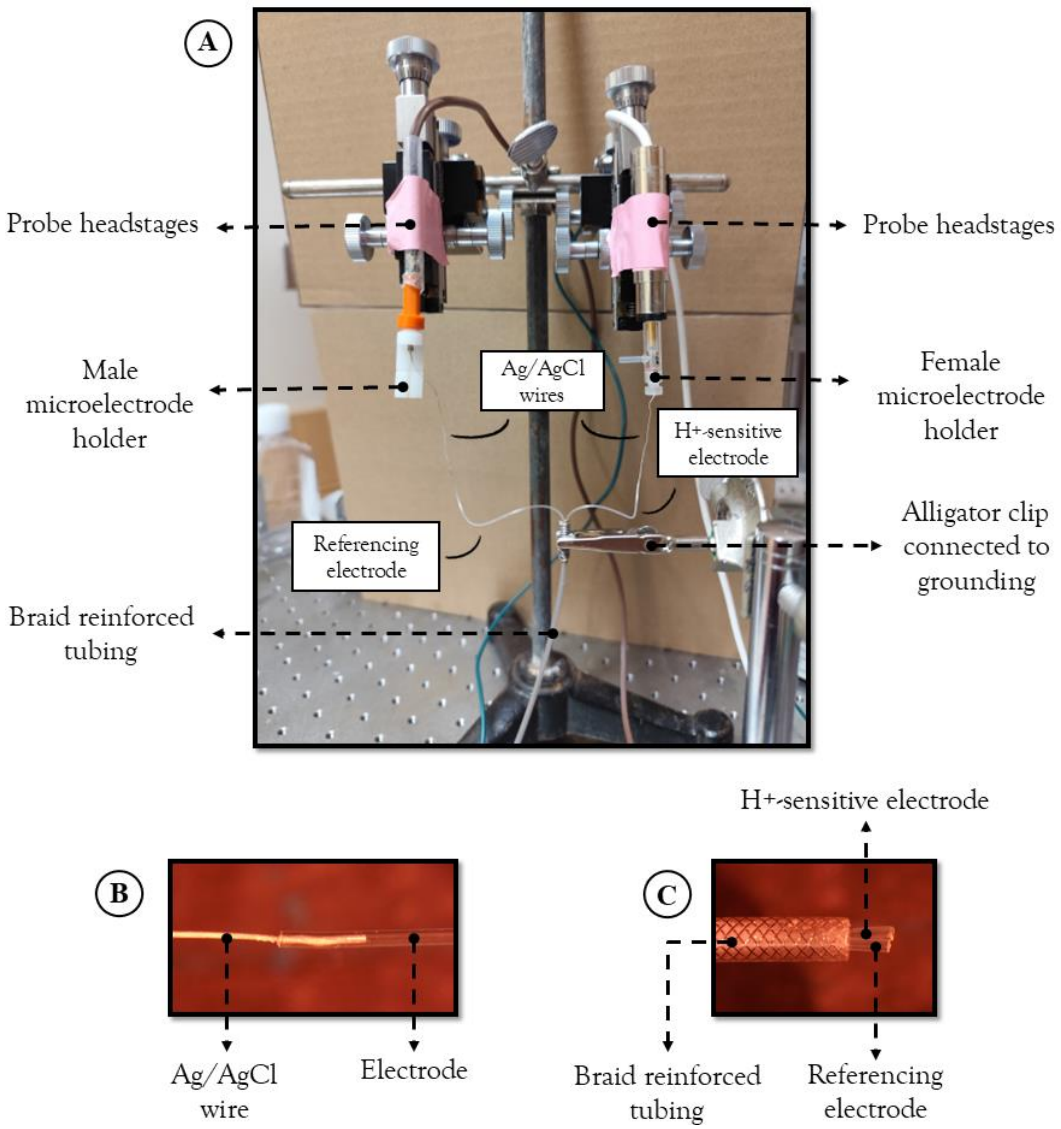

Figure 3.5. Assembly of a plastic H^+-selective electrode cell in a pair of microelectrode holders and being fed through a grounded stainless-steel braid reinforced tubing.

3.2.4. Plastic H^+-selective electrode characterization

A series of tests were performed in a set of electrodes to assess their performance over time in terms of Nernstian slope, adjusted R^2, and response times. Also, the degree of noise seen on the recordings at different setups and the effects of temperature on the measurements were observed. All assays were developed outside of the Faraday cage to simulate the experimental setup to be used in the in vivo experiment. A single RE was used for all measurements, being paired with different ISEs to perform the recordings. The electrode cells, composed of the RE and one ISE, were assembled as previously described. The dual-channel electrometer's range was set to 200 mV and a digital low-pass filter with a top-cut of 50 Hz was set in the analytical software to filter the EMI from alternate current running in the laboratory room. All tests except when described otherwise were performed at room temperature (approximately 22 °C).

Performance over time

The Nernstian slope, adjusted R^2, and response time of 10 H^+-selective electrodes were assessed daily to evaluate their performance over time. For this purpose, the same calibration procedure using solutions of known pH was carried out for 4 consecutive days. The calibration process followed the dipping method (Maccà, 2004), in which the ISE cells are submerged into a series of solutions of known pH while continuously recording the resultant voltage. Before each calibration, three PBS solutions (Cytiva, Cat. No. SH30256.FS, Marlborough, MA, USA) were fixed to pH 6, 7 and 8 according to a calibrated bench pH meter (Thermo Fisher Scientific Inc., Cat. No. 13-620-183A, Waltham, MA, USA) by adding either HCl or NaOH to the solutions. These calibration solutions were chosen based on the expected pH range to be measured in the ASL of the piglet during the in vivo experiment (pH ≈ 7). Aliquots of 1 mL of each solution were then added to 1.5 mL plastic safe-lock tubes for easy handling, in which the ISE cells were submerged (Figure 3.6).

Initially, the tips of the ISE and RE were submerged into the pH 7 calibration solution until the reading stabilized, which took up to 5 minutes. After 30 seconds of stable measurements, the electrodes were removed from the first calibration solution, rinsed with distilled water and dried by gently tapping them with a paper wipe. Then, the electrodes were submerged into the second calibrating solution of pH 6. The transfer from one solution to the next one occurred within 5 seconds, minimizing the time the electrode circuit was left open. To transfer the electrode cell to the third and last calibration solution, of pH 8, the previous

steps were repeated. The voltage recorded at each calibration solution of different pHs was used to calculate the Nernstian slope and the adjusted R^2 by performing a linear regression (Baucke et al., 1993).

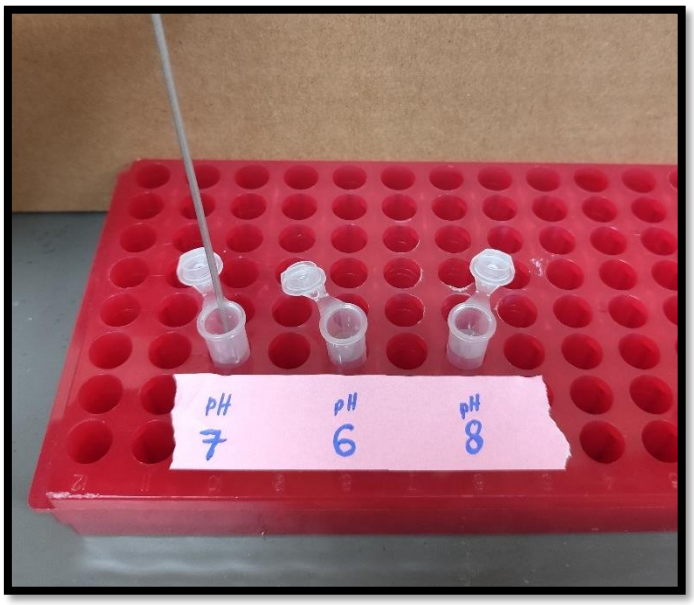

Figure 3.6.Aliquots of three calibrating solutions were placed in 1.5 mL plastic safe-lock tubes to facilitate the calibration of the H^+-selective electrode cells.

Voltage recordings from the calibration process were also used to calculate the electrodes' response time. This parameter (t^*) is defined by the time elapsed from the instant in which the electrode cell is removed from the first calibration solution to the instant in which the recording reaches 1 mV from the final stable voltage while the electrode cell is submerged into the second solution (Guilbault et al., 1976).

Noise

The noise detected in the ISE cells recordings was used to test the EMI shielding efficacy of the grounded stainless-steel braid reinforced tubing. These assays also aimed to assess the compatibility of the electrodes with an endoscope. Since the endoscope is an electrical device, the tests evaluated whether using ISE cells concurrently with the endoscope would introduce noise into the readings. The equipment used was a 140 m long veterinary endoscope (Karl Storz SE & Co., Cat. No. 13820 NKS, Tuttlingen, Germany) with a working

channel 2.8 mm wide. Recordings made in a pH 7 calibration solution after the ISE cells had stabilized were used to measure the noise intensity. This parameter was determined by subtracting the lowest voltage reading from the highest reading within a 1-second interval, resulting in the signal noise amplitude.

Four different setups were tested: (1) ISE cells inserted through the grounded stainless-steel braid reinforced tubing (shielded), (2) shielded ISE cells inserted through the working channel of the endoscope with the illumination system turned off (end. light off), (3) shielded ISE cells inserted through the working channel of the endoscope with the illumination system turned on (end. light on), and (4) ISE cells without any shielding (unshielded) (Figure 3.7). The endoscope monitor was left on throughout the experiment; the only difference between setups 2 and 3 was whether the endoscope's light was turned on or off.

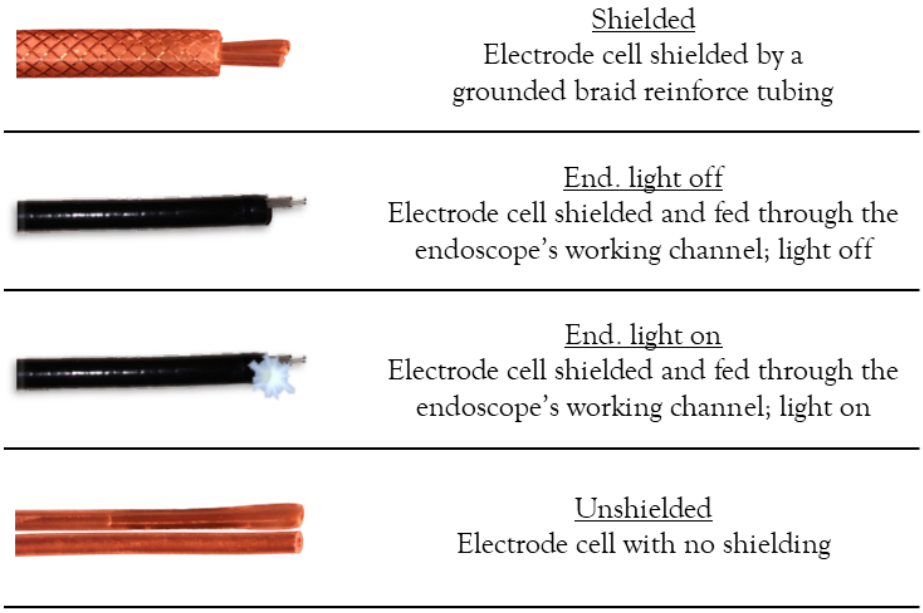

Figure 3.7. Four different electrode shielding setups tested.

Additionally, data from the daily calibration procedure performed to assess the ISE performance over time was used to compare the noise observed in recordings from pH 7 calibration solutions throughout four days after the electrodes manufacture. Data from the assay studying the effects of temperature on the ISE Nernstian slope (see below) was also

used to compare the noise between readings performed at different temperatures. Recordings performed in pH 7 calibration solutions at 23, 27 and 32 °C were used to assess if heated samples introduced larger measurement oscillations.

Effect of temperature on Nernstian slope

To assess the effect of temperature on the ISE Nernstian slope, three sets of calibration solutions of pHs 6, 7 and 8 at different temperatures were used. One set of solutions was kept at room temperature (22 °C) and a pair of heat plates were used to warm one set of calibration solutions at 27 °C and another at 32 °C. Table 3.1 depicts the order of solutions in which the ISE cells were submerged. This order was chosen to avoid repeated large H^+ concentration changes. Data from this assay was used to calculate three Nernstian slopes, respectively to the temperature of the calibration solutions set.

Table 3.1. Order of the different pH calibration solutions and temperatures used to determine the effect of temperature on ISE Nernstian slope.

Solution order	1st	2nd	3rd	4th	5th	6th	7th	8th	9th
Solution (pH)	7	7	7	6	6	6	8	8	8
Temperature (°C)	22	27	32	22	27	32	22	27	32

Statistical analysis

Raw data was exported from the software LabChart (Version 7.3.8; ADInstruments, 2016) to an Excel spreadsheet (Version 2407, Microsoft Corporation, Inc., 2024). Statistical analyses were performed using the Stata Statistical Software (Version 18; StataCorp LLC, 2024) and graphs were made using the software OriginLab (Version 2024b; OriginLab Corporation, 2024).

Initially, the distribution of each variable was assessed for normality by Shapiro-Wilk tests. In the results topic, the mean and standard deviation (SD) of normally distributed variables were reported, while the median and interquartile range (IQR) were given for variables with a non-normal distribution.

Generalized estimating equations (GEEs) were used to compare the Nernstian slope, response time and noise intensity across four days after the ISEs' manufacture. GEEs allow

the calculation of regression estimates for datasets with repeated measures whose variables have non-normal distributions (Zeger & Liang, 1986). It calculates the population average, including the within-subject correlation (each ISE, in this case) in the model. Therefore, GEEs are an interesting approach to analyzing clustered data with repeated measures. In the model, "day" was included as the time variable relative to the repeated measures, and "electrode" was included as the cluster to indicate non-independence between the recordings. Results were calculated using robust standard errors, which correct for possible misspecifications in the model without altering the coefficients (Tang & Wang, 2019). The regression estimates were calculated with a 95% confidence interval, using "day 1" as the baseline for comparisons. Additionally, the overall effects of time were calculated.

GEEs were also used to compare the noise intensity between the different shielding setups and between the calibration solutions' temperatures, as well as to compare the Nernstian slope resultant from calibration procedures at different temperatures. "Electrode" was included in the model as the cluster and robust standard errors were calculated with a 95% confidence interval. Noise analysis used "shielded" as the baseline for comparisons, while "22 °C" was the reference for the temperature assay.

3.3. Results

3.3.1. Building technique

A total of 20 plastic H^+-selective electrodes were manufactured to test the building techniques, from which 17 passed through visual quality control and succeeded in the calibration procedure. Although a single RE was used for all tests, 5 electrodes were manufactured to test the built techniques. All 5 REs showed adequate performances. The most common reason for ISE non-compliance with the quality standards was the presence of air bubbles trapped between the ionophore cocktail and the PVC sealing. This issue was readily observed through microscopy after the PVC cure, being fixed by simply cutting a few centimetres from the plastic tubing tip using a razor blade and resuming the manufacturing process on the filling step. Overall, the ISE and RE built success rates were 85% and 100%, respectively. The approximate time for building an individual ISE was 5 minutes, while only 3 minutes were necessary to prepare a RE. Therefore, a set of 10 ISE and one RE could be manufactured within an hour. On the other hand, preparing the grounded reinforced braid tubing took around 20 minutes. Although it was considerably more time-consuming than building the electrodes themselves, a single braid tubing was used for all assays.

3.3.2. ISEs characterization

Performance over time

Figure 3.8 shows a typical recording from the calibration procedure performed at room temperature using the H^+-selective electrode #7 one day after its manufacture. It is possible to observe that a 58 mV increase in the voltage occurred from moving the electrode cell from the first calibration solution of pH 7 (initially set at 0 mV) to the second solution of pH 6. Then, moving the electrode cell to the third and last solution of pH 8 induced a drop in the recording to -56.5 mV. As a result, it was calculated that this electrode had a Nernstian slope of 57.25 mV and an adjusted R^2 of 0.9996. This figure also shows that the reading was "out of range" for a brief period in two circumstances, observed as a spike reaching 200 and a dip down to -200 mV approximately at 11 and 22 seconds, respectively. These steep voltage changes were due to the transient opening of the electrode's circuit that occurred between the instant that it was removed from a calibration solution and the instant that it was re-submerged into the following one. The time elapsed from the submersion of the electrode in the solution of pH 6 and the voltage recording achieving stability was recorded, corresponding to the response time of the electrode.

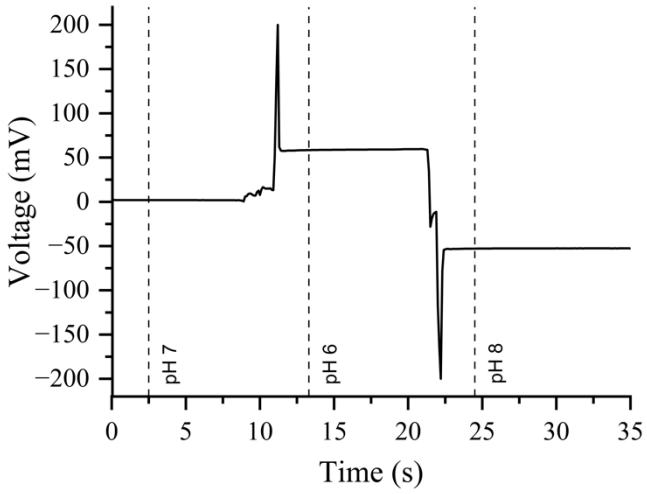

Figure 3.8. Typical recording from the calibration process performed using the H^+-selective electrode #7 one day after its manufacture. Dashed vertical lines mark the pH of the calibration solutions used in each stage.

The performance over time of a total of 10 H^+-selective electrodes was assessed (Table S1 in Appendix A). Table 3.2 shows a summary of their Nernstian slope, adjusted R^2, and

response time over time, including the coefficient and p-value for comparison against day 1 and the overall effect of time. Graphical representations of the Nernstian slope decrease over time and the distribution of adjusted R^2 and response time day by day are also available in Figures 3.9, 3.10, and 3.11, respectively.

Table 3.2. Nernstian slope, adjusted R^2, and response time from 10 H^+-selective electrodes over four days after manufacture.

	Overall	Day			
		1	2	3	4
Nernstian slope (mV/[H^+] decade)					
Mean (SD)	52.2 (2.7)	53.7 (3.7)	51.6 (2.3)	52.6 (1.6)	50.9 (2.5)
Minimum	46.1	46.1	46.4	50.6	46.2
Maximum	57.5	57.5	54.4	54.8	54.9
Coefficient (SE)	-0.71 (0.4)	-	-2.08 (1.4)	-1.03 (1.2)	-2.73 (1.3)
p-value	.053	-	.144	.376	.032
Adjusted R^2					
Median (IQR)	0.9983 (0.995-0.999)	0.9979 (0.9959-0.9996)	0.9973 (0.9942-0.9995)	0.9992 (0.9973-1)	0.9977 (0.9945-0.9999)
Minimum	0.9829	0.9829	0.9924	0.9944	0.9938
Maximum	1	1	1	1	0.9999
Coefficient (robust SE)	0.0005 (0)	-	0.0008 (0)	0.0022 (0)	0.0011 (0)
p-value	.427	-	.542	.246	.544
Response time (s)					
Median (IQR)	1.5 (0.9-2.8)	1.1 (0.8-1.7)	1.5 (1.1-3.1)	1.8 (0.8-2.2)	2.6 (1.8-4.8)
Minimum	0.2	0.3	0.2	0.3	0.4
Maximum	8.3	2.6	3.2	4.1	8.3
Coefficient (SE)	0.68 (0.2)	-	0.52 (0.2)	0.72 (0.4)	2.19 (0.8)
p-value	.004	-	.002	.045	.005

Abbreviations: SD, standard deviation; SE, standard error; IQR, interquartile range.

It was observed a trend towards the decrease in the Nernstian slope of the electrodes over time (p=.053); on average, for each day passed after the electrodes' manufacture, the slope decreased by 0.71 ± 0.4 mV/[H^+] decade. The average slopes from day 2 and 3 were shallower when compared to day 1 (Figure 3.9), although they were not significantly different (p=.144 and .376, respectively). On the other hand, on day 4 the mean slopes were found to be statistically different from those observed on day 1 (p=.032), resulting in a mean 2.73 ± 1.3 mV/[H^+] decade decrease over this period. Regardless of this overall trend toward the reduction of slope over time, it is important to note that slopes as high as 54.9 (steeper than the mean slope on day 1) were measured on day 4. On the other hand, the adjusted R^2 resulting from the linear regressions calculated using the daily calibration data was not affected by time (p=.427). With the exception of electrode #4 on day 1 that showed an adjusted R^2 of 0.9829, all other were above 0.990 regardless of the day. As a result, the overall adjusted R^2 median (interquartile range) was 0.9983 (0.995-0.999).

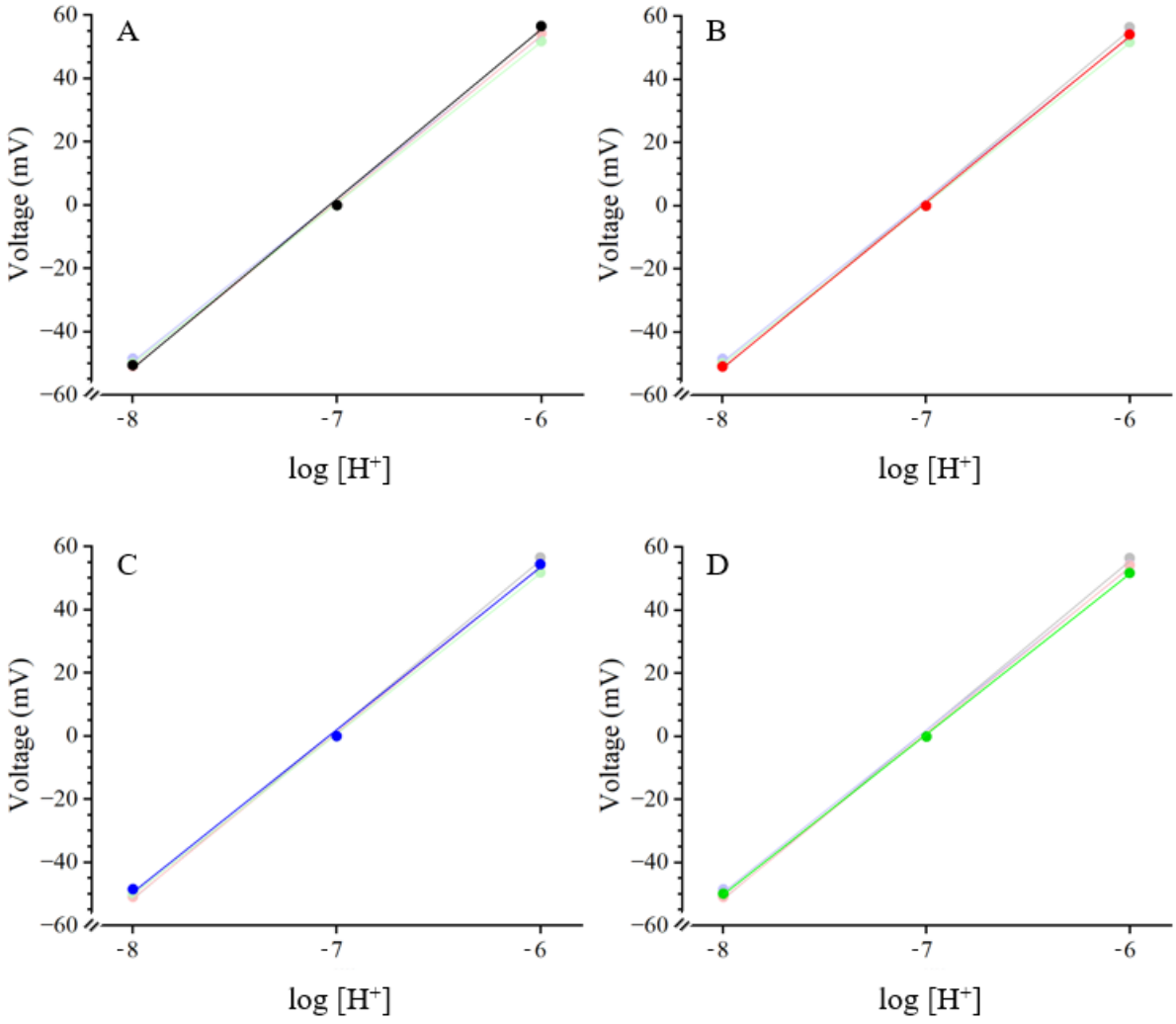

Figure 3.9. Graphical representation of the mean calibration curve from 10 H^+-selective electrodes over four days after manufacture. Black, day 1 (highlighted in A, top left); Red, day 2 (highlighted in B, top right); Blue, day 3 (highlighted in C, bottom left); Green, day 4 (highlighted in D, bottom right).

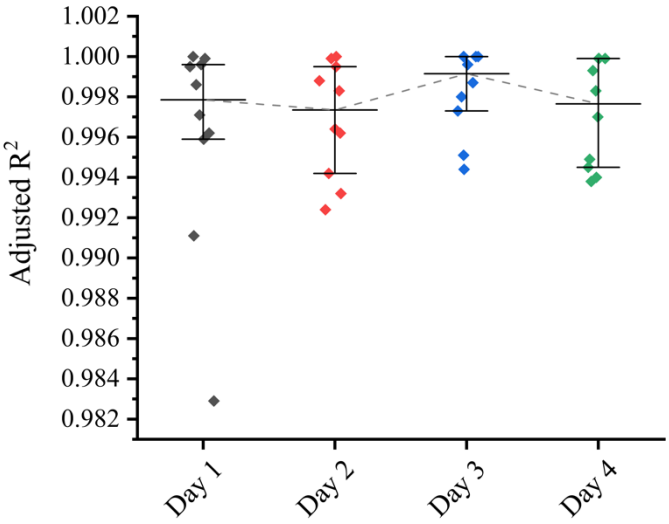

Figure 3.10. Scatter interval plot of the adjusted R^2 from 10 H^+-selective electrodes over four days after manufacture, including median and interquartile range. The dashed line shows the median trend over time.

The response time was found to be significantly dependent on the electrodes freshness (p=.004), as for each day after manufacture, the response time increased by 0.68 ± 0.2 s. Additionally, the electrodes' responsiveness observed on days 2 through 4 was significantly slower compared to day 1 (p=.002, .045, and .005, respectively). Although the overall response time was increased by 0.52 ± 0.2 and 0.72 ± 0.4 s on days 2 and 3, respectively, the difference was more pronounced on day 4, corresponding to a 2.19 ± 0.8 s increase. Nevertheless, one electrode on day 4 showed a response time <1s, comparable to those seen on day 1. On the other hand, response times as large as 8.3 s were observed on day 4, showcasing the increased variability in the electrodes' performance with the time passing, as observed in Figure 3.11.

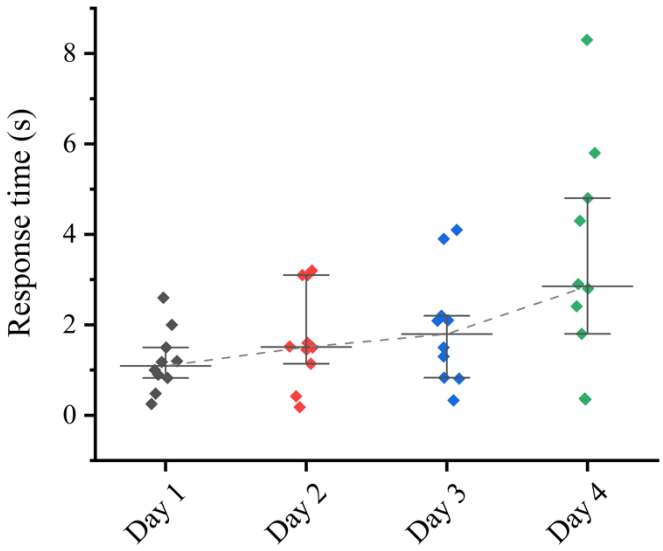

Figure 3.11. Scatter interval plot of the response time from 10 H^+-selective electrodes over four days after manufacture, including median and interquartile range. The dashed line shows the median trend over time.

Noise

Figure 3.12 shows the noise observed in the recordings from electrode #15 throughout one second at four different setups: while shielded by the grounded stainless-steel braid reinforced tubing, shielded and fed through an endoscope working channel with its lights off and on, and without any electromagnetic shielding. The voltage oscillations from the unshielded electrode were visually larger than the ones with the shielded electrode (Figure 3.12 A, left). Figure 3.12 B, right, shows these voltage oscillations at a scale 10 times smaller than the one in Figure 3.12 A for a more precise comparison between the three shielded categories, which have visually similar amplitudes.

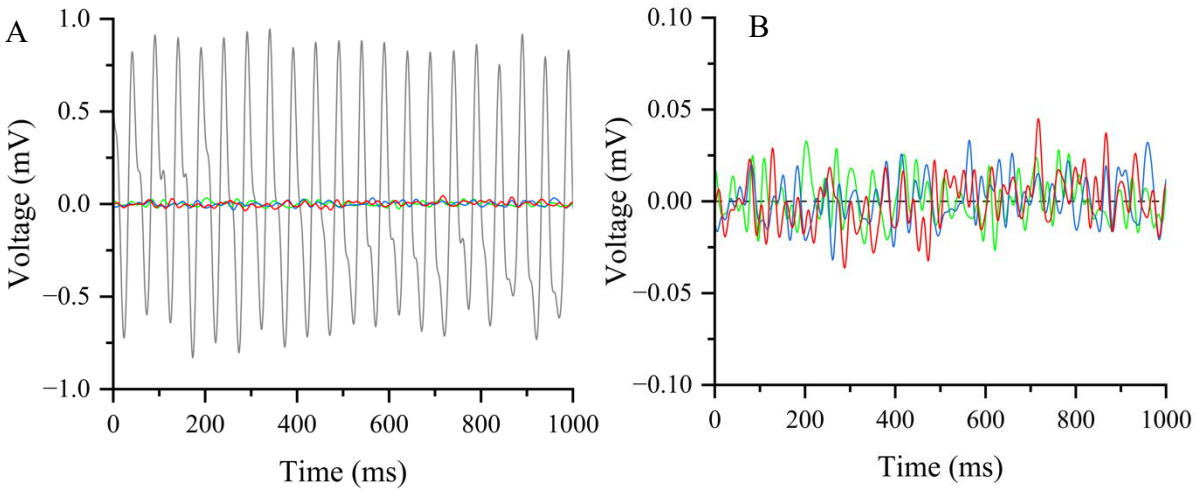

Figure 3.12. Typical recording from the H^+-selective electrode #15 showing voltage oscillations (mV) at four different electromagnetic shielding settings over a 1-second period. A (left) displays all settings assessed, while B (right) excludes the unshielded category. Red, shielded; Blue, endoscope with lights off; Green, endoscope with lights on; Gray, unshielded. The dashed line (B) was set at 0 mV for parameter.

Table 3.3. Noise amplitude (mV) recorded by 17 H^+-selective electrodes at four different electromagnetic shielding categories.

	Shielding category			
	Shielded	End. lights off	End. lights on	Unshielded
Mean (SD)	0.11 (0.03)	0.09 (0.02)	0.11 (0.03)	2.15 (0.7)
Minimum	0.06	0.06	0.07	0.56
Maximum	0.19	0.13	0.18	3.7
Coefficient (SE)	-	-0.01 (0.01)	0.00 (0.01)	2.05 (0.2)
p-value	-	.220	.966	<.001

Abbreviations: End, endoscope; SD, standard deviation; SE, standard error.

The noise amplitude observed in each one of the 17 H^+-selective electrodes recorded under the different setups is available in Table S2 in Appendix A. Table 3.3 shows a summary of the noise measured in all four shielding categories assessed, including the coefficient and p-value for comparison against shielded electrodes.

Compared to just surrounding the electrodes with the braid reinforced tubing, passing the electrodes and shielding assembly through the endoscope did not induce statistically larger noise fluctuations (p=.220 and .966, respectively). On the other hand, the mean noise intensity observed in recordings from unshielded electrodes was significantly larger than when shielded (p<.001). From a relatively small noise amplitude of 0.11 ± 0.03 mV observed in shielded electrodes, the absence of electromagnetic shielding resulted in an average 2.05 ± 0.2 mV larger noise. This difference corresponds to an almost 20-fold increase in noise intensity. Given this large variance from unshielded to the other setups, Figure 3.13 shows data from all categories together (A, left) as well as only the shielded setups (B, right) for a closer comparison. It is observed a large variance in the noise of unshielded electrodes, ranging from 0.56 to 3.7 mV (Table 3.3). Although shielded, endoscope with lights off and on showed relatively large standard deviations, the largest noises seen in these categories were significantly smaller than the best readings in unshielded electrodes.

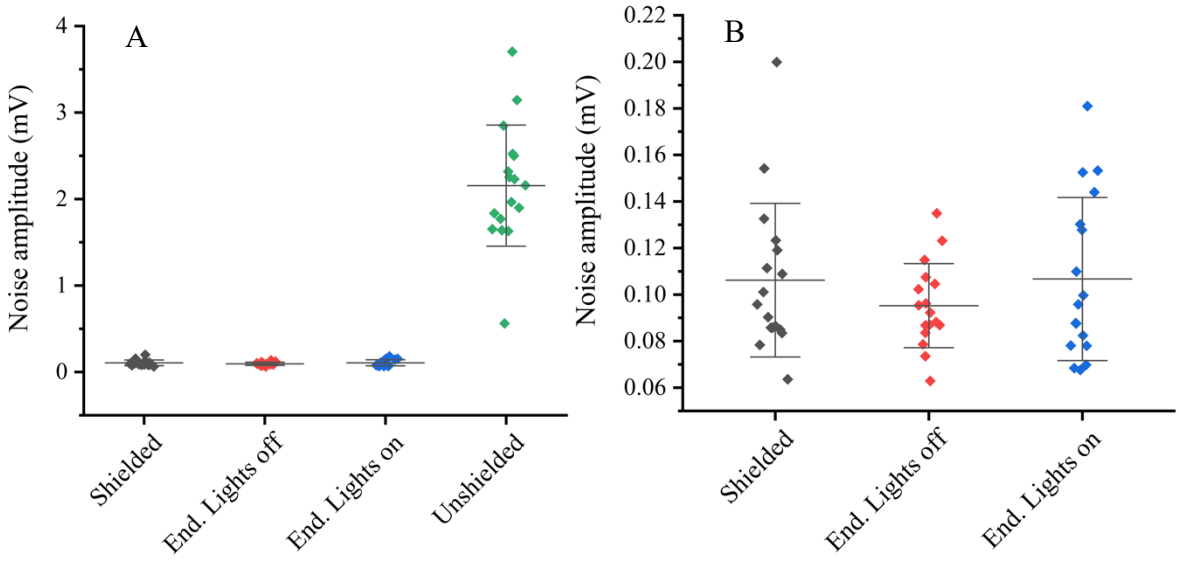

Figure 3.13. Scatter interval plot of the noise amplitude (mV) recorded by 17 H^+-selective electrodes at four different electromagnetic shielding categories, including mean and standard deviation. A (left) displays all settings assessed, while B (right) excludes the unshielded category.

Additionally, Table 3.4 summarizes the noise intensity observed in readings from 10 electrodes for four consecutive days while shielded by the grounded braid reinforced tubing. It includes comparisons between the first and subsequent days after the electrodes manufacture and calculation of the overall time effect. Table S3 in Appendix A provides the individual noise observed in the readings from all electrodes per day.

Table 3.4. Noise amplitude (mV) recorded by 10 shielded H+-selective electrodes in a calibration solution of pH 7 on 4 consecutive days.

	Overall	Day			
		1	2	3	4
Mean (SD)	0.15 (0.07)	0.13 (0.06)	0.13 (0.04)	0.15 (0.07)	0.19 (0.1)
Minimum	0.06	0.07	0.07	0.09	0.06
Maximum	0.38	0.27	0.19	0.29	0.38
Coefficient (SE)	0.02 (0.01)	-	0 (0.01)	0.02 (0.02)	0.07 (0.02)
p-value	<.001	-	.857	.401	.001

Abbreviations: SD, standard deviation; SE, standard error.

No statistically significant differences were observed in the noise amplitude on days 2 and 3 compared to those seen on day 1 (p=.857 and .401, respectively). On the other hand, the mean noise amplitude recorded on day 4 was 0.07 ± 0.02 mV larger than on day 1, corresponding to a significant increase (p=.001). An overall effect of time was observed (p<.001), showing that for each day after the electrodes manufacture, the noise amplitude was increased by 0.02 ± 0.01 mV. This trend was also visually demonstrated in Figure 3.14. Further, this figure shows that the noise amplitude dispersion between electrodes turned wider as the days passed, although 6 of the devices had noise intensities like those seen on day 1.

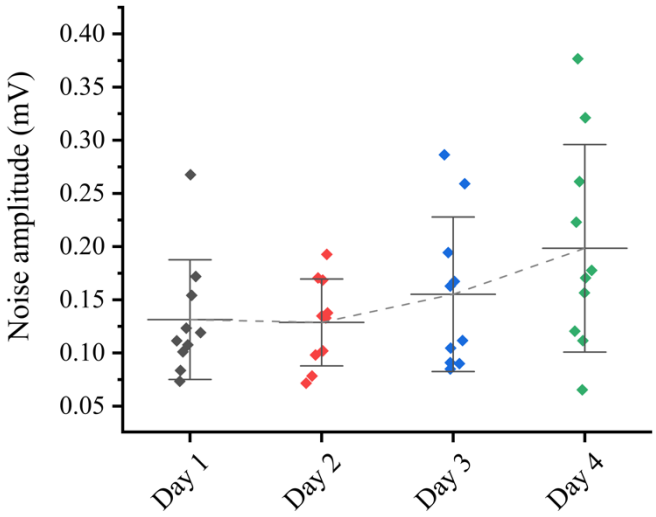

Figure 3.14. Scatter interval plot of the noise amplitude (mV) recorded by 10 shielded H^+-selective electrodes in calibration solution of pH 7 at 4 consecutive days, including mean and standard deviation.

Table 3.5 shows the overview of the calibration solutions temperature effect on the mean noise amplitude as observed in recordings from 12 electrodes. Comparisons between 22, 27 and 32 °C are provided, as well as the overall effect of temperature on the readings. The complete dataset used for these calculations is available in Table S4 in Appendix A.

Table 3.5. Noise amplitude (mV) recorded by 12 shielded H^+-selective electrodes in calibration solutions of pH 7 at three different temperatures.

	Overall	Temperature (°C)		
		22	27	32
Mean (SD)	0.14 (0.06)	0.11 (0.04)	0.14 (0.06)	0.16 (0.06)
Minimum	0.06	0.06	0.08	0.08
Maximum	0.33	0.19	0.27	0.33
Coefficient (SE)	0.005 (0.002)	-	0.03 (0.01)	0.05 (0.02)
p-value	.017	-	.016	.017

Abbreviations: SD, standard deviation; SE, standard error.

The mean noise amplitude from readings performed at 27 and 32 °C were statistically larger than the mean noise recorded at 22 °C (p=.016 and .017, respectively). Furthermore, an overall effect of temperature was observed (p=.017), representing an increase of 0.005 ± 0.002 mV in the noise intensity for each degree Celsius increment, or an increase of 0.05 ± 0.02 mV for each 10 degrees Celsius increment. Additionally, Figure 3.15 shows that, besides an average increase in noise amplitude, the readings performed in warmer solutions also provided a more spread dataset, ranging from 0.08 to 0.33 mV in the solutions at 32 °C.

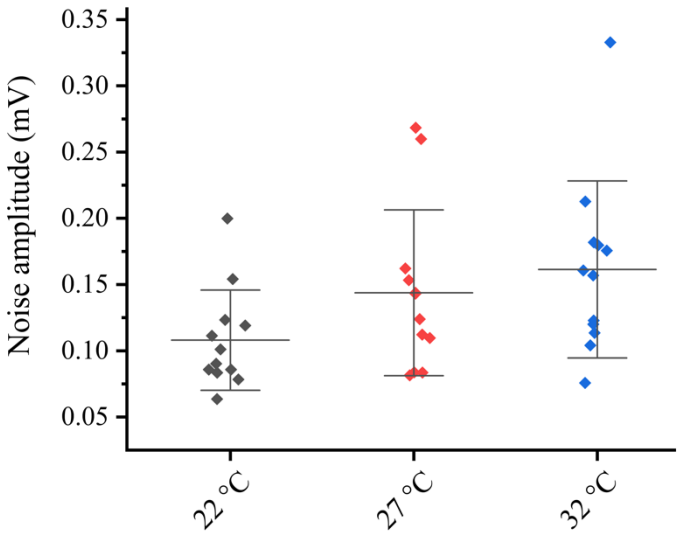

Figure 3.15. Scatter interval plot of the noise amplitude (mV) recorded by 12 shielded H^+-selective electrodes in calibration solutions of pH 7 at three different temperatures, including mean and standard deviation.

Effect of temperature on Nernstian slope

Table 3.6 describes the effect of calibration solutions' temperature on the mean Nernstian slope observed in 12 electrodes. Comparisons between 22, 27 and 32 °C are described, and the overall effect of temperature on the slope was calculated. The complete dataset of this assay is available in Table S5 in Appendix A.

Table 3.6. Nernstian slope (mV/[H^+] decade) from 12 H^+-selective electrodes at three different temperatures.

	Overall	Temperature (°C)		
		22	27	32
Mean (SD)	52.9 (1.6)	52.2 (2.0)	53.3 (1.2)	53.2 (1.3)
Minimum	49.5	49.5	51.9	50.5
Maximum	56.1	56.1	55.6	54.8
Coefficient (SE)	0.1 (0.05)	-	1.11 (0.4)	1.04 (0.5)
p-value	.047	-	.002	.047

Abbreviations: SD, standard deviation; SE, standard error.

By calibrating the electrodes in 5 and 10 °C warmer solutions, it was observed a significantly steeper Nernstian slope (p=.002 and .047, respectively) compared to solutions at room temperature (22 °C). Although the relative differences from 22 °C to 27 °C and from 22 °C to 32 °C were similar and not twice as large as one another, as expected, an overall effect of temperature was identified (p=.047). In this case, for each Celsius degree increment in the calibration solutions, the Nernstian slope was increased by 0.1 ± 0.05 mV/[H^+] decade, or for each 10 Celsius degree increment in the calibration solutions, the Nernstian slope was increased by 1 ± 0.05 mV/[H^+] decade. This trend can also be observed graphically in Figure 3.16, where steeper slopes are seen as the calibration solutions are warmer.

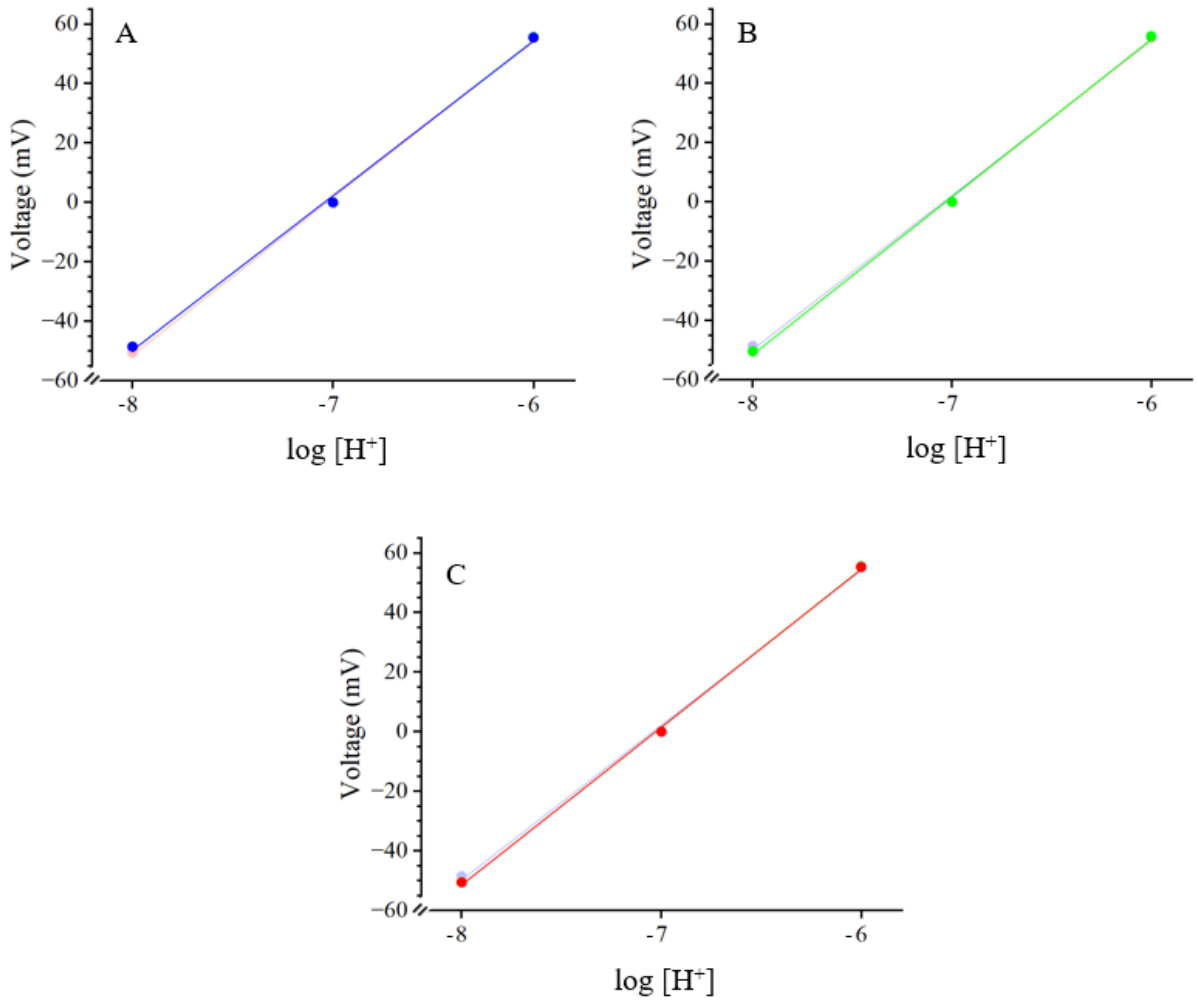

Figure 3.16. Graphical representation of the mean calibration curve from 12 H^+-selective electrodes at three different temperatures. Blue, 22 °C (highlighted in A, top left); Green, 27 °C (highlighted in B, top right); Red, 32 °C (highlighted in C, bottom).

3.4. Discussion

Using PE tubing is an effective alternative for manufacturing long and flexible ISEs. The building process presented in this chapter followed steps like those described for manufacturing plastic electrodes made of PE syringes (O'Donnell, 1992). Switching the raw material to pre-molded tubing greatly simplified the electrode preparation process, as evidenced by the relatively short time required to construct these devices. Within an hour, it was possible to produce up to 10 ISEs and one RE. Minimal practice was required to achieve these results, thanks to the ease of handling the PE tubing and the simpler building process compared to previously described techniques.

First, using PE tubing eliminates the need for pulling a syringe barrel through heat. This is the most time-consuming step and greatly relies on the researcher's manual skills when using a syringe as the raw material. Furthermore, it limits the final electrode length and inputs important variability to the tip diameter. Kim and coworkers (2021) reported that plastic electrodes manufactured using PE syringes had tips with diameters ranging from 150 to 550 micrometres, representing a difference of almost 4 times from the thinnest to the thickest electrode produced. The use of PE tubing allows the manufacture of considerably longer devices and results in more uniform electrodes with a constant diameter throughout its length and equal tip diameter among duplicates. This technique does not require the manipulation of melted plastic during the pulling step, making it a safer and user-friendly alternative to flexible electrode manufacture.

Although possible, the tubing was not bevelled in this research. Having a blunt tip is safer for the measurement of ASL pH in vivo, since using a sharp end could risk damaging the delicate airways mucous tissue. Silanization is a necessary step in manufacturing glass electrodes because glass micropipettes are hydrophilic and need to be made hydrophobic before being filled. In contrast, PE plastic is inherently hydrophobic. As a result, silanization is not required for manufacturing plastic electrodes using PE syringes or the PE tubing used in this investigation.

The ISE sealing technique described by O'Donnell (1992) involved filling the tips of the electrodes with a mixture consisting of one part ionophore cocktail and two parts of a 15% (w/v) PVC solution in tetrahydrofuran. Alternatively, simply dipping the electrodes' tips in the PVC/tetrahydrofuran mixture without the ionophore cocktail has been shown effective in preventing liquid leakage while maintaining a proper sensitivity to hydrogen ions. However, it was necessary to incubate the mixture overnight at room temperature or for a couple of hours in a 37 °C hot bath to ensure that the PVC was completely dissolved. This step was crucial for achieving the ideal viscosity needed for sealing the plastic tubing. If the electrodes were dipped into a heterogeneous PVC-tetrahydrofuran mixture, the sealing layer would cure too quickly, leading to a brittle coating that could easily crack and allow the solution to leak.

A slightly different method was used to seal the REs in this experiment compared to O'Donnell's approach. O'Donnell's electrodes, made from PE syringes, were fully filled with a 3% (w/v) agar mixture in 3M KCl, the referencing solution (RS). However, filling a longer PE tube with this mixture proved impractical. Saturating a 1.7-meter-long tube with the

referencing solution took about 15 seconds. Although this might not seem long, it was sufficient for the agar to harden inside the tube before reaching the end, which blocked further solution flow. To address this issue, the tubing was first filled with RS alone, and then a 1 cm column of the RS-agar mixture was drawn into it. This approach allowed the electrode to effectively interface with the calibration solutions and Ag/AgCl wires from the microelectrode holders, while the agar at the tip of the electrodes prevented fluid leakage.

O'Donnell (1992) reported that sealing ISEs with a mixture of ionophore cocktail, PVC, and tetrahydrofuran extended their lifetime to over four weeks. However, no details were provided about the storage conditions. Initial tests showed that storing the electrodes in open air caused the PVC sealing to lose its rubber-like properties, resulting in a thin, brittle layer that failed to prevent fluid leakage in the ISEs. Similarly, the agar-RS mixture dried out, leading to the formation of air bubbles at the lower end of the REs. To address this, the present experiment tested storing the electrodes submerged in solutions. It was found that immersing the tips of plastic H^+-selective electrodes in pH 7 PBS solution and REs in 3M KCl effectively preserved the seals for several days, allowing the use of the same set of electrodes for different assays. Rolling the long electrodes around the Falcon™ tubes also helped to keep them organized and untangled.

The most common method for reducing electromagnetic interference (EMI) and achieving cleaner readings is to conduct ion concentration assays inside a Faraday cage (Glasscott et al., 2022). However, this approach is not feasible for in vivo measurements in humans or larger animal models such as pigs. Therefore, this project aimed to develop an alternative electromagnetic shielding method that allows the use of electrodes outside of a Faraday cage for in vivo experiments. The choice of a grounded stainless-steel reinforced braid tubing for shielding the ISE cells from EMI proved effective. Although preparing the tubing for grounding was more challenging and time-consuming than constructing the electrodes, a single braid tubing can be used for multiple assays if properly maintained safe from twists and folds. The tubing inner diameter comfortably accommodated an ISE and a RE, while its outer diameter was just right for fitting through the endoscope working channel. Additionally, the tubing's flexibility facilitated handling the ISE cell-braid tubing assembly, allowing for curving and easy positioning of the device. Besides enhancing the maneuverability of the electrodes, grounding the braid tubing effectively reduced noise in the readings. It permitted its use outside of a Faraday cage, as demonstrated by the ISE characterization assay results and discussed further in this topic.

The novel plastic ISE design showed adequate and similar performances compared to previously described devices. One day after their manufacture, the mean Nernstian slope of the 10 ISEs tested was 53.7 ± 3.7 mV/[H^+] decade, slightly lower than those reported by O'Donnel (1992). The slopes measured by electrodes made of PE syringes were between 56 and 58 mV/[H^+] decade, but the experimental parameters used (i.e., pH and nature of the calibration solutions, profile of confounding ions, and temperature) were not described. Additionally, the electrodes used were 50 cm long, significantly shorter than the 1.7 m-long devices built for this assay. On the other hand, 32 1 m-long plastic electrodes used by Kim and collaborators (2021) showed mean slopes of 51.1 ± 3.0 mV/[H^+] decade. Regardless of this shallower slope, the authors succeeded in measuring large pH oscillations in the noses of healthy and CF subjects, suggesting that the device had the sensitivity required to perform this investigation. Unfortunately, the temperature under which the calibration was carried out was also not reported. Therefore, the mean Nernstian slope observed in the present experiment was within the range of published similar devices and within the range of adequate function (Luxardi et al., 2015).

A trend of decreasing slope over time was observed, indicating that, overall, the electrodes became less sensitive to [H^+] changes as time passed. However, this loss of sensitivity was only statistically significant on day 4 compared to day 1. Given that all electrodes must be calibrated immediately after each measurement to ensure an accurate calibration curve, the relatively small change in their Nernstian slope (-0.71 ± 3.7 mV per [H^+] decade per day) will be factored into the pH calculation for the sample, minimizing potential inaccuracies. The mean slope was found to be significantly lower only on day 4 compared to day 1, suggesting that the electrodes maintained their functionality for up to 3 days after manufacture. It is important to note, however, that a large variability was seen in all days. For example, one of the electrodes showed a slope of 54.9 mV/[H^+] decade on day 4, which is larger than the average slope observed one day after their build. This interesting finding suggests that these electrodes undergo individual changes in functionality over time. While some electrodes experienced an abrupt decrease in slope within the first few days, others maintained good performance throughout the 4-day testing period. Therefore, it is suggested that in future research an individualized assessment of the electrodes' viability and performance be carried out immediately prior to the investigation.

This trend was not observed when comparing the linear regressions adjusted R^2 resulting from the calibration data points over 4 days after the electrodes manufacture. No

overall time effect was observed, and the medians from days 2 to 4 were not significantly different from day 1. The adjusted R^2 value of the linear regression should be higher than 0.9 to consider an electrode efficient (Luxardi et al., 2015). In this experiment, adjusted R^2 medians were above 0.99 on each day, and only one electrode had a value below 0.9 (0.9829, electrode 4 on day 1). These results confirm the proper performance of the electrodes, showing overall adjusted R^2 above the cutting point and stable over time. Furthermore, the values observed in this assay were superior to those reported in similar plastic ISE made from PE disposable syringes, with a mean ± SE of 0.9851 ± 0.0027 (Kim et al., 2021).

The maintenance of an acceptable performance over time is beneficial because it would allow the same electrode to be used in a series of subjects, allowing for intra-electrode variability analysis that could demonstrate if the same device behaves differently according to the patient.

Although other methods for measuring response time are available, assays performed in this work followed the most used and reported definition of response time (time for achieving 1 mV from the stable reading in the new solution, t^*). Unfortunately, works from O'Donnel (1992) and Kim and coworkers (2021) did not elucidate the method used, but they likely employed either the t_{90} or t^* definitions given that they reported response times in seconds.

Results showed that the electrode response time was more significantly affected by the passage of time than their Nernstian slope. In fact, for each day after manufacture, the response time was increased by 0.68 ± 0.2 s. From day 2 to 4, this parameter was found to be significantly different from the first day after the electrodes were built. However, similarly to the assessment of slope over time, larger differences were found between day 4 and day 1. From day 1 to day 3 the response time increased by ≈ 64%, while on day 4 it escalated to ≈ 236%. The average response time observed in this experiment was similar to those reported by O'Donnel (1992), ranging from 2 to 4 s. Kim and coworkers (2021), however, reported substantially faster electrodes, with response times under 1 s. Unfortunately, neither publications described in detail the assay used to measure the response time, nor did they provide a clear definition of this parameter, hampering further comparisons with the results presented in this dissertation. Kim et al. (2021) reported using solutions with pH values of 6.96, 7.62, 8.01, 8.60, and 9.10 for electrode calibration. It's important to note that the pH differences between these solutions (0.66, 0.39, 0.59, and 0.5 pH units, respectively) are

considerably smaller than the 1 pH unit intervals used in the present study. This difference in calibration protocols is likely responsible for the varying response times, as electrodes would stabilize more quickly when moved between solutions with smaller pH differences compared to a 1 pH unit gap.

The plastic electrodes made with PE syringes used by Kim and colleagues (2021) showed good responsiveness and, regardless of a relatively small Nernstian slope compared to the original devices described by O'Donnel (1992), were able to measure large pH oscillations in the noses of pH of non-CF patients, ranging from 0.7 and 1.4 pH units between inspiration and expiration. It suggests that using electrodes with faster responses is more relevant to measuring pH during quick dynamic processes such as the breathing cycle than electrodes with a larger Nernstian slope.

Previous work using long plastic electrodes made with PE syringes did not mention if strategies against EMI were implemented during the recordings (Kim et al., 2021; O'Donnell, 1992). The present investigation proved that surrounding the electrodes with a grounded stainless steel braid reinforced tubing significantly reduced the noise amplitude seen in stable recordings in pH 7 solutions. A significant noise amplitude reduction was achieved, from 2.15 ± 0.7 mV to 0.11 ± 0.03 mV, representing a ≈ 95% reduction. The possibility of collecting accurate and stable ion concentration data outside of a Faraday cage represents an important advancement in the area, especially for assays involving large in vivo models or human subjects.

Furthermore, shielding the electrodes enabled its use with an endoscope by passing it through the endoscope working channel. The mean noise amplitude observed while through the endoscope, regardless of whether the optical light was on or off was not significantly different from the recordings independent from the endoscope. It was confirmed that the proposed electrode cell and shielding assembly are compatible with endoscope equipment. This compatibility is crucial for future assays involving live patients, as it allows researchers to visualize sites of interest while performing ASL pH measurements. The electrode-endoscope assembly enables real-time visualization and pH measurement at various airway sites, facilitating data collection across different regions and allowing for comparisons between diseased and healthy lung areas within the same subject.

As observed regarding the Nernstian slope and response time, the time after the electrodes manufacture significantly influenced the noise amplitude observed in shielded

electrode cells. Given the time overall effect, the noise amplitude increased by 0.02 ± 0.01 mV/day. Statistically significant differences were only observed on day 4 compared to day 1, representing a ≈ 46% increase. Nevertheless, the mean noise amplitude of 0.19 ± 0.1 mV measured on day 4 is relatively low, given the expected voltage oscillations during breathing, reported to be as large as 1.4 pH units in healthy subjects (Kim et al., 2021). As previously discussed in terms of performance, the noise amplitude observed over time is highly dependent on the individual devices. Of note, the smaller noise amplitude observed throughout the assay (0.06 mV) was measured on day 4. The noise amplitude has also been found to be influenced by the temperature under which the assays were conducted. For each 10 °C increment, an increase of 0.05 ± 0.02 in the noise amplitude was observed. Although statistical significance was achieved, this factor would hardly be of concern for practical reasons given the relatively small temperature effect in terms of reading stability.

Although previous work done with plastic ISE did not assess the temperature effects on the device performance, it is known that the electrode calibration curve is directly influenced by the media temperature (Lee et al., 2013), as described by the Nernstian equation (2.1). For this reason, it is theoretically expected that Nernstian slopes resulting from calibrations performed in heated solutions will be steeper than those carried out at room temperature. Assays performed in the present work have confirmed this proposition. An overall effect of temperature has been observed, representing an increase of 1 ± 0.5 mV/[H^+] decade for each 10 °C increment. Further, the mean Nernstian slopes observed at 27 and 32 °C were statistically steeper compared to the mean slopes seen at room temperature (22 °C). This result confirms the recommendation of calibrating the electrodes at the same temperature as the sample or tissue of interest (Voipio et al., 1994). Previous work done with plastic ISE did not assess the temperature effects on the device performance.

3.5. Conclusion

Both the general and specific objectives outlined in this chapter have been successfully met. Using polyethylene tubing to manufacture H^+-selective and referencing electrodes is a feasible alternative to building plastic, long electrodes. This novel design showed similar performance compared to previously described plastic electrodes in terms of the Nernstian slope, adjusted R^2 values, and response time. The grounded stainless steel tubular mesh developed has proven effective in shielding the electrodes from electromagnetic interference. Additionally, it has been proven that the electrode cell-shielding assembly is compatible with an endoscope.

3.6. Transition

The plastic ISEs and electromagnetic shielding developed in Chapter 3 performed as expected, demonstrating that this novel design can accurately measure ASL pH, even when used through the working channel of an endoscope. These results support further testing in live piglets, as described in Chapter 4, to measure airway surface liquid pH. This second investigation is crucial for confirming the usability of the plastic ISEs, as it will evaluate their performance on biological tissues, whereas the tests in Chapter 3 only used pH calibration solutions.

CHAPTER 4 - EFFECTIVENESS OF THE PLASTIC H^+-SELECTIVE ELECTRODE FOR IN VIVO pH MEASUREMENTS OF AIRWAY SURFACE LIQUID

4.1. Introduction

The airway surface liquid (ASL) is a ~10 µm thick bilayer fluid that revests the airway epithelium (Zajac et al., 2021). The ASL serves as a pH buffer fluid due to its high bicarbonate content, which is transported from epithelial cells to the airway lumen via cystic fibrosis transmembrane conductance regulator (CFTR) channels (Smith & Welsh, 1992; Thomas & Adams, 1965). CF is commonly accompanied by a lowered ASL pH due to absent or insufficient CFTR function (Coakley et al., 2003). Results from in vivo studies comparing ASL pH in the lower airways between CF and non-CF animal subjects are inconsistent. No significant differences between tracheal ASL pH in CF and wild-type mice were found by Jayaraman and colleagues (2001), whereas Pezzulo and coworkers (2012) observed a significantly more acidic tracheal ASL in CFTR -/- swine compared to non-CF subjects. Research conducted on human volunteers on the same topic also has conflicting results depending on the portion of the airway assessed and on the age of the subjects. McShane and coworkers (2003) found significantly more acidic distal nasal ASL in CF adults compared to the control group, but the authors found no significant differences when comparing ASL pH in the lower respiratory tract of CF and non-CF children. However, this experiment only included 5 CF and 6 non-CF children, which may have impacted its capacity to detect significant differences between the groups. Abou Alaiwa and colleagues (2014) observed significantly lower nasal ASL pH in CF neonates compared to non-CF subjects. Kim and collaborators (2021) observed a significantly lower mean nasal ASL pH in CF patients compared to non-CF subjects. However, Schultz and coworkers (2017) found no significant differences in ASL pH between CF and non-CF children in the lower airways. With 37 CF and 30 non-CF children included, this research provides the strongest evidence to date that CF infants do not experience ASL pH imbalances early in life.

The ASL is largely dependent on bicarbonate to maintain its pH within the physiological range (Berkebile & McCray, 2014). However, CO_2 levels in the respiratory gas

also play a crucial role in pH fluctuations during different phases of breathing. Carbon dioxide concentrations in the airways vary significantly, from 0.035% during inhalation to as high as 6% during exhalation (Kim et al., 2021). ASL, as an open pH buffer system with a large surface area-to-volume ratio, allows CO_2 to diffuse quickly through its thin aqueous layer (Thomas & Adams, 1965). This CO_2 variation can cause the nasal ASL pH to largely oscillate in healthy individuals, ranging from pH 9 during inhalation to pH 7.5 during exhalation, reflecting a more than 10-fold change in H^+ concentration in just one breathing cycle (Kim et al., 2021). In contrast, individuals with CF show significantly smaller pH fluctuations, ranging from 7 to 7.7, between inhalation and exhalation (Kim et al., 2021). Interestingly, when a bicarbonate solution was applied locally, CF patients experienced an increase of more than 1 pH unit during exhalation and over 0.5 pH unit during inhalation, resulting in an overall pH fluctuation of approximately 1 unit, similar to non-CF subjects (Kim et al., 2021).

The ASL has an important physiological role in the host-defence against inhaled pathogens, containing bactericide peptides such as lactoferrin, lysozyme, LL-37, β-defensins, secretory leukocyte peptidase inhibitor (SLPI), SP-A and SP-D (Meyerholz et al., 2010). Innate immune system cells such as macrophages and neutrophils are also found in the ASL, being involved in the removal of microbial debris (Berkebile & McCray, 2014). Furthermore, proper mucociliary clearance is directly dependent on the ASL physiological properties, since cilia from ciliated cells beat in the interface between the periciliary liquid (PCL) and the mucus layer (MCL) of the ASL (Zajac et al., 2021). Research have appointed that the acidification of the ASL has the potential to reduce the peptides' antimicrobial potential against pathogens commonly involved in CF, such as *S. aureus* and *P. aeruginosa* (Abou Alaiwa et al., 2014; Pezzulo et al., 2012; Stoltz et al., 2015). This acid-basic alteration in the ASL has been shown to predispose swine CF models and CF patients to persistent bacterial infection (Kim et al., 2021; Pezzulo et al., 2012). Not only the overall acidification of the ASL but also the decrease in the ASL pH oscillation during breathing in CF subjects may diminish their bacterial killing capacities (Kim et al., 2021).

In CF, the PCL portion of the ASL loses humidity secondarily to an increased NaCl and water epithelial absorption through osmosis (Bergeron & Cantin, 2019). Consequently, the PCL/MCL ratio is reduced, resulting in an ASL with higher viscosity (Hoegger et al., 2014). This alteration makes the mucociliary clearance of the airways less effective, which predisposes CF patients to airway obstruction and microbial infections (Berkebile & McCray,

2014). The acidification of the ASL further contributes to the thickening of the fluid, possibly by altering pH-sensitive noncovalent interactions in the mucus (Tang et al., 2016).

In sum, the ASL increased viscosity and altered pH concomitantly contribute to impairing the host defence against inhaled microorganisms, predisposing CF patients to chronic bacterial infections (Bergeron & Cantin, 2019; Gustafsson et al., 2012; Pezzulo et al., 2012; Shah et al., 2016). The onset of airway inflammation and tissue remodelling is primarily triggered by microbial contamination, which is the leading cause of morbidity and mortality in cystic fibrosis-related lung disease (Conese & Di Gioia, 2021). Therefore, understanding how these two key imbalances in the ASL contribute to the heightened susceptibility to infections in CF patients is essential.

The two experimental chapters available in this dissertation (Chapters 3 and 4) are part of a larger multidisciplinary project. Among other objectives, this project aims to assess pH levels and potential fluctuations in the lower airways of CF pigs and, eventually, CF human volunteers. These assays have the potential to deepen our knowledge of the role of ASL pH imbalances in CF patients and aid in the development of new therapies for the disease. To acquire data required to fulfil this objective, it is necessary to develop a precise, financially accessible and easy-handle method to measure ASL pH.

Various techniques have been employed to measure ASL pH in vivo, with pH-sensitive dyes the most commonly used. While these methods are accessible and relatively easy to use, they have significant limitations, such as the inability to measure pH in real time; they are effective for capturing pH at a specific moment but cannot provide continuous recordings. In contrast, plastic ion-selective electrodes (ISEs) offer several advantages for measuring ASL pH in the lower airways. ISEs can record ion concentrations in real-time, enabling researchers to accurately monitor pH fluctuations during dynamic processes such as the breathing cycle. Additionally, plastic ISEs can be made long enough for use during bronchoscopy, allowing visual assessment of the target tissue before and during recording.

The novel plastic ISE design made of polyethylene (PE) tubing described in Chapter 3 showed adequate performance in tests developed using calibration solutions. Its Nernstian slope, adjusted R^2, and response time, three main factors related to ISE usability and precision, were similar to those reported in earlier electrode designs made of PE disposable syringes (Kim et al., 2021; O'Donnell, 1992). Although this prototype has performed well in assays using pH calibration solutions, measuring pH in the airways of live subjects presents

several challenges. The pH meter must maintain stable readings, which can be complicated by the breathing movements. Additionally, the ASL is a thin layer covering the airway epithelium, which results in a reduced contact area between the ISEs and the fluid, compared to submerging the electrodes in calibration solutions. The equipment also needs to be shielded from external disturbances, such as electromagnetic interference (EMI). Tests conducted in Chapter 3 showed that surrounding the ISE cell with grounded stainless steel braided tubing significantly reduced noise in the recordings. However, applying this setup to a living organism might introduce other sources of EMI, such as electrical currents from the heartbeat.

This chapter tests the effectiveness of the plastic H^+-selective electrodes characterized in Chapter 3 in dynamically measuring ASL pH in a live healthy piglet. This in vivo proof-of-concept assay represents the first use of a device of this kind in the lower airways. Characterizing its performance and assessing the investigation setup is essential before performing further experiments in CF swine and human patients, providing relevant information on the device and experimental setup that can contribute to a better assay comparing CF and non-CF patients in the future.

To achieve this goal, this chapter outlines two general objectives, and several specific objectives are defined, which are addressed through measurements performed by a set of plastic H^+-selective electrodes in an anesthetized tracheostomized 1-week-old piglet.

General objective 1: To assess the effectiveness of plastic H^+-selective electrodes in dynamically measuring ASL pH in a live healthy piglet.

1.1. To characterize the electrodes used in terms of their Nernstian slope, adjusted R^2, response time, and noise.

1.2. To calculate the minimum, maximum, and ΔpH in the piglet ASL throughout 5 consecutive breathing cycles according to the voltage measured by the electrodes.

1.3. To assess relationships between pH measurements and parameters such as $[CO_2]$, respiratory rate, Nernstian slope, adjusted R^2, and response time.

1.4. To assess potential interferences of the cardiac cycles on pH measurements.

General objective 2: To assess the experimental setup used in terms of practicality and synergism between equipment.

2.1. To evaluate the technique's feasibility in terms of the resultant electromagnetic noise, breathing movement, and ease of performing the intended measurements.

2.2. To discuss the synergism between the equipment simultaneously used to gather data.

4.2. Material and methods

The study was approved by the University of Saskatchewan's Animal Care Committee Animal Research Ethics Board (Animal Use Protocol #20110047 with Dr. Juan Ianowski as the principal investigator).

4.2.1. H^+-selective electrodes and electromagnetic shielding

A set of 10 ISEs and one RE were manufactured and stored overnight according to the specifications described in item 3.2.2. To reduce the effects of electromagnetic interference (EMI) in the signals, one ISE and one RE (constituting an ISE cell) at a time were fed through a grounded stainless steel braid reinforced tubing (prepared as described in item 3.2.3). The electrodes were connected to a pair of microelectrode holders and probe head stages which were secured by a tripod, as shown in 3.2.4. To further shield the apparatus against EMI, a custom-built Faraday cage was used to surround the microelectrode holders, probe head stages, and the braid reinforced tubing head. This device was constructed by surrounding a 16''x16''x16'' cardboard box with a stainless-steel woven wire mesh (1mm hole diameter), which was grounded to the building's system using an insulated 2.5 mm thick stranded copper wire and a male cord connector (Figure 4.1). The probe head stages cables and the tubing grounding wire passed through a small circle opening (3 cm wide) made on the mesh on the side of the Faraday cage.

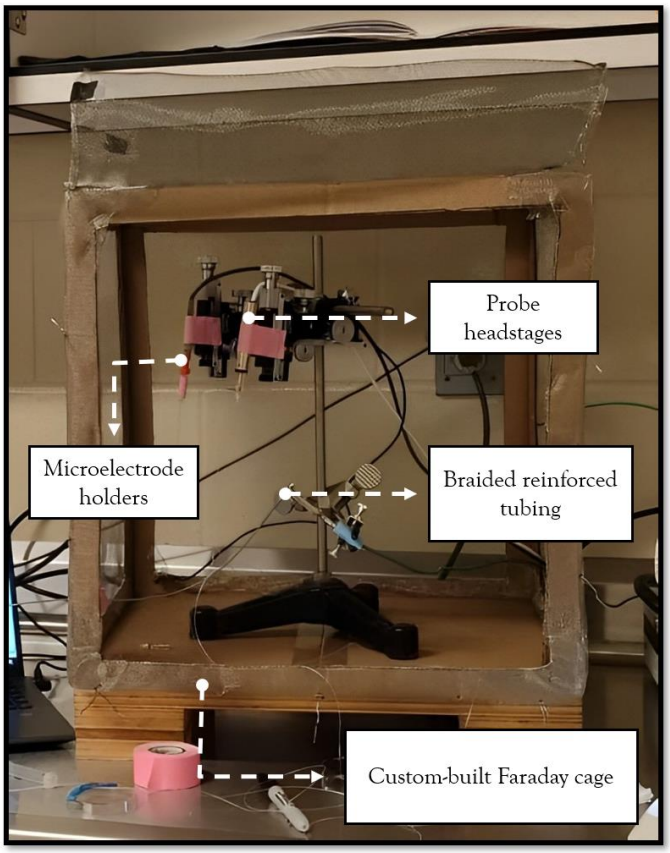

Figure 4.1. Custom-built Faraday cage used to shield the microelectrode holders and probe head stages against electromagnetic interference.

4.2.2. Animal model

A female, 1-week-old, 3.8 kg bodyweight healthy piglet from the University of Saskatchewan's Prairie Swine Centre (2105 – 8th Street East, Saskatoon, SK, S7H 5N9) was used. This investigation was performed in the University of Saskatchewan's Lab Animal Services Unit (LASU), located in the Health Sciences building (107 Wiggins Rd, Saskatoon, SK, S7N 5E5). Anesthesia was induced and maintained using isoflurane inhalation (Fresenius Kabi Canada Ltd., Cat. No. CP0406V2, Toronto, ON, Canada). The subject's muzzle was secured into a mask connected to an anesthetic bracket unit operating on a non-rebreathing circuit (VetTech Solutions Ltd., Cat. No. AN009CO, North-West England, UK). To induce anesthesia, isoflurane was administered at a 5% concentration, which was then reduced to 2% for maintenance. The anesthetic bracket unit was supplied with 100% oxygen from a gas tank, set to a flow rate of 1.5–2.0 L/min. Anesthesia depth was assessed by ocular position and digital pinch reflex. The piglet was placed in a supinated position on top of an electric heating

pad on a 'V' top operating table to help maintain its body temperature. Rectal temperature and blood oxygenation were constantly monitored using a digital thermometer (Braun, Cat. No. PRT2000CA, Taunus, Germany) and a Pulse CO-Oximeter (Woodley Equipment Company Ltd., Cat. No. 504, Bolton, UK). At the end of the assay when all measurements were completed, the piglet was, still under anesthesia, euthanized by a 2 mL Euthanyl (Bimeda-MTC Animal Health Inc., DIN 00141704, Cambridge, ON, Canada) intracardial bolus. The carcass was discarded as per the University of Saskatchewan's biological material disposal procedure.

4.2.3. Data collection

Besides measuring tracheal ASL pH, other physiological parameters were simultaneously assessed. Once the subject was stable after the anesthetic induction, a 3-lead ECG was placed to collect cardiac cycle data throughout the experiment using a differential biological potential amplifier (ADInstruments, Dual Bio Amp, Cat. No. FE232, Sydney, Australia). It was used to evaluate if the cardiac cycle introduces noise, seen as spikes or dips on the ISE recording. The positive electrode (red) was placed on the piglet's right forelimb, the negative electrode (white) on its left forelimb, and the grounding electrode (black) on the left side of its abdomen. Additionally, a pulse transducer (ADInstruments, Cat. No. MLT1010, Sydney, Australia) was placed on the piglet's abdomen at the diaphragm height to track breathing movements (Figure 4.2). This data was used to calculate the subject's breathing rate.

Once the peripheric instruments were placed and working properly, surgical procedures to access the subject's tracheal lumen started. Lidocaine spray (Odan Laboratories Ltd., DIN 02231147, Pointe-Claire, QC, Canada) was topically applied on the ventral aspect of the neck and left for 2 minutes to desensitize the skin. The piglet's trachea was exposed by making a 5-cm long longitudinal incision using a surgical scalpel blade No. 15. Surgical gauze pads were used to clean and dry the exposed region, and one pad was placed caudally to the incision to contain a small bleeding. A pair of surgical thumb forceps were used to hold both sides of the incision, facilitating access to the trachea. Using the scalpel blade, a 1-cm long longitudinal incision was made on the trachea, corresponding to two tracheal rings. The tips of a crucible tong were placed inside of the trachea access to help keep it slightly open, exposing the tracheal lumen. An ISE cell involved by the grounded braid reinforced tubing was then carefully inserted into this opening, assuring that both electrodes' tips were contacting the ASL on the internal tracheal wall. Efforts were made to prevent the application of excessive mechanical pressure that could trigger ion movement toward the trachea lumen.

pH data was collected after 1 minute after stabilization of the recordings. To dynamically measure O_2 and CO_2 concentrations in the inhaled and exhaled air, a 10µl micropipette tip connected to a 3-mm thick, 1-m long plastic transparent tubing was inserted on the same opening. This tubing was connected to a respiratory gas analyzer (ADInstruments, Cat. No. ML206, Sydney, Australia). Differently from the electrodes, the tip of the micropipette tip was positioned in the tracheal lumen, slightly above the tracheal epithelia to allow the passage of air through it. The electrodes and gas tubing were secured in place by a pair of alligator clips connected to flexible plastic arms clamped on the procedure table.

The differential biological potential amplifier, pulse transducer, respiratory gas analyzer and dual channel differential electrometer were connected to a data acquisition hardware device (ADInstruments, PowerLab 8/35, Sydney, Australia). A USB cable connected this device to a computer that used the software LabChart (Version 7.3.8; ADInstruments, 2016, Sydney, Australia) to collect data from all investigational equipment simultaneously (Figure 4.2). A range of 200 mV was set on the dual-channel electrometer and a digital low-pass filter with a top-cut of 50 Hz was added in the ISE channel in analytical software.

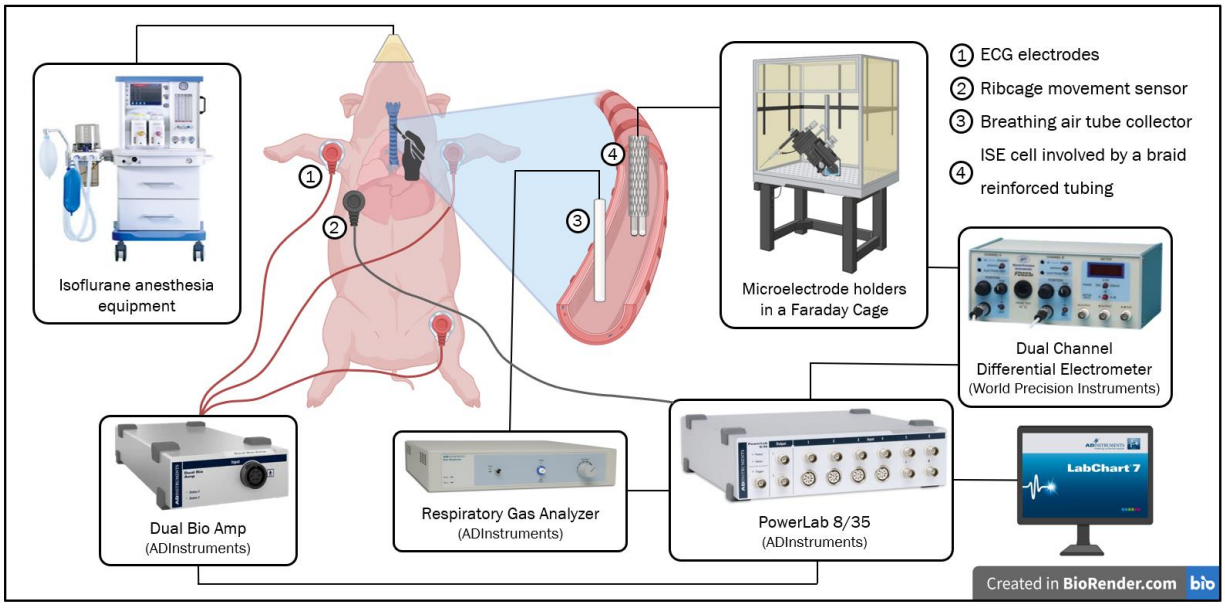

Figure 4.2. Diagram of all equipment used in the in vivo data collection.

This setup was used to record minimum and maximum [CO_2], breathing rate, and minimum and maximum voltage recorded by the ISE cells. Once all readings stabilized, data from 5 consecutive breathing cycles were collected and averaged. Then, each electrode cell was calibrated. Calibration data was used to measure the electrodes response time and noise, as described in 3.2.5. Linear regression was performed using the three calibration data points, resulting in an equation of the line from where the Nernstian slope and the line adjusted R^2 were acquired. Furthermore, each individual electrode cell's equation of the line was used to calculate the minimum and maximum ASL pH according to the voltage recorded. Finally, the $\Delta[CO_2]$ and ΔASL pH were also calculated.

4.2.4. Statistical analysis

The data was initially exported from LabChart software (Version 7.3.8; ADInstruments, 2016) to an Excel spreadsheet (Version 2407, Microsoft Corporation, Inc., 2024), where the $\Delta[CO_2]$ and ΔASL pH were calculated. Statistical analyses were conducted with Stata Statistical Software (Version 18; StataCorp LLC, 2024), and the graphs were generated using OriginLab software (Version 2024b; OriginLab Corporation, 2024).

The normal distribution of each variable was confirmed through Shapiro-Wilk tests, being reported as mean (SD, standard deviation). Pearson's correlations were calculated between all variables with a 95% confidence interval. Linearity between variables of interest and pairs with strong and very strong correlations ($r > 0.7$, Schober et al., 2018) were assessed by performing univariate linear regressions with a confidence of 95%. Test assumptions including linearity between variables, normal distribution of residuals, and constant variance of residuals (heteroskedasticity) were confirmed for each significant linear regression ($p < 0.05$). Significant relationships were also graphically represented, including a fitting line with a 95% confidence interval area.

4.3. Results

4.3.1. Experimental procedure

It took approximately 1:15h between inducing anesthesia on the subject to finish setting up the equipment to record the tracheal ASL pH and respiratory gas composition. The first data collection was longer compared to the following ones, lasting for approximately one hour, due to the need to fine-tune and test all equipment before beginning to acquire data. Once the experimental setup was ready, data collection from each ISE cell lasted from 5 to 10 minutes, including the calibration. The process of disassembling a pair of electrodes after data

collection/calibration and assembling a new ISE cell took approximately 5 minutes. Therefore, between 10 and 15 minutes were necessary to collect tracheal ASL pH data, calibrate the ISE cell, and prepare a new one for the following measurements. In sum, the whole assay including all preparatory processes mentioned above and collecting data from 10 ISE cells lasted for approximately 4:30 hours. No intercurrences related to the subject well-being occurred. The piglet was maintained stable throughout the experiment, showing blood oxygenation above 95% and even rectal temperature.

4.3.2. In vivo measurements

All the 10 ISEs used in the assay were able to measure tracheal ASL pH oscillations during the breathing cycle. However, one electrode (electrode #2) malfunctioned during the calibration process. The reason for this occurrence couldn't be determined, since under visual inspection no flaws were noted. As a result of the impossibility of calibrating this electrode, its data was not included in the analysis. Therefore, measurements from 9 ISE cells were used to assess the ASL pH oscillations in the live piglet, representing a 90% success. No other issue occurred in the equipment employed; this experiment was successful in recording ECG, breathing movements, respiratory gas profile and tracheal ASL pH simultaneously. Figure 4.3 shows a typical recording performed by electrode #8.

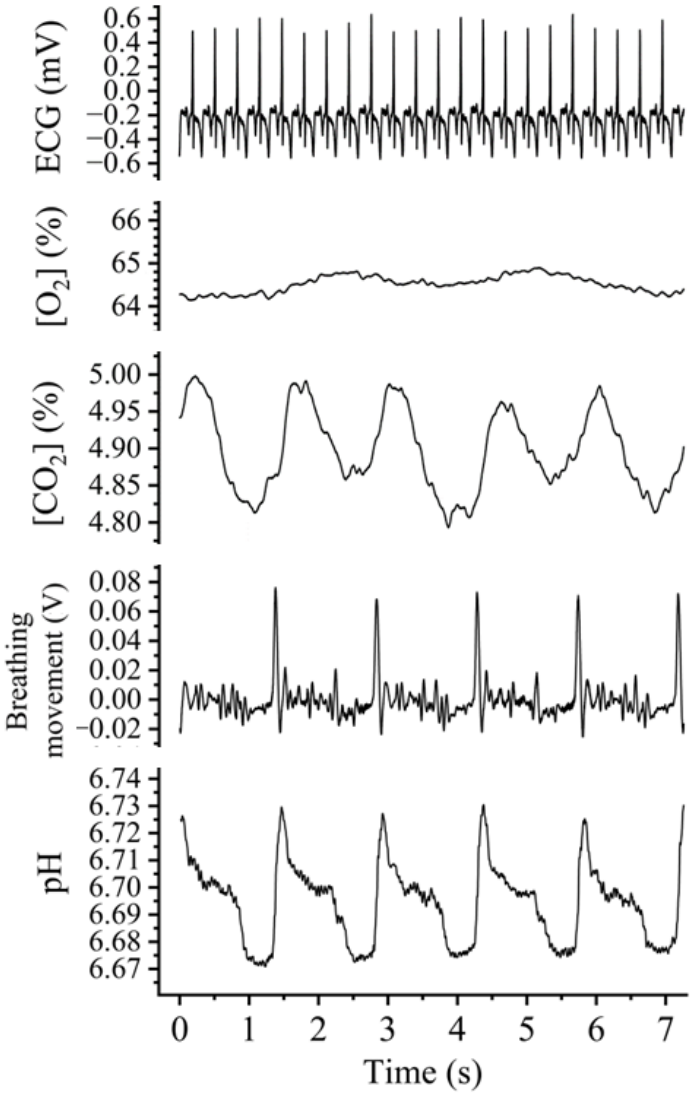

Figure 4.3. Typical ECG, respiratory gas analysis, breathing movement and ASL pH recording throughout 5 breathing cycles in a tracheostomized piglet.

According to the simultaneous recordings shown in Figure 4.3, no periodic interference on ASL pH readings that could be caused by the subject's cardiac cycle was noticed. The oxygen concentration on the respiratory gas was relatively stable throughout the assay, not fluctuating according to the breathing cycle. On the other hand, periodic oscillations in CO_2 concentrations were observed. Carbon dioxide concentrations dropped approximately 30 seconds after each inspiratory movement, shown as a spike on the breathing movement graph. Conversely, CO_2 concentrations rose slightly after the expiratory movement was recorded, seen as a dip on the graph right after the inspiration. This delay between the breathing movement and CO_2 concentration oscillation is likely due to the length of the

respiratory gas tube; probably, this is relative to the time elapsed from the air collection in the trachea to the air achieving the gas analyzer. The inspiratory movements were seen more marked on the graph compared to expiratory ones, which were followed by a post-expiratory pause when little diaphragmatic movement was measured. It was also noted that the respiratory rate (RR) was relatively constant throughout each 10 to 15-minute long assay, although it varied between assays as shown below. pH recordings were clean, with little to no EMI visually observable. A low ASL pH plateau was recorded during the post-expiratory pause, followed by a peak immediately after inspiration. Soon after the peak, the pH decreased quickly as the piglet expired.

Table 4.1 presents respiratory parameters, including minimum, maximum, and ΔCO_2 concentrations, respiratory rate (RR), as well as key characteristics of the H^+-selective electrodes. These characteristics include the Nernstian slope (NS), adjusted R^2, response time (RT), and noise levels based on 9 individual recordings from each ISE cell assay. The table also provides the mean (SD), overall minimum, and maximum values of each variable measured. Additionally, it reports the minimum, maximum, and ΔpH values, which were calculated using the calibration points, the equation of the line, and the measured voltages. Raw voltage data and the equation of the line for each electrode can be found in Table S6.

The CO_2 concentration in respiratory air fluctuated from 5.04 ± 0.3% during inspiration to 5.15 ± 0.3% during expiration, representing an average oscillation of 0.11 ± 0.03% within five consecutive breathing cycles. A relatively high variance was seen in the piglet's respiratory rate, ranging from 40 to 57.69 breaths per minute (bpm) between assays, resulting in a mean of 49.35 ± 5.9. The mean Nernstian slope of the electrode cells was 58.65 ± 0.9 mV/[H^+] decade, ranging from 56.8 to 59.8. The smallest adjusted R^2 calculated was 0.9896, while the largest ones were close to 1. The average adjusted R^2 was 0.9951 ± 0.003. Electrodes showed a response time ranging from 0.3 to 1.76 seconds, resulting in an average of 1.16 ± 0.4 seconds. The mean noise observed was 0.14 ± 0.04 mV, ranging from 0.09 to 0.23 mV. Immediately after inspiration, the mean maximum ASL pH measured was 6.91 ± 0.4, which dropped to 6.84 ± 0.4 after expiration. This oscillation resulted in a mean ΔpH of 0.07 ± 0.4 throughout 5 consecutive breathing cycles, ranging from 0.02 to 0.16 pH units.

Figure 4.4 displays a correlation matrix illustrating the interactions between the variables listed in Table 4.1. To aid in interpretation, the matrix cells are color-coded based on the strength of the correlation coefficients. Dark blue represents a perfect positive correlation

(r = 1), white indicates no correlation (r = 0), and red signifies a perfect negative correlation (r = -1). Relationships between variables that were found to be moderately or strongly correlated, and relevant for assessing the ISE characteristics concerning ASL pH measurements, were further analyzed using a series of univariate linear regressions. The results of linear regression analysis between dependent (y) and independent variables (x) are presented in Table 4.2, including the Pearson's correlation coefficient (r), linear regression coefficient, p-value, and adjusted R^2.

Table 4.1. Respiratory parameters and airway surface liquid pH measurements performed using 9 H^+-selective electrodes in a tracheostomized piglet.

Elect. #	Min. $[CO_2]$ (%)	Max. $[CO_2]$ (%)	$\Delta[CO_2]$ (%)	RR (bpm)	NS (mV/ $[H^+]$ decade)	Adj. R^2	RT (s)	Noise (mV)	Min. pH	Max. pH	ΔpH
1	5.07	5.18	0.11	54.1	58.75	0.9998	0.94	0.23	7.54	7.62	0.08
3	5.2	5.31	0.11	51.1	59.2	0.9991	1.13	0.09	7.32	7.42	0.1
4	4.99	5.05	0.06	57.7	56.8	0.9896	0.98	0.17	6.45	6.51	0.06
5	5.56	5.65	0.09	50	57.8	0.9926	1.76	0.14	6.32	6.34	0.02
6	5.11	5.2	0.09	48.8	59.8	0.9942	1.16	0.19	7.03	7.08	0.05
7	4.97	5.11	0.13	40	59.25	0.9957	0.3	0.12	6.6	6.75	0.16
8	4.87	5.03	0.16	40.3	58.75	0.9932	1.42	0.1	6.82	6.88	0.06
9	5.05	5.17	0.13	52.9	59.2	0.9970	1.6	0.1	6.72	6.75	0.03
10	4.54	4.67	0.12	49.4	58.3	0.9947	1.16	0.15	6.8	6.84	0.03
Mean (SD)	5.04 (0.3)	5.15 (0.3)	0.11 (0.03)	49.35 (5.9)	58.65 (0.9)	0.9951 (0.003)	1.16 (0.4)	0.14 (0.04)	6.84 (0.4)	6.91 (0.4)	0.07 (0.4)
Minimum	4.54	4.67	0.06	40	56.8	0.9896	0.3	0.09	6.32	6.34	0.02
Maximum	5.56	5.65	0.16	57.69	59.8	0.9998	1.76	0.23	7.54	7.62	0.16

Abbreviations: Elect, electrode; Min, minimum; Max, maximum; RR, respiratory rate; bpm, breaths per minute; NS, Nernstian slope; Adj, adjusted; RT, response time; SD, standard deviation.

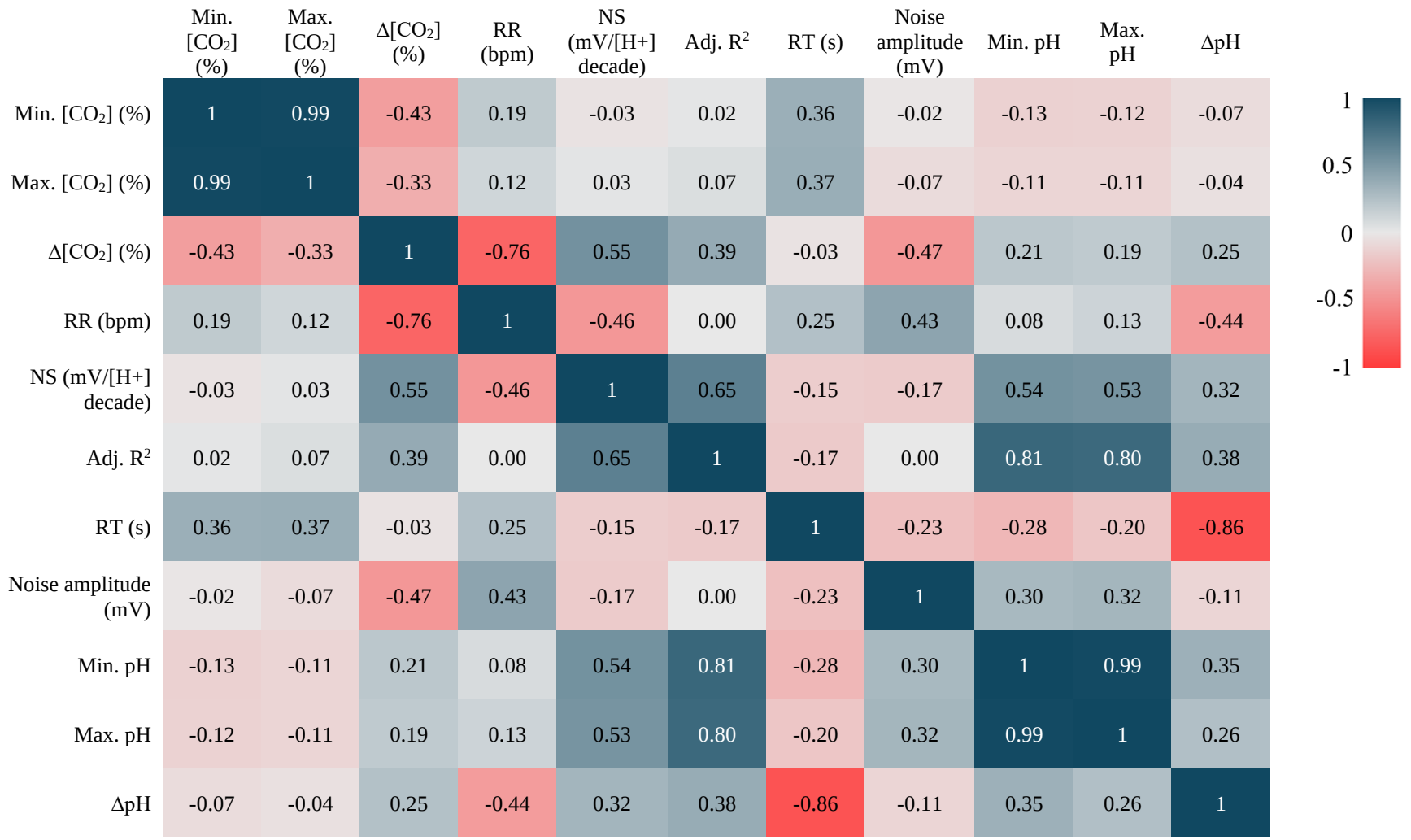

Figure 4.4. Correlation matrix of respiratory parameters and airway surface liquid pH measurements performed using 9 H^+-selective electrodes in a tracheostomized piglet. Abbreviations: Elect, electrode; Min, minimum; Max, maximum; RR, respiratory rate; bpm, breaths per minute; NS, Nernstian slope; Adj, adjusted; RT, response time; SD, standard deviation.

It was observed a very strong positive correlation (0.99) between minimum and maximum CO_2 concentrations, and a moderate negative correlation between these parameters and ΔCO_2 concentrations (-0.43 and -0.33, respectively). Similarly to what was found in CO_2 concentrations, a very strong positive correlation (0.99) between minimum and maximum pH was seen. ΔCO_2 concentrations and RR had a strong negative correlation (-0.76). These variables have a linear relationship ($p = .018$), as for each bpm increment, the oscillations in CO_2 concentration decreased by 0.004%. Conversely, measurements at 10 bpm higher resulted in 0.04% lower ΔCO_2. This relationship can be seen in Figure 4.5 A, where a fitting line between these two variables has a negative slope. RR and ΔpH were moderately negatively correlated (-0.44), however this is not statistically significant ($p = .239$). ΔpH and ΔCO_2 were weakly positively correlated (0.25) and were also not linearly correlated with each other ($p = .521$).

On the other hand, besides the large negative correlation coefficient (-0.86), ΔpH and the electrodes RT are significantly related ($p = .003$). For each second added in the electrode RT, the pH oscillation measurement decreased by 0.086 ± 0.02 pH units. In other words, a faster electrode showing an RT 1 second shorter than another electrode was able to measure ASL pH fluctuations almost 0.09 units larger. Figure 4.5 B graphically demonstrates this phenomenon, where faster electrodes measured larger pH oscillations whereas slower ones recorded significantly shorter pH fluctuations.

The electrodes NS had a moderate positive correlation with the adjusted R^2, minimum and maximum ASL pH (0.65, 0.54, and 0.53, respectively), but none of these relationships were found statistically significant ($p = .058.,146$, and .131, respectively). The adjusted R^2 was also moderately positively correlated to minimum and maximum ASL pH (0.81 and 0.80, respectively), with a statistically significant linear relationship ($p = .01$ and .008, respectively). For each 0.001 increment in the adjusted R^2, such as increasing from 0.990 to 1, the minimum and maximum ASL pHs measured increased by 0.098 and 0.103 pH units, respectively. These relationships can be visualized in Figures 4.5 C and D, respectively. The positive slopes of the fitting lines indicate that electrodes with higher adjusted R^2 recorded higher minimum and maximum ASL pHs. Noise and RR had a moderate positive correlation (0.43), but they were found to have a non-linear relationship ($p = .254$). All assumptions of the linear regression analysis were met by each statistically significant univariate test.

Table 4.2. Univariate linear regressions assessing relevant relationships between respiratory parameters and airway surface liquid pH measurements performed using 9 H^+-selective electrodes in a tracheostomized piglet.

y	x	r	Coefficient (SE)	p-value	Adjusted R^2
$\Delta[CO_2]$ (%)	RR (bpm)	-0.76	-0.004 (0)	.018	0.5106
ΔpH	RR (bpm)	-0.44	-0.003 (0)	.239	0.0757
	$\Delta[CO_2]$ (%)	0.25	0.35 (0.5)	.521	-0.073
	RT (s)	-0.86	-0.086 (0.02)	.003	0.7024
NS (mV/ $[H^+]$ decade)	Min. pH	0.54	1.2 (0.7)	.146	0.1736
	Max. pH	0.53	1.2 (0.7)	.131	0.1942
Adjusted R^2	NS (mV/$[H^+]$ decade)	0.65	0.002 (0)	.058	0.3416
	Min. pH	0.81	98.3 (28)	.01	0.5836
	Max. pH	0.80	103.2 (28)	.008	0.6093
Noise (mV)	RR (bpm)	0.43	0.0032 (0.003)	.254	0.0636

Abbreviations: y, dependent variable; x, independent variable; r, Pearson's correlation coefficient; SE, standard error; RR, respiratory rate; bpm, breaths per minute; RT, response time; NS, Nernstian slope; Min, minimum; Max, maximum.

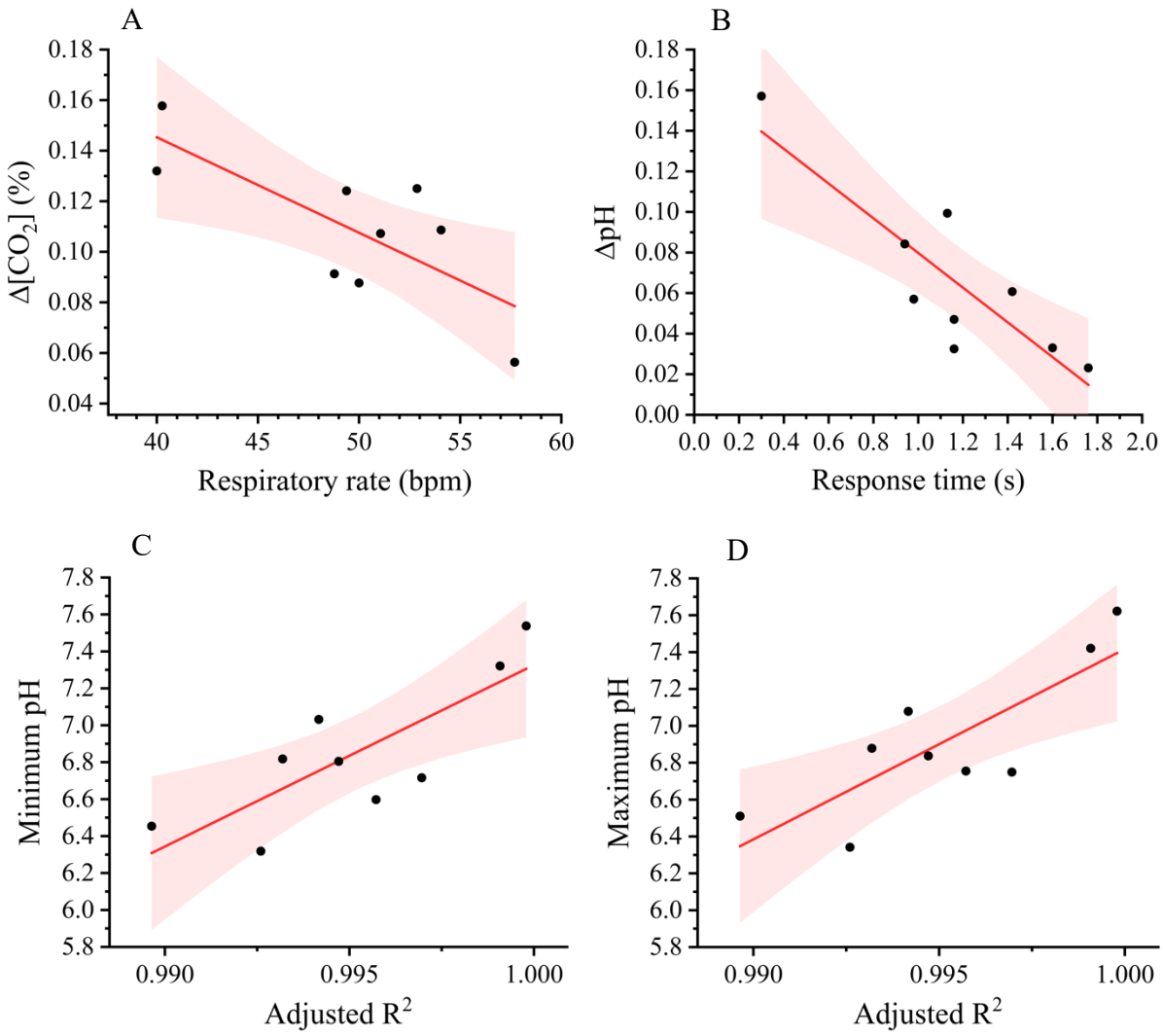

Figure 4.5. Scatter plot with fitting line and 95% confidence intervals for significant linear regressions calculated between respiratory parameters and airway surface liquid pH measurements performed using 9 H^+-selective electrodes in a tracheostomized piglet.

To further examine the relationship between the electrodes' response time and ASL pH fluctuations, Figure 4.6 shows the CO_2 concentration, breathing movement and ASL pH recording performed using a fast and a slow response ISE. A shape difference between the two pH curves was noted. The pH recording from the faster ISE (#7, left) besides having a large amplitude, shows a steep increase immediately after the subject inspired, rapidly lowering down after expiration to a low valley, with values maintained throughout the post-expiratory pause until a new peak resulting of the following inspiration movement. On the other hand, the pH curve from the slow response electrode (#5, right) did not show a peak after the inspiration movement. Instead, a much less steep and slower rise was observed,

reaching a plateau and then decreasing during expiration. The different pH curve shapes seen according to the responsiveness of the electrodes might be indicative of the negative relationship between RT and ASL pH oscillations.

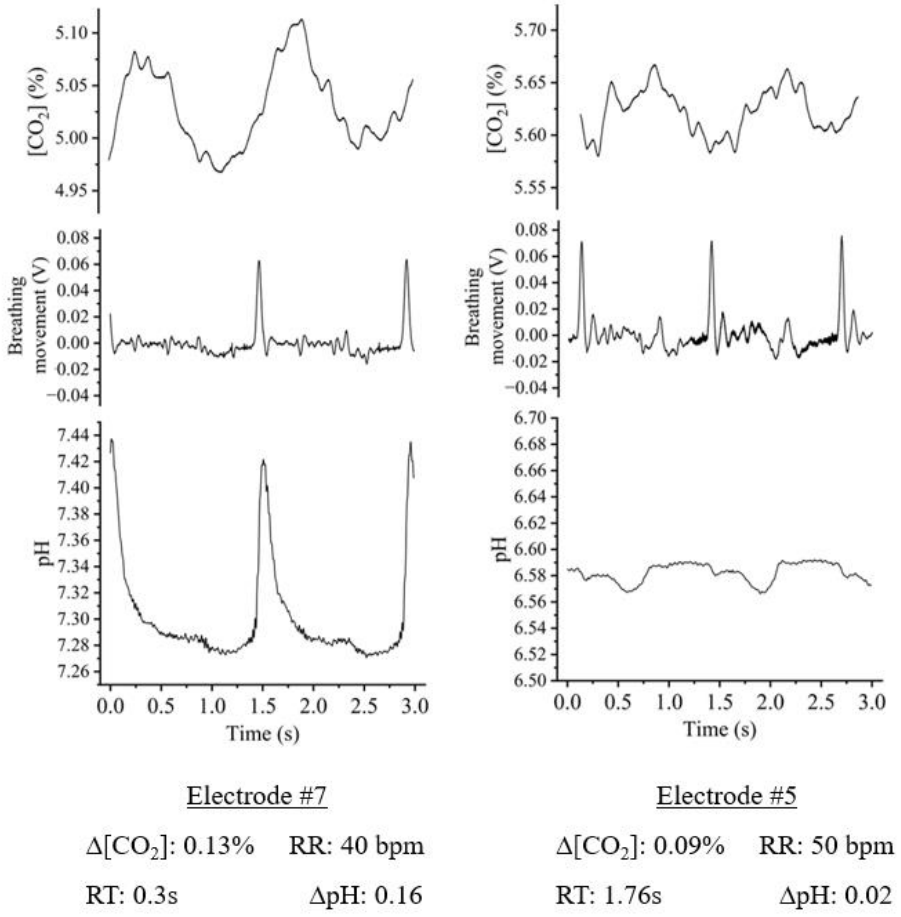

Figure 4.6. Comparison between [CO_2], breathing movement and ASL pH measurements during tests with H^+-selective electrodes with low and high response times.

4.4. Discussion

Pigs are considered a good animal model to study CF for several reasons. The porcine CFTR amino acid sequence is 92% identical to the human one (Liu et al., 2017) and they show similar disease progress and phenotype to what is observed in humans (Keiser & Engelhardt, 2011). Furthermore, pigs have important anatomical similarities with humans, such as the size and structure of the airways and lungs (Donnelley et al., 2019; Rogers et al., 2008). These characteristics are mainly relevant for in vivo studies since the swine model has significantly

larger airways compared to other commonly used animal models, being beneficial for studies on measurements of ASL pH. Pigs are the second most used animal model for studying CF, only being behind the murine model according to a systematic review of 636 papers describing 751 animal models used in CF research (Leenaars et al., 2020). Using a 1-week-old piglet in this assay was found to be adequate for measuring tracheal ASL pH. Handling the subject during anesthesia induction did not impose difficulties, since the size and behavior of the animal facilitated the process. Also, it had a tracheal size large enough to perform the surgical procedure and place the ISE cells while still allowing the free passage of air through the airway.

This was the first experiment successful in recording ASL pH fluctuations in the lower airways. For that purpose, 10 plastic ISE were placed into contact with the tracheal ASL of a tracheostomized piglet. Nine out of 10 ISEs tested were able to measure tracheal ASL pH oscillations and be calibrated using 3 calibration solutions of known pHs. Unfortunately, one ISE presented a malfunction during the calibration process, which made its recording to be excluded from analysis. Nevertheless, a success rate of 90% was achieved, indicating adequate manufacturing of the electrodes and good usage of the materials incorporated into their build. The microelectrode holders and braid reinforced tubing system was very practical, allowing the disassembly of an ISE cell and the assembly of a new one within 5 minutes. Recordings from each ISE cell lasted from 5 to 10 minutes, which allowed 4 to 6 ASL pH measurements within an hour. The relatively short time needed to repeat readings with different electrodes is advantageous for future research. Repeating readings with different instruments on the same subject can be beneficial for investigational device development since it allows for intra-device comparisons and variability assessments.

The ISEs used in this experiment showed adequate working parameters, also being similar to those described in Chapter 3 one day after manufacture. The 9 ISEs had a mean Nernstian slope (NS) of 58.65 ± 0.9 mV/[H^+] decade, considered ideal for this type of device (Luxardi et al., 2015). Besides being slightly larger than those observed in the ISE set characterized in Chapter 3 (mean of 53.7 mV/[H+] decade), NS of electrodes in the current assays had a smaller variability (0.9 vs 3.7 mV/[H+] decade). The average adjusted R^2 was also above the usability threshold of 0.9 (0.9951 ± 0.003) (Luxardi et al., 2015), also being similar to previous devices tested (0.9979, 0.9959-0.9996). Finally, the mean response time (RT) measured in the present assays was slightly larger than those observed in ISEs described in Chapter 3 (1.16 ± 0.4 vs 1.1 (0.8-1.7) seconds). In terms of noise and electromagnetic

shielding, recordings of ASL pH in vivo had slightly larger mean noise amplitudes 0.14 ± 0.04 mV) compared to tests performed in pH calibration solutions (0.11 ± 0.03 mV). Therefore, the electromagnetic shielding developed and described in Chapter 3 was found to be efficient in reducing influences of environmental interferences even in in vivo assays, resulting in a clean pH recording with little noise present.

The equipment setup used showed adequate usefulness, providing accurate and reliable recordings of the subject's ECG, breathing movement, respiratory gas analysis and tracheal ASL pH simultaneously with little to no interference observed. Performing these measurements at the same time allowed for tracing cause-effect links between the distinct physiological phenomena observed over time. For example, it was observed that CO_2 concentration and ASL pH oscillated depending on the piglet's breathing phase, as seen by its diaphragm movement. In healthy humans, CO_2 concentrations in the respiratory gas fluctuate from 0.035% during inspiration of room air up to 5.6% during expiration (Kim et al., 2021). Although CO_2 oscillations were observed in the present study, its amplitude was significantly smaller than the more than 140-fold variance reported in humans (Kim et al., 2021). This study found an average $\Delta[CO_2]$ of 0.11 ± 0.03% (n=9), with the largest variation being 0.16%. The discrepancy with Kim and colleagues' work in humans may be partially explained by the anesthesia system chosen in the present study, versus free room air breathing.

Given that a non-rebreathing circuit was used, maintaining a sufficiently high oxygen flow is crucial to remove CO_2 from the subjects lungs, as this system lacks a CO_2 absorber. The anesthesia equipment was supplied with 100% O_2 from a gas tank, so oxygen levels above 90% would typically be expected throughout the breathing phases. However, although not included in the statistical analysis, O_2 concentrations were found to range between 65% and 70%. This suggests that room air, with an oxygen concentration of approximately 21%, may have entered the breathing system, either through the mask-muzzle interface or, more likely, via the tracheostomy site. As a result, the mixing of oxygen and room air likely led to lower oxygen concentrations reaching the subjects lungs. This, in turn, caused rebreathing of air with a high CO_2 concentration, maintaining elevated CO_2 levels during both the inspiration (5.04 ± 0.3%) and expiration (5.15 ± 0.3%) phases. In summary, the low $\Delta[CO_2]$ observed in this experiment is likely attributable to the inability of exhaled CO_2 to fully exit the system because of insufficient oxygen flow, resulting in persistently high concentrations of CO_2.

The hypercapnia may also have influenced the subject's respiratory rate (RR), as a normal compensatory response to remove more CO_2. This assumption is supported by previous research in which higher respiratory frequencies have been observed in healthy human subjects when exposed to CO_2 concentrations of 5 and 7% compared to lower CO_2 concentrations (Schaefer, 1958). The mean RR of the piglet was 49.35 ± 5.9 bpm, with a maximum of 57.69 bpm, values considerably higher than the RR of human subjects breathing room air at rest. Although Kim and colleagues (2021) did not explicitly state the RR of their patients, according to the graphs provided it is possible to estimate that an interval of approximately 5 seconds occurred between breathings, resulting in an RR of approximately 12 bpm. In fact, the authors asked the subjects "to hold their breath for 10 s, then take 5–10 slow breaths while pH was being recorded", reinforcing the assumption that their RR was lower than the mean observed in the present experiment. This is of special importance when analyzing CO_2 concentration fluctuations since a statistically significant negative linear relationship between RR and $\Delta[CO_2]$ has been observed in the present experiment ($p = .018$). As such, smaller oscillations in CO_2 concentration were measured when the piglet was breathing at a higher rate, which could be expected since when at a high RR, the gas exchange has less time to occur. Consequently, the subject would exhale a smaller amount of CO_2 when compared to if it was at a lower RR, which results in a smaller $\Delta[CO_2]$ between inspiration and expiration. Therefore, the different breathing systems (room air in an open system vs anesthesia and 100% oxygen system) and different subjects' RR make it difficult to directly compare the CO_2 oscillations found in this experiment and with Kim and coworkers' study.

Through the breathing movement graphs, it was observed that inspiratory and expiratory movements occurred within a very short period, with a short post-inspiration phase. Also, inspiratory movements were more intense than the expiratory, seen as taller spikes on the readings as shown in Figure 4.3. Moreover, a long post-expiratory phase was observed. For example, in electrode #8's assay at an RR of 40.3 bpm (corresponding to 1 breathing cycle every 1.5 seconds), the time from the end of expiration to the beginning of the following inspiration took approximately 1 second, corresponding to 2/3 of the full breathing cycle. It is possible that the piglet's non-physiological position during the assays contributed to this abnormal breathing pattern. The subject's abdominal organs might have compressed the lungs making it difficult for them to fully expand during inspiration, resulting in a shallower breath that could also influence the low $\Delta[CO_2]$ observed.

Besides the lower $\Delta[CO_2]$ observed in the respiratory gas when compared to previous similar work from Kim and coworkers (2021), the present study found lower tracheal ASL pH oscillations compared to ASL pH on the nasal mucous of healthy human subjects. The acid-base equilibrium in the ASL is highly dependent on the CO_2 concentration in the respiratory gas, as CO_2 quickly diffuses through the thin ASL revesting airway epithelia (Thomas & Adams, 1965). In aqueous systems, CO_2 and water (H_2O) combine, resulting in carbonic acid (H_2CO_3) (Wang et al., 2016). The formation of carbonic acid in the ASL during expiration, when the carbon dioxide concentration in the respiratory gas is high, contributes to the transient ASL acidification during this respiratory phase seen as large $[H^+]$ oscillations (Kim et al., 2021). In their experiment, human subjects voluntarily breathed room air, which suggests that this large ASL pH oscillation was accompanied by also large $[CO_2]$ fluctuations in the respiratory gas. This study found that ASL pH fluctuates from 7.5 during exhalation up to 9 during inhalation on the nasal walls of non-CF human subjects (Kim et al., 2021). In the present experiment, tracheal ASL pH measurements ranged from 6.84 ± 0.4 to 6.91 ± 0.4 pH units, corresponding to an average oscillation of 0.07 ± 0.4 pH units. Given these results, it is suggested that the lower tracheal ASL ΔpH measured in the present experiment have been a result of a significantly lower $\Delta[CO_2]$ compared to previous works. Nevertheless, this study did not find a statistically significant linear relationship between $\Delta[CO_2]$ and ΔpH ($p = .521$). Given the close physiological relationship between these two parameters, it would be expected that, in an open room air breathing system where larger CO_2 concentration oscillations occur, a linear relationship between $\Delta[CO_2]$ and ΔpH be found.

Tracheal ASL pH values recorded in the present experiment were more acidic than nasal ASL pH reported by Kim and colleagues (2021). However, previous studies on lower airways found more acidic ASL compared to the upper respiratory tract. All these studies used techniques that do not allow recording pH values in real-time, so ASL pH fluctuation in the lower airways data has been published. McShane and collaborators (2003) recorded a mean pH of 7.1 ± 0.1 in the ASL of the lower respiratory tract of non-CF children. Schultz and colleagues (2017) found even lower values in the lobe bronchi of healthy children, with an average of 7.00 ± 0.12. In a similar study by Pezzulo and coworkers (2012), a mean tracheal ASL pH of around 7.2 was observed in non-CF piglets maintained in a >5% CO_2 concentration environment. The mean upper end of the ASL pH range observed in the present study was 6.91 ± 0.4 pH units, slightly more acidic than the mean Pezzulo and coworkers (2012) found. They used a pH-sensitive planar optical probe, a sensor that relies on the

fluorescence decay time of pH-sensitive indicator dyes incorporated into a polymer matrix (Blossfeld & Gansert, 2007). ISEs used in this experiment measure pH by recording difference in potential between two solutions divided by a hydrogen-permeable membrane (Lee et al., 2013). The difference between tracheal ASL pH observed may be, at least in part, due to the different methods used since one is based on indicator dyes and the other on potentiometric measurements. This investigation found a moderately high variance in the ASL pH between electrodes (SD = 0.4). It might have been due to the prolonged period between the first and last assays while the piglet's trachea remained opened, causing localized ASL physiological alterations that impacted the pH balance, or small inconsistencies between devices. Further research evaluating multiple plastic ISEs in different subjects would be relevant to establish this novel device's accuracy and the repeatability of its measurements.

The relationships between ASL pH and other variables were also evaluated. Interestingly, it was found that the ISE RT showed a negative linear correlation with the measured pH amplitude ($p = .003$). In this sense, an electrode with a response time 1 second shorter than another could detect pH fluctuations in ASL that were nearly 0.09 units larger. This effect on recording pH oscillation is relevant, since the average ΔpH measured was 0.07 ± 0.4 units. It is suggested that electrodes with larger RT are not fast enough to accurately record ASL pH fluctuations on time. This proposition is supported by the difference in the pH curve shape between a fast and a slow ISE as depicted in Figure 4.6. The fast electrode (RT = 0.3s) was able to record a steep peak in ASL pH immediately after inspiration followed by a drop and plateau during the post-expiratory phase. Contrarily, the pH value from the electrode with higher RT (RT = 1.76s) slowly increases after inspiration, stabilizes and decreases slowly during expiration. The ASL pH curve shape from the fast ISE in this study resembles those recorded in the noses of non-CF human patients (Kim et al., 2021). A peak pH is seen during inspiration in both profiles, but graphs from Kim and colleagues (2021) present a plateau during the post-inspiratory pause before reducing during expiration. This temporary maintenance of a high ASL pH is likely a result of a lower RR compared to the one seen in the present study (approximately 12 vs 49.35 ± 5.9 bpm), as previously discussed. Kim and coworkers (2021) reported that only plastic ISEs with response times below 1 second were used, reinforcing the hypothesis that fast-responding electrodes are essential for accurately measuring pH fluctuations in the ASL. Additionally, the adjusted R^2 from the electrodes' calibration curve was found to have a positive linear correlation with minimum and maximum ASL pH ($p = .01$ and .008, respectively). The equation of the calibration curve fitted line is

used to calculate the log of hydrogen ion concentration (Baucke et al., 1993). Thus, having a large adjusted R^2 indicates an adequate goodness of fit, resulting in accurate calculations made using the equation of the line. For this reason, a minimum adjusted R^2 of 0.9 is preconized for ISEs. In sum, the present study showed that, besides a Nernstian slope close to 58mV, ISEs must have a high adjusted R^2 and low response time (<1 s) to accurately measure ASL pH fluctuations in vivo.

The main limitation of this study is the use of a single subject. Testing multiple ISEs in different animals would provide relevant information to assess the device's accuracy and precision. Nevertheless, this was a proof-of-concept experiment that aimed to assess if plastic ISEs were able to measure tracheal ASL pH fluctuations in vivo, which has been successfully accomplished. Another significant limitation involved the anesthesia and ventilation system. The subject's ability to exhale and eliminate CO_2 was compromised due to the insufficient O_2 flow on a non-rebreathing system, which affected the recorded $\Delta[CO_2]$ and likely reduced the ASL pH oscillations. As a result, using such breathing system to monitor respiratory gases proved inadequate, limiting further conclusions.

4.5. Conclusion

In conclusion, the novel plastic ISE design was able to measure tracheal ASL pH fluctuations in a healthy one-week-old piglet. Lower CO_2 and pH oscillations were observed compared to previous work, which might have been due to limitations in the experimental setup. Besides the Nernstian slope, the adjusted R^2 and response time of the electrodes were found to influence the ASL pH measurements, indicating that devices with a Nernstian slope close to 58 mV/$[H^+]$ decade, a large adjusted R^2, and low response time (<1 s) should be considered in future in vivo ASL pH fluctuations assays.

CHAPTER 5 - GENERAL DISCUSSION AND FUTURE DIRECTIONS

5.1. General discussion

The experiments described in this thesis are part of a multidisciplinary project funded by the CIHR, whose objectives include assessing pH levels and potential fluctuations in the lungs of cystic fibrosis (CF) pigs and human volunteers, comparing diseased and healthy regions within the same lung. To aid in the fulfillment of this research framework, assays performed on the present work had two main objectives: to optimize building techniques of long plastic H^+-selective electrodes and to assess its effectiveness in measuring ASL pH in vivo. All general and specific objectives proposed were met by performing two experiments, described in Chapters 3 and 4.

Chapter 3 describes a novel building technique of plastic ISEs using polyethylene tubing, which facilitates the manufacture of long (>1.7m long), uniform and thin electrodes. These characteristics combined with a custom-built grounded stainless-steel braid reinforced tubing that reduces the electromagnetic interference enabled the use of the ISEs through endoscopy with little noise observed on the readings. This novel device showed comparable Nernstian slope, adjusted R^2 values, and response time with other plastic electrodes previously described. Furthermore, consecutive daily tests performed on the same electrodes showed that they can be used for at least 2 days after manufacture without significantly reducing their performance. While the electrodes performed adequately in pH calibration solutions (as tested in Chapter 3), these assays differ in nature from those conducted on biological tissues, which may affect the device's functionality. Therefore, Chapter 4 focused on testing these ISEs in a live piglet to confirm their suitability for recording ASL pH in vivo.

In line with the results from Chapter 3, the experiments conducted in Chapter 4 demonstrated that the devices previously described and characterized performed adequately, successfully measuring tracheal ASL pH in a live piglet. Although limitations on the experimental setup were present, namely the difficulty of the subject to adequately exhale,

CO_2 and ASL pH oscillations were recorded. It is suggested that, due to the insufficient O_2 flow on a non-rebreathing system leading to the maintenance of a high [CO_2], the CO_2 fluctuations in the respiratory gas were significantly smaller than those previously reported. As a consequence, ASL pH oscillations were also smaller than expected. Furthermore, results indicate that the Nernstian slope, the calibration curve's adjusted R^2 and the response time of the electrodes are parameters that should be considered when selecting ISEs for measuring ASL pH. Thus, it is preconized that electrodes with a Nernstian slope close to 58 mV/[H^+] decade, large adjusted R^2, and low response time (<1 s) should be used in future in vivo assays to measure ASL pH fluctuations.

In conclusion, the novel plastic ISE design has shown adequate performance and usability during the tests described in this thesis, being a promising device for future in vivo assays through bronchoscopy in CF pigs and human subjects. Nevertheless, a few modifications outlined in the considerations for future research, detailed below, should be taken into account.

5.2. Future directions

Using one-week-old piglets has shown to be adequate for performing assays aiming to record ASL pH fluctuation in vivo, but it is suggested that the anesthesia and/or breathing system be modified in future research. The maintenance of anesthesia through inhalation demands a constant airflow from the anesthetic machine to the mask. Results from the in vivo study strongly indicate that the subject was not appropriately exhaling the CO_2 produced by its organism. Consequently, a high CO_2 concentration in the respiratory gas throughout the breathing stages was maintained and, therefore, reduced CO_2 oscillations were observed. Ultimately, this might have impacted the ASL acid-base equilibrium, resulting in overall more acidic ASL and smaller pH fluctuations. Therefore, alternatives for anesthesia and breathing methods that allow the subject to properly eliminate CO_2, as in free room air breathing should be considered. Future research will not involve performing tracheostomy, thus solving the room air contamination and low O_2 flow, which were main issues observed in the present setup. In studies involving inhaled anesthesia, a closed breathing system with a CO_2 absorber would be a better choice, permitting a proper carbon dioxide elimination and controlling the gas fluctuation. Maintaining anesthesia through intravenous injection could be another alternative, although it has limitations such as a higher risk during prolonged (>1 hour) sessions when compared to inhaled isoflurane, for example. Nonetheless, it is suggested that future studies also assess breathing gas profiles, as correlating CO_2 parameters with ASL pH

measurements could result in novel data in the lower airways. Another important parameter to be considered is the respiratory rate (RR) of the subjects. It was found that the RR is negatively correlated with CO_2 oscillations which, in turn, may influence ASL pH fluctuations. For this reason, it is suggested that future research try to control the RR of the subjects included, which could contribute to a more uniform CO_2 oscillation among recordings and higher statistical power to determine differences between CF and non-CF groups.

As previously mentioned, faster electrodes measured significantly larger ASL pH fluctuations in vivo. Moreover, the calibration curve's adjusted R^2 was found to be positively correlated with the minimum and maximum ASL pH measurements. Given the relationship between the electrodes' working parameters and the recorded ASL pH, it is suggested that each electrode be thoroughly tested immediately before the assay and only those with the best performance (high adjusted R^2 and low response time) be used, to reduce the variability and improve recordings accuracy.

Noise assays performed in Chapter 3 did not identify significantly larger electromagnetic interferences in the recordings when ISEs were used inside a working channel of a bronchoscope. These results demonstrate that the plastic ISEs are compatible with bronchoscopy techniques, which would yield several advantages in future research. This technique would enable the researchers to record and compare pH at different areas of interest in the airway epithelia, such as healthy vs diseased, upper vs lower respiratory tract, etc. Results from these assays could enlighten the involvement of ASL acidification in CF disease progression, correlating the severity of the disease at a given site to its ASL pH profile. Furthermore, using plastic ISEs through bronchoscopy could result in even more stable and trustworthy data, since it would allow investigators to visually ensure a proper interface between the electrodes tips and the ASL. With the breathing movement, the contact between the electrodes and the fluid revesting the site of interest may be lost, which if happens even during a few milliseconds could result in loss of relevant data. Using the electrodes through bronchoscopy, this issue is reduced since an in-real-time observation of the ISE placement is possible.

The setup developed to simultaneously record breathing movements, respiratory gas analysis and ASL pH has shown to be user-friendly and practical. The ISE, holders and braid reinforced tubing system used was a practical way to quickly assemble and disassemble ISE

cells, enabling a complete recording process to be performed within 10-15 minutes. This practicality would allow researchers to collect data from the same patient using different devices, which is suggested for future studies. It would be advantageous since recordings from a few electrodes could be compared and averaged, decreasing the likelihood of using poor-performing devices and reducing the impact of individual variances, resulting in more accurate results.

In summary, the use together of the novel plastic ISE developed, described and tested in this thesis and bronchoscopy techniques in a perfectioned breathing system will enable researchers to study the ASL pH role in CF pathogenesis, potentially contributing to the development of therapies that can positively impact the well-being and prolong the CF patient's lifespan.

The combination of the novel plastic ISE design developed and tested in this thesis, along with bronchoscopy techniques in an optimized breathing system that allows larger CO_2 concentration fluctuations, will enable researchers to thoroughly investigate the role of ASL pH in CF pathogenesis. This research may not only contribute to the advancement of scientific knowledge but also offer a significant, positive impact on the lives of those suffering from this debilitating disease by aiding in the development of therapies that can improve the well-being and extend the lifespan of individuals with CF.

REFERENCES

Abou Alaiwa, M. H. A., Reznikov, L. R., Gansemer, N. D., Sheets, K. A., Horswill, A. R., Stoltz, D. A., Zabner, J., & Welsh, M. J. (2014). pH modulates the activity and synergism of the airway surface liquid antimicrobials β-defensin-3 and LL-37. *Proceedings of the National Academy of Sciences of the United States of America*, *111*(52), 18703–18708. https://doi.org/10.1073/pnas.1422091112

Abou Alaiwa, M. H., Beer, A. M., Pezzulo, A. A., Launspach, J. L., Horan, R. A., Stoltz, D. A., Starner, T. D., Welsh, M. J., & Zabner, J. (2014). Neonates with cystic fibrosis have a reduced nasal liquid pH; A small pilot study. *Journal of Cystic Fibrosis*, *13*(4), 373–377. https://doi.org/10.1016/j.jcf.2013.12.006

Abou Alaiwa, M. H., Launspach, J. L., Grogan, B., Carter, S., Zabner, J., Stoltz, D. A., Singh, P. K., McKone, E. F., & Welsh, M. J. (2018). Ivacaftor-induced sweat chloride reductions correlate with increases in airway surface liquid pH in cystic fibrosis. *JCI Insight*, *3*(15). https://doi.org/10.1172/jci.insight.121468

Abou Alaiwa, M. H., Launspach, J. L., Sheets, K. A., Rivera, J. A., Gansemer, N. D., Taft, P. J., Thorne, P. S., Welsh, M. J., Stoltz, D. A., & Zabner, J. (2016). Repurposing tromethamine as inhaled therapy to treat CF airway disease. *JCI Insight*, *1*(8). https://doi.org/10.1172/jci.insight.87535

ADInstruments. (n.d.). Dual Bio Amp FE232. [Apparatus]. https://www.adinstruments.com/products/bio-amps

ADInstruments. (2016). LabChart (Version 7.3.8). [Computer software]. https://www.adinstruments.com/support/downloads/windows/labchart-0

ADInstruments. (n.d.). PowerLab 8/35. [Apparatus]. https://www.adinstruments.com/products/powerlab-daq-hardware

ADInstruments. (n.d.). Pulse Transducer MLT1010. [Apparatus]. https://m-cdn.adinstruments.com/product-data-cards/MLT1010-DCW-15A.pdf

ADInstruments. (n.d.). Respiratory Gas Analyzer ML206. [Apparatus]. https://www.adinstruments.com/products/gas-analyzer

Ammann, D. (1986). Potentiometric measurements of ion activities with neutral carrier-based electrodes. *Ion-selective Microelectrodes: Principles, design and application*, 65-96.https://doi.org/10.1007/978-3-642-52507-0_5

Ammann, D., Pretsch, E., Simon, W., Lindner, E., Bezegh, A., & Pungor, E. (1985). Lipophilic salts as membrane additives and their influence on the properties of macro- and micro-electrodes based on neutral carriers. *Analytica Chimica Acta*, *171*, 119–129. https://doi.org/10.1016/S0003-2670(00)84189-6

Ammann, Daniel., Lanter, Franz., Steiner, R. A., Schulthess, Peter., Shijo, Yoshio., & Simon, Wilhelm. (1981). Neutral carrier based hydrogen ion selective microelectrode for extra- and intracellular studies. *Analytical Chemistry*, *53*(14), 2267–2269. https://doi.org/10.1021/ac00237a031

Andersen, D. H. (1938). Cystic fibrosis of the pancreas and its relation to celiac disease: a clinical and pathologic study. *American journal of Diseases of Children, 56*(2), 344-399. https://doi.org/10.1001/archpedi.1938.01980140114013

Armstrong, D. S., Grimwood, K., Carlin, J. B., Carzino, R., Gutierrez, J. P., Hull, J., ... & Phelan, P. D. (1997). Lower airway inflammation in infants and young children with cystic fibrosis. *American journal of respiratory and critical care medicine, 156*(4), 1197-1204. https://doi.org/10.1164/ajrccm.156.4.96-11058

Ask, P., Edwall, G., Johansson, K. E., & Tibbling, L. (1982). On the use of monocrystalline antimony pH electrodes in gastro-oesophageal functional disorders. *Medical and*

Biological Engineering and Computing, 20, 383-389. https://doi.org/10.1007/BF02442809

Bansil, R., & Turner, B. S. (2006). Mucin structure, aggregation, physiological functions and biomedical applications. *Current opinion in colloid & interface science, 11*(2-3), 164-170. https://doi.org/10.1016/j.cocis.2005.11.001

Baucke, F. G. K., Naumann, Renate., & Alexander-Weber, Christine. (1993). Multiple-point calibration with linear regression as a proposed standardization procedure for high-precision pH measurements. *Analytical Chemistry*, *65*(22), 3244–3251. https://doi.org/10.1021/ac00070a013

BD Intramedic™. (n.d.). PE Tubing, cat 14-170-12P. [Apparatus]. https://www.fishersci.ca/shop/products/intramedic-pe-tubing-16/1417012p

Bergeron, C., & Cantin, A. M. (2019). Cystic fibrosis: pathophysiology of lung disease. *Seminars in Respiratory and Critical Care Medicine*, *40*(6), 715–726. https://doi.org/10.1055/s-0039-1694021

Berkebile, A. R., & McCray Jr, P. B. (2014). Effects of airway surface liquid pH on host defense in cystic fibrosis. *The international journal of biochemistry & cell biology, 52*, 124-129. https://doi.org/10.1016/j.biocel.2014.02.009

Bhaskar, K. R., Gong, D. H., Bansil, R. A. M. A., Pajevic, S. I. N. I. S. A., Hamilton, J. A., Turner, B. S., & LaMont, J. T. (1991). Profound increase in viscosity and aggregation of pig gastric mucin at low pH. *American Journal of Physiology-Gastrointestinal and Liver Physiology, 261*(5), G827-G832. https://doi.org/10.1152/ajpgi.1991.261.5.G827

Bijman, J., & Fromter, E. (1986). Direct demonstration of high transepithelial chloride-conductance in normal human sweat duct which is absent in cystic fibrosis. *Pflugers Archiv European Journal of Physiology*, *407*(S2), S123–S127. https://doi.org/10.1007/BF00584941

Bimeda-MTC Animal Health Inc. (n.d.). Euthanyl, DIN 00141704. [Pharmaceutical product]. https://www.bimedacanada.com/products?issearch=1&ordering=alpha&category_id=1&xf_1[0]=2&xf_1[1]=15&xf_1[2]=4&xf_1[3]=3

Blossfeld, S., & Gansert, D. (2007). A novel non-invasive optical method for quantitative visualization of pH dynamics in the rhizosphere of plants. *Plant, Cell and Environment*, *30*(2), 176–186. https://doi.org/10.1111/j.1365-3040.2006.01616.x

Braun. (n.d.). Age Precision™ Digital Thermometer, Cat. No. PRT2000CA. [Apparatus]. https://www.braunhealthcare.com/ca_en/thermometer/braun-digital-thermometer-with-age-precision/

Buck, R. P., & Lindner, E. (1994). Recommendations for nomenclature of ionselective electrodes (IUPAC Recommendations 1994). *Pure and Applied Chemistry*, *66*(12), 2527–2536. https://doi.org/10.1351/pac199466122527

Bucki, R., Byfield, F. J., & Janmey, P. A. (2007). Release of the antimicrobial peptide LL-37 from DNA/F-actin bundles in cystic fibrosis sputum. *European Respiratory Journal*, *29*(4), 624–632. https://doi.org/10.1183/09031936.00080806

Cao, H., Ouyang, H., Ip, W., Du, K., Duan, W., Avolio, J., Wu, J., Duan, C., Yeger, H., Bear, C. E., Gonska, T., Hu, J., & Moraes, T. J. (2015). Testing gene therapy vectors in human primary nasal epithelial cultures. *Molecular Therapy Methods and Clinical Development*, *2*, 15034. https://doi.org/10.1038/mtm.2015.34

Coakley, R. D., Grubb, B. R., Paradiso, A. M., Gatzy, J. T., Johnson, L. G., Kreda, S. M., ... & Boucher, R. C. (2003). Abnormal surface liquid pH regulation by cultured cystic fibrosis bronchial epithelium. *Proceedings of the National Academy of Sciences*, 100(26), 16083-16088. https://doi.org/10.1073/pnas.2634339100

Conese, M., & Di Gioia, S. (2021). Pathophysiology of lung disease and wound repair in cystic fibrosis. *Pathophysiology*, *28*(1), 155–188. https://doi.org/10.3390/pathophysiology28010011

Cutting, G. R. (2005). Modifier genetics: cystic fibrosis. *Annual Review of Genomics and Human Genetics*, *6*(1), 237–260. https://doi.org/10.1146/annurev.genom.6.080604.162254

Cystic Fibrosis Canada. (2023). The Canadian Cystic Fibrosis Registry 2022 Annual Data report. Retrieved July 31, 2024, from www.cysticfibrosis.ca

Cystic Fibrosis Foundation. (2023). Patient Registry Highlights, Bethesda, Maryland. Retrieved July 31, 2024, from https://www.cff.org/medical-professionals/patient-registry

Cytiva. (n.d.). HyClone Phosphate Buffered Saline solution, Cat. No. SH30256.FS. [Chemical product]. https://www.cytivalifesciences.com/en/us/shop/cell-culture-and-fermentation/buffers-and-process-liquids/balanced-salt-solutions/hyclone-phosphate-buffered-saline-solution-p-00520?srsltid=AfmBOoqdW8UPx7pX9RzrcL1QNpcIDYEwJe1B8yxHhNDntrDP2mWwLXF0

di Sant'Agnese, P. A., Darling, R. C., Perera, G. A., & Shea, E. (1953). Abnormal electrolyte composition of sweat in cystic fibrosis of the pancreas: clinical significance and relationship to the disease. *Pediatrics*, 12(5), 549-563. https://doi.org/10.1542/peds.12.5.549

Donnelley, M., Morgan, K. S., Gradl, R., Klein, M., Hausermann, D., Hall, C., Maksimenko, A., & Parsons, D. W. (2019). Live-pig-airway surface imaging and whole-pig CT at the Australian Synchrotron Imaging and Medical Beamline. *Journal of Synchrotron Radiation*, *26*(1), 175–183. https://doi.org/10.1107/S1600577518014133

Fan, Z., Perisse, I. V., Cotton, C. U., Regouski, M., Meng, Q., Domb, C., Van Wettere, A. J., Wang, Z., Harris, A., White, K. L., & Polejaeva, I. A. (2018). A sheep model of cystic fibrosis generated by CRISPR/Cas9 disruption of the CFTR gene. *JCI Insight*, *3*(19). https://doi.org/10.1172/jci.insight.123529

Farber, S., Shwachman, H., & Maddock, C. L. (1943). Pancreatic function and disease in early life. I. Pancreatic enzyme activity and the celiac syndrome. *The Journal of clinical investigation, 22*(6), 827-838. https://doi.org/10.1172/JCI101456

Felgentreff, K., Beisswenger, C., Griese, M., Gulder, T., Bringmann, G., & Bals, R. (2006). The antimicrobial peptide cathelicidin interacts with airway mucus. *Peptides*, *27*(12), 3100–3106. https://doi.org/10.1016/j.peptides.2006.07.018

Fresenius Kabi Canada Ltd. (n.d.). Isoflurane USP, DIN 02237518, Cat. No. CP0406V2. [Pharmaceutical product]. https://www.fresenius-kabi.com/en-ca/products/animal-health-isoflurane-usp

Gangell, C., Gard, S., Douglas, T., Park, J., De Klerk, N., Keil, T., Brennan, S., Ranganathan, S., Robins-Browne, R., & Sly, P. D. (2011). Inflammatory responses to individual microorganisms in the lungs of children with cystic fibrosis. *Clinical Infectious Diseases*, *53*(5), 425–432. https://doi.org/10.1093/cid/cir399

Gentzsch, M., Dang, H., Dang, Y., Garcia-Caballero, A., Suchindran, H., Boucher, R. C., & Stutts, M. J. (2010). The cystic fibrosis transmembrane conductance regulator impedes proteolytic stimulation of the epithelial Na+ channel. *Journal of Biological Chemistry*, *285*(42), 32227–32232. https://doi.org/10.1074/jbc.M110.155259

Gibson, L. E., & Cooke, R. E. (1959). A test for concentration of electrolytes in sweat in cystic fibrosis of the pancreas utilizing pilocarpine by iontophoresis. *Pediatrics*, *23*(3), 545–549. https://doi.org/10.1542/peds.23.3.545

Glasscott, M. W., Brown, E. W., Dorsey, K., Laber, C. H., Conley, K., Ray, J. D., Moores, L. C., & Netchaev, A. (2022). Selecting an optimal faraday cage to minimize noise in

electrochemical experiments. *Analytical Chemistry*, *94*(35), 11983–11989. https://doi.org/10.1021/acs.analchem.2c02347
Goetz, D., & Ren, C. L. (2019). Review of cystic fibrosis. *Pediatric Annals*, *48*(4), e154–e161. https://doi.org/10.3928/19382359-20190327-01
Guilbault, G. G. (1980). Recommendations for publishing manuscripts on ion-selective electrodes. *Ion-Selective Electrode Reviews, 1*, 139-143. https://doi.org/10.1016/B978-0-08-026044-0.50008-1
Guilbault, G. G. (1981). Recommendations for publishing manuscripts on ion-selective electrodes. *Pure and Applied Chemistry*, *53*(10), 1907–1912. https://doi.org/10.1351/pac198153101907
Guilbault, G. G., Durst, R. A., Frant, M. S., Freiser, H., Hansen, E. H., Light, T. S., ... & Thomas, J. D. R. (1976). Recommendations for nomenclature of ion-selective electrodes. Pure Appl. Chem, 48(1), 127-132. https://doi.org/10.1351/pac197648010127
Guo, J., Garratt, A., & Hill, A. (2022). Worldwide rates of diagnosis and effective treatment for cystic fibrosis. *Journal of Cystic Fibrosis*, *21*(3), 456–462. https://doi.org/10.1016/j.jcf.2022.01.009
Gustafsson, J. K., Ermund, A., Ambort, D., Johansson, M. E. V., Nilsson, H. E., Thorell, K., Hebert, H., Sjövall, H., & Hansson, G. C. (2012). Bicarbonate and functional CFTR channel are required for proper mucin secretion and link cystic fibrosis with its mucus phenotype. *Journal of Experimental Medicine*, *209*(7), 1263–1272. https://doi.org/10.1084/jem.20120562
Hamilton Company. (n.d.). 31 gauge, Metal Hub Needle, 2 in, point style 3, Cat. No. 91031. [Apparatus]. https://www.hamiltoncompany.com/laboratory-products/needles/91031
Han, J., & Burgess, K. (2010). Fluorescent indicators for intracellular pH. *Chemical Reviews*, *110*(5), 2709–2728. https://doi.org/10.1021/cr900249z
Hoegger, M. J., Awadalla, M., Namati, E., Itani, O. A., Fischer, A. J., Tucker, A. J., Adam, R. J., McLennan, G., Hoffman, E. A., Stoltz, D. A., & Welsh, M. J. (2014). Assessing mucociliary transport of single particles in vivo shows variable speed and preference for the ventral trachea in newborn pigs. *Proceedings of the National Academy of Sciences of the United States of America*, *111*(6), 2355–2360. https://doi.org/10.1073/pnas.1323633111
Hoegger, M. J., Fischer, A. J., McMenimen, J. D., Ostedgaard, L. S., Tucker, A. J., Awadalla, M. A., Moninger, T. O., Michalski, A. S., Hoffman, E. A., Zabner, J., Stoltz, D. A., & Welsh, M. J. (2014). Impaired mucus detachment disrupts mucociliary transport in a piglet model of cystic fibrosis. *Science*, *345*(6198), 818–822. https://doi.org/10.1126/science.1255825
Jayaraman, S., Song, Y., Vetrivel, L., Shankar, L., & Verkman, A. S. (2001). Noninvasive in vivo fluorescence measurement of airway-surface liquid depth, salt concentration, and pH. *Journal of Clinical Investigation*, *107*(3), 317–324. https://doi.org/10.1172/JCI11154
Johansson, G., Karlberg, B., & Wikby, A. (1975). The hydrogen-ion selective glass electrode. *Talanta*, *22*(12), 953–966. https://doi.org/10.1016/0039-9140(75)80109-3
Johansson, J., Gudmundsson, G. H., Rottenberg, M. E., Berndt, K. D., & Agerberth, B. (1998). Conformation-dependent antibacterial activity of the naturally occurring human peptide LL-37. *Journal of Biological Chemistry*, *273*(6), 3718–3724. https://doi.org/10.1074/jbc.273.6.3718
Karl Storz SE & Co. (n.d.). Silver Scope, Cat. No. 13820 NKS. [Apparatus]. https://www.karlstorz.com/ca/en/small-animals.htm
Keiser, N. W., & Engelhardt, J. F. (2011). New animal models of cystic fibrosis: what are they teaching us? *Current opinion in pulmonary medicine, 17*(6), 478-483.https://doi.org/10.1097/MCP.0b013e32834b14c9

Kessler, W. R., & Andersen, D. H. (1951). Heat prostration in fibrocystic disease of the pancreas and other conditions. *Pediatrics*, 8(5), 648-656. https://doi.org/10.1542/peds.8.5.648

Kim, D., Liao, J., Scales, N. B., Martini, C., Luan, X., Abu-Arish, A., Robert, R., Luo, Y., McKay, G. A., Nguyen, D., Tewfik, M. A., Poirier, C. D., Matouk, E., Ianowski, J. P., Frenkiel, S., & Hanrahan, J. W. (2021). Large pH oscillations promote host defense against human airways infection. *Journal of Experimental Medicine*, *218*(4). https://doi.org/10.1084/JEM.20201831

Kim, K., Lane, E. A., Saftien, A., Wang, H., Xu, Y., Wirtz-Peitz, F., & Perrimon, N. (2020). Drosophila as a model for studying cystic fibrosis pathophysiology of the gastrointestinal system. *Proceedings of the National Academy of Sciences*, *117*(19), 10357–10367. https://doi.org/10.1073/pnas.1913127117

Kinetic Systems, Inc. (n.d.). Enclosures and Faraday Cages. [Apparatus]. https://kineticsystems.com/products/enclosures-and-faraday-cages/

Knowles, M., Gatzy, J., & Boucher, R. (1983). Relative ion permeability of normal and cystic fibrosis nasal epithelium. *Journal of Clinical Investigation*, *71*(5), 1410–1417. https://doi.org/10.1172/JCI110894

Kopelman, H., Corey, M., Gaskin, K., Durie, P., Weizman, Z., & Forstner, G. (1988). Impaired chloride secretion, as well as bicarbonate secretion, underlies the fluid secretory defect in the cystic fibrosis pancreas. *Gastroenterology*, *95*(2), 349–355. https://doi.org/10.1016/0016-5085(88)90490-8

Kreindler, J. L. (2010). Cystic fibrosis: exploiting its genetic basis in the hunt for new therapies. *Pharmacology & therapeutics, 125*(2), 219-229. https://doi.org/10.1016/j.pharmthera.2009.10.006

Kunzelmann, K., Schreiber, R., & Hadorn, H. B. (2017). Bicarbonate in cystic fibrosis. *Journal of Cystic Fibrosis, 16*(6), 653-662. https://doi.org/10.1016/j.jcf.2017.06.005

Lavelle, G. M., White, M. M., Browne, N., McElvaney, N. G., & Reeves, E. P. (2016). Animal models of cystic fibrosis pathology: Phenotypic parallels and divergences. *BioMed Research International*, *2016*. https://doi.org/10.1155/2016/5258727

Lee, S. K., Boron, W. F., & Parker, M. D. (2013). Monitoring ion activities in and around cells using ion-selective liquid-membrane microelectrodes. *Sensors, 13*(1), 984-1003. https://doi.org/10.3390/s130100984

Leenaars, C. H., De Vries, R. B., Heming, A., Visser, D., Holthaus, D., Reijmer, J., ... & Ritskes-Hoitinga, M. (2020). Animal models for cystic fibrosis: a systematic search and mapping review of the literature–Part 1: genetic models. *Laboratory animals*, 54(4), 330-340. https://doi.org/10.1177/0023677219868502

Liu, F., Zhang, Z., Csanády, L., Gadsby, D. C., & Chen, J. (2017). Molecular Structure of the Human CFTR Ion Channel. *Cell*, *169*(1), 85-95.e8. https://doi.org/10.1016/j.cell.2017.02.024

Lozo Vukovac, E., Miše, K., Gudelj, I., Perić, I., Duplančić, D., Vuković, I., Vučinović, Z., & Lozo, M. (2019). Bronchoalveolar pH and inflammatory biomarkers in patients with acute exacerbation of chronic obstructive pulmonary disease. *Journal of International Medical Research*, *47*(2), 791–802. https://doi.org/10.1177/0300060518811560

Luan, X., Tam, J. S., Jagadeeshan, S., Grishchenko, N., Hassan, N., Gioino, P., Shipley, A. M., Machen, T. E., & Ianowski, J. P. (2020). Airway submucosal glands from cystic fibrosis swine suffer from abnormal ion transport across the serous acini, collecting duct, and ciliated duct. *American Journal of Physiology-Lung Cellular and Molecular Physiology*, *318*(5), L931–L942. https://doi.org/10.1152/ajplung.00219.2019

Luxardi, G., Reid, B., Ferreira, F., Maillard, P., & Zhao, M. (2015). Measurement of extracellular ion fluxes using the ion-selective self-referencing microelectrode technique. *Journal of Visualized Experiments*, *99*. https://doi.org/10.3791/52782

Maccà, C. (2004). Response time of ion-selective electrodes: Current usage versus IUPAC recommendations. *Analytica Chimica Acta*, *512*(2), 183–190. https://doi.org/10.1016/j.aca.2004.03.010

Madeira, G. D. M., N. P. Dias Mello, H. J., Faleiros, M. C., & Mulato, M. (2021). Model improvement for super-Nernstian pH sensors: the effect of surface hydration. *Journal of Materials Science*, *56*(3), 2738–2747. https://doi.org/10.1007/s10853-020-05412-w

Marson, F. A. L., Bertuzzo, C. S., & Ribeiro, J. D. (2016). Classification of CFTR mutation classes. *The Lancet Respiratory Medicine*, 4(8), e37-e38. https://doi.org/10.1016/S2213-2600(16)30188-6

McCarron, A., Donnelley, M., & Parsons, D. (2018). Airway disease phenotypes in animal models of cystic fibrosis. *Respiratory research, 19*, 1-12. https://doi.org/10.1186/s12931-018-0750-y

McCarron, A., Parsons, D., & Donnelley, M. (2021). Animal and cell culture models for cystic fibrosis: which model is right for your application? *The American journal of pathology, 191*(2), 228-242. https://doi.org/10.1016/j.ajpath.2020.10.017

McShane, D., Davies, J. C., Davies, M. G., Bush, A., Geddes, D. M., & Alton, E. W. F. W. (2003). Airway surface pH in subjects with cystic fibrosis. *European Respiratory Journal*, *21*(1), 37–42. https://doi.org/10.1183/09031936.03.00027603

Meyerholz, D. K., Stoltz, D. A., Namati, E., Ramachandran, S., Pezzulo, A. A., Smith, A. R., Rector, M. V., Suter, M. J., Kao, S., McLennan, G., Tearney, G. J., Zabner, J., McCray, P. B., & Welsh, M. J. (2010). Loss of cystic fibrosis transmembrane conductance regulator function produces abnormalities in tracheal development in neonatal pigs and young children. *American Journal of Respiratory and Critical Care Medicine*, *182*(10), 1251–1261. https://doi.org/10.1164/rccm.201004-0643OC

MG Chemicals. (n.d.). Super Shield Silver Conductive Paint, Cat. No. 842AR-P. [Chemical product]. https://mgchemicals.com/products/conductive-paint/conductive-acrylic-paints/silver-conductive-paint/

Mise, K., Capkun, V., Jurcev-Savicevic, A., Sundov, Z., Bradaric, A., & Mladinov, S. (2010). The influence of gastroesophageal reflux in the lung: A case-control study. *Respirology*, *15*(5), 837–842. https://doi.org/10.1111/j.1440-1843.2010.01777.x

Montoro, D. T., Haber, A. L., Biton, M., Vinarsky, V., Lin, B., Birket, S. E., Yuan, F., Chen, S., Leung, H. M., Villoria, J., Rogel, N., Burgin, G., Tsankov, A. M., Waghray, A., Slyper, M., Waldman, J., Nguyen, L., Dionne, D., Rozenblatt-Rosen, O., … Rajagopal, J. (2018). A revised airway epithelial hierarchy includes CFTR-expressing ionocytes. *Nature*, *560*(7718), 319–324. https://doi.org/10.1038/s41586-018-0393-7

Murshed, R., Spitz, L., Kiely, E., & Drake, D. (1997). Meconium Ileus: A Ten-Year Review of Thirty-Six Patients. *European Journal of Pediatric Surgery*, *7*(05), 275–277. https://doi.org/10.1055/s-2008-1071170

Nakayama, K., Jia, Y. X., Hirai, H., Shinkawa, M., Yamaya, M., Sekizawa, K., & Sasaki, H. (2002). Acid stimulation reduces bactericidal activity of surface liquid in cultured human airway epithelial cells. *American journal of respiratory cell and molecular biology*, 26(1), 105-113. https://doi.org/10.1165/ajrcmb.26.1.4425

Narishige. (n.d.). Micromanipulator, Cat. No. MM-3. [Apparatus]. https://products.narishige-group.com/group1/MM-3/electro/english.html

New England Tubing Technologies. (n.d.). Braid Reinforced Tubing To 0.057" ID x 0.076" OD-Cut To 59 +/- 0.5 in., Cat. No. NETT01218-C1. [Apparatus]. https://newenglandtubing.com/product/braid-reinforced-tubing/

Odan Laboratories Ltd. (n.d.). Lidodan® Endotracheal, DIN 02231147. [Pharmaceutical product]. https://odanlab.com/product/lidodan-endotracheal/

O'Donnell, M. J. (1992). Short communication. A simple method for construction of 983 flexible, subminiature ion-selective electrodes. *Journal of Experimental Biology, 162*(353-359), 984-985. https://doi.org/10.1242/jeb.162.1.353

OriginLab Corporation. (2024). OriginLab (Version 2024b) [Computer software]. https://www.originlab.com/

Ostedgaard, L. S., Meyerholz, D. K., Chen, J.-H., Pezzulo, A. A., Karp, P. H., Rokhlina, T., Ernst, S. E., Hanfland, R. A., Reznikov, L. R., Ludwig, P. S., Rogan, M. P., Davis, G. J., Dohrn, C. L., Wohlford-Lenane, C., Taft, P. J., Rector, M. V., Hornick, E., Nassar, B. S., Samuel, M., … Stoltz, D. A. (2011). The ΔF508 Mutation Causes CFTR Misprocessing and Cystic Fibrosis–Like Disease in Pigs. *Science Translational Medicine*, *3*(74). https://doi.org/10.1126/scitranslmed.3001868

O'Sullivan, B. P., & Freedman, S. D. (2009). Cystic fibrosis. *The Lancet*, *373*(9678), 1891–1904. https://doi.org/10.1016/S0140-6736(09)60327-5

Paemka, L., McCullagh, B. N., Abou Alaiwa, M. H., Stoltz, D. A., Dong, Q., Randak, C. O., Gray, R. D., & McCray, P. B. (2017). Monocyte derived macrophages from CF pigs exhibit increased inflammatory responses at birth. *Journal of Cystic Fibrosis*, *16*(4), 471–474. https://doi.org/10.1016/j.jcf.2017.03.007

Pezzulo, A. A., Tang, X. X., Hoegger, M. J., Abou Alaiwa, M. H., Ramachandran, S., Moninger, T. O., Karp, P. H., Wohlford-Lenane, C. L., Haagsman, H. P., Eijk, M. Van, Bánfi, B., Horswill, A. R., Stoltz, D. A., Mc Cray, P. B., Welsh, M. J., & Zabner, J. (2012). Reduced airway surface pH impairs bacterial killing in the porcine cystic fibrosis lung. *Nature, 487*(7405), 109-113. https://doi.org/10.1038/nature11130

Plasschaert, L. W., Žilionis, R., Choo-Wing, R., Savova, V., Knehr, J., Roma, G., ... & Jaffe, A. B. (2018). A single-cell atlas of the airway epithelium reveals the CFTR-rich pulmonary ionocyte. Nature, 560(7718), 377-381. https://doi.org/10.1038/s41586-018-0394-6

Pula, K., Sudarsan, V., Rallapalli, D., KG, S. N., Baskaradas, J. A., & Balasubramanian, M. (2019, December). Analysis of shielding effectiveness of a faraday cage for high voltage laboratory. In *2019 IEEE Indian Conference on Antennas and Propogation (InCAP)* (pp. 1-4). IEEE. https://doi.org/10.1109/InCAP47789.2019.9134498

Quinton, P. M., & Bijman, J. (1983). Higher bioelectric potentials due to decreased chloride absorption in the sweat glands of patients with cystic fibrosis. *New England Journal of Medicine*, *308*(20), 1185–1189. https://doi.org/10.1056/NEJM198305193082002

Reid, B., & Zhao, M. (2011). Ion-selective self-referencing probes for measuring specific ion flux. *Communicative & Integrative Biology*, *4*(5), 524–527. https://doi.org/10.4161/cib.16182

Rescorla, F. J., & Grosfeld, J. L. (1993). Contemporary management of meconium ileus. *World Journal of Surgery*, *17*(3), 318–325. https://doi.org/10.1007/BF01658698

Riordan, J. R. (2008). CFTR function and prospects for therapy. *Annu. Rev. Biochem., 77*(1), 701-726. https://doi.org/10.1146/annurev.biochem.75.103004.142532

Riordan, J. R., Rommens, J. M., Kerem, B. S., Alon, N. O. A., Rozmahel, R., Grzelczak, Z., ... & Tsui, L. C. (1989). Identification of the cystic fibrosis gene: cloning and characterization of complementary DNA. *Science, 245*(4922), 1066-1073. https://doi.org/10.1126/science.2475911

Rodrigo, G. C., & Chapman, R. A. (1990). A novel resin-filled ion-sensitive micro-electrode suitable for intracellular measurements in isolated cardiac myocytes. *Pflugers Archiv European Journal of Physiology*, *416*(1–2), 196–200. https://doi.org/10.1007/BF00370242

Rogers, C. S., Abraham, W. M., Brogden, K. A., Engelhardt, J. F., Fisher, J. T., McCray, P. B., McLennan, G., Meyerholz, D. K., Namati, E., Ostedgaard, L. S., Prather, R. S., Sabater, J. R., Anthony Stoltz, D., Zabner, J., Welsh, M. J., & Jr, M. P. (2008). The porcine lung as a potential model for cystic fibrosis. *Am J Physiol Lung Cell Mol Physiol*, *295*, 240–263. https://doi.org/10.1152/ajplung.90203.2008

Rogers, C. S., Stoltz, D. A., Meyerholz, D. K., Ostedgaard, L. S., Rokhlina, T., Taft, P. J., Rogan, M. P., Pezzulo, A. A., Karp, P. H., Itani, O. A., Kabel, A. C., Wohlford-Lenane, C. L., Davis, G. J., Hanfland, R. A., Smith, T. L., Samuel, M., Wax, D., Murphy, C. N., Rieke, A., … Welsh, M. J. (2008). Disruption of the CFTR gene produces a model of cystic fibrosis in newborn pigs. *Science*, *321*(5897), 1837–1841. https://doi.org/10.1126/science.1163600

Saha, A., Yermembetova, A., Mi, Y., Gopalakrishnan, S., Sedaghat, S., Waimin, J., Wang, P., Glassmaker, N., Mousoulis, C., Raghunathan, N., Bagchi, S., Rahimi, R., Shakouri, A., Wei, A., & Alam, M. A. (2022). Temperature self-calibration of always-on, field-deployed ion-selective electrodes based on differential voltage measurement. *ACS Sensors*, *7*(9), 2661–2670. https://doi.org/10.1021/acssensors.2c01163

Schaefer, K. E. (1958). Respiratory pattern and respiratory response to CO2. *Journal of Applied Physiology*, *13*(1), 1–14. https://doi.org/10.1152/jappl.1958.13.1.1

Schober, P., Boer, C., & Schwarte, L. A. (2018). Correlation coefficients: Appropriate use and interpretation. *Anesthesia & Analgesia*, *126*(5), 1763–1768. https://doi.org/10.1213/ANE.0000000000002864

Schultz, A., Puvvadi, R., Borisov, S. M., Shaw, N. C., Klimant, I., Berry, L. J., Montgomery, S. T., Nguyen, T., Kreda, S. M., Kicic, A., Noble, P. B., Button, B., & Stick, S. M. (2017). Airway surface liquid pH is not acidic in children with cystic fibrosis. *Nature Communications*, *8*(1). https://doi.org/10.1038/s41467-017-00532-5

Scudieri, P., Musante, I., Venturini, A., Guidone, D., Genovese, M., Cresta, F., Caci, E., Palleschi, A., Poeta, M., Santamaria, F., Ciciriello, F., Lucidi, V., & Galietta, L. J. V. (2020). Ionocytes and CFTR Chloride Channel Expression in Normal and Cystic Fibrosis Nasal and Bronchial Epithelial Cells. *Cells*, *9*(9). https://doi.org/10.3390/cells9092090

Semaniakou, A., Croll, R. P., & Chappe, V. (2019). Animal models in the pathophysiology of cystic fibrosis. *Frontiers in pharmacology, 9*, 1475. https://doi.org/10.3389/fphar.2018.01475

Shah, V. S., Meyerholz, D. K., Tang, X. X., Reznikov, L., Alaiwa, M. A., Ernst, S. E., Karp, P. H., Wohlford-Lenane, C. L., Heilmann, K. P., Leidinger, M. R., Allen, P. D., Zabner, J., Mccray, P. B., Ostedgaard, L. S., Stoltz, D. A., Randak, C. O., & Welsh, M. J. (2016). Airway acidification initiates host defense abnormalities in cystic fibrosis mice. *Science, 351*(6272), 503-507. https://doi.org/10.1126/science.aad5589

Siemens Healthcare Limited. Multistix® 10 SG Reagent Strips. Retrieved July 31, 2024, from https://www.siemens-healthineers.com/en-ca/urinalysis-products/urinalysis-reagents/multistix-10-sg-reagent-strips

Sigma Aldrich. (n.d.). Agar, CAS-No 9002-18-0, Cat. No. A1296. [Chemical product]. https://www.sigmaaldrich.com/CA/en/product/sigma/a1296?srsltid=AfmBOoo-Q6PvbYOKKSkwsKD24712x_0r-YMc83slQZrtuK5FMhL_6um4

Sigma Aldrich. (n.d.). Hydrogen ionophore I - cocktail B, Cat. No. 95293. [Chemical product]. https://www.sigmaaldrich.com/CA/en/product/sial/95293?srsltid=AfmBOooa0bGXZ_zAD1hcwMA6X7U4EBS3_mydqQK7RaLr1lDHhIfpXhsA

Sigma Aldrich. (n.d.). Poly(vinyl chloride), CAS-No 9002-86-2, Cat. No. 81392. [Chemical product]. https://www.sigmaaldrich.com/CA/en/product/sial/81392?srsltid=AfmBOorTu-zrGsjKLUx2SJ_RE-JvdVbgq_RXft9fOUY_MbAmyjnr57jb

Sigma Aldrich. (n.d.). Tetrahydrofuran, CAS-No 109-99-9, Cat. No. 401757. [Chemical product]. https://www.sigmaaldrich.com/CA/en/product/sial/401757?srsltid=AfmBOopzkt-H9Gt5OD6BBSQdUszbM1SFl1ffMQFnmGIDa1_SCuC2PxCA

Smith, J. J., & Welsh, M. J. (1992). cAMP stimulates bicarbonate secretion across normal, but not cystic fibrosis airway epithelia. *Journal of Clinical Investigation*, *89*(4), 1148–1153. https://doi.org/10.1172/JCI115696

Snouwaert, J. N., Brigman, K. K., Latour, A. M., Malouf, N. N., Boucher, R. C., Smithies, O., & Koller, B. H. (1992). An animal model for cystic fibrosis made by gene targeting. *Science*, *257*(5073), 1083–1088. https://doi.org/10.1126/science.257.5073.1083

Song, Y., Salinas, D., Nielson, D. W., & Verkman, A. S. (2006). Hyperacidity of secreted fluid from submucosal glands in early cystic fibrosis. *Am J Physiol Cell Physiol*, *290*, 741–749. https://doi.org/10.1152/ajpcell.00379.2005

SparkFun Electronics. (n.d.). Copper Tape - Conductive Adhesive, 5mm (50ft), Cat. No. 13827. [Apparatus]. https://www.sparkfun.com/products/13827

StataCorp LLC. (2024). Stata Statistical Software (Version 18) [Computer software]. https://www.stata.com/

Stoltz, D. A., Meyerholz, D. K., Pezzulo, A. A., Ramachandran, S., Rogan, M. P., Davis, G. J., Hanfland, R. A., Wohlford-Lenane, C., Dohrn, C. L., Bartlett, J. A., Nelson, G. A., Chang, E. H., Taft, P. J., Ludwig, P. S., Estin, M., Hornick, E. E., Launspach, J. L., Samuel, M., Rokhlina, T., … Welsh, M. J. (2010). Cystic fibrosis pigs develop lung disease and exhibit defective bacterial eradication at birth. *Science Translational Medicine*, *2*(29). https://doi.org/10.1126/scitranslmed.3000928

Stoltz, D. A., Meyerholz, D. K., & Welsh, M. J. (2015). Origins of cystic fibrosis lung disease. *New England Journal of Medicine*, *372*(4), 351–362. https://doi.org/10.1056/nejmra1300109

Stoltz, D. A., Rokhlina, T., Ernst, S. E., Pezzulo, A. A., Ostedgaard, L. S., Karp, P. H., Samuel, M. S., Reznikov, L. R., Rector, M. V., Gansemer, N. D., Bouzek, D. C., Alaiwa, M. M. A., Hoegger, M. J., Ludwig, P. S., Taft, P. J., Wallen, T. J., Wohlford-Lenane, C., McMenimen, J. D., Chen, J. H., … Welsh, M. J. (2013). Intestinal CFTR expression alleviates meconium ileus in cystic fibrosis pigs. *Journal of Clinical Investigation*, *123*(6), 2685–2693. https://doi.org/10.1172/JCI68867

Sun, X., Sui, H., Fisher, J. T., Yan, Z., Liu, X., Cho, H. J., Joo, N. S., Zhang, Y., Zhou, W., Yi, Y., Kinyon, J. M., Lei-Butters, D. C., Griffin, M. A., Naumann, P., Luo, M., Ascher, J., Wang, K., Frana, T., Wine, J. J., … Engelhardt, J. F. (2010). Disease phenotype of a ferret CFTR-knockout model of cystic fibrosis. *Journal of Clinical Investigation*, *120*(9), 3149–3160. https://doi.org/10.1172/JCI43052

Tam, A., Wadsworth, S., Dorscheid, D., Man, S. P., & Sin, D. D. (2011). The airway epithelium: more than just a structural barrier. *Therapeutic advances in respiratory disease, 5*(4), 255-273. https://doi.org/10.1177/1753465810396539

Tang, N., & Wang, W. (2019). Robust estimation of generalized estimating equations with finite mixture correlation matrices and missing covariates at random for longitudinal data. *Journal of Multivariate Analysis*, *173*, 640–655. https://doi.org/10.1016/j.jmva.2019.05.006

Tang, X. X., Ostedgaard, L. S., Hoegger, M. J., Moninger, T. O., Karp, P. H., McMenimen, J. D., Choudhury, B., Varki, A., Stoltz, D. A., & Welsh, M. J. (2016). Acidic pH increases airway surface liquid viscosity in cystic fibrosis. *Journal of Clinical Investigation*, *126*(3), 879–891. https://doi.org/10.1172/JCI83922

Thermo Fisher Scientific Inc. (n.d.). Falcon™ 50 mL High Clarity Conical Centrifuge Tubes, Cat. No. 14-432-22. [Apparatus]. https://www.fishersci.ca/shop/products/falcon-50ml-conical-centrifuge-tubes-2/p-193321

Thermo Fisher Scientific Inc. (n.d.). Fisherbrand™ accuTupH™ Rugged Bulb pH Combination Electrodes - Mercury-Free, Cat. No. 13-620-183A. [Apparatus]. https://www.fishersci.ca/shop/products/fisher-scientific-accutuph-rugged-bulb-ph-combination-electrodes-mercury-free-5/13620183a

Thiagarajah, J. R., Song, Y., Haggie, P. M., & Verkman, A. S. (2004). A small molecule CFTR inhibitor produces cystic fibrosis-like submucosal gland fluid secretions in normal airways. *The FASEB Journal*, *18*(7), 875–877. https://doi.org/10.1096/fj.03-1248fje

Thomas, J. A., Buchsbaum, R. N., Zimniak, A., & Racker, E. (1979). Intracellular pH measurements in Ehrlich ascites tumor cells utilizing spectroscopic probes generated in situ. *Biochemistry*, *18*(11), 2210–2218. https://doi.org/10.1021/bi00578a012

Thomas, R. C. (1978). *Ion-sensitive intracellular microelectrodes: how to make and use them* (Vol. 1). London: Academic Press.

Thomas, W. J., & Adams, M. J. (1965). Measurement of the diffusion coefficients of carbon dioxide and nitrous oxide in water and aqueous solutions of glycerol. *Transactions of the Faraday Society*, *61*, 668. https://doi.org/10.1039/tf9656100668

Travis, S. M., Singh, P. K., & Welsh, M. J. (2001). Antimicrobial peptides and proteins in the innate defense of the airway surface. *Current Opinion in Immunology*, *13*(1), 89–95. https://doi.org/10.1016/S0952-7915(00)00187-4

Tsien, R. Y., & Rink, T. J. (1980). Neutral carrier ion-selective microelectrodes for measurement of intracellular free calcium. *Biochimica et Biophysica Acta (BBA)-Biomembranes, 599*(2), 623-638. https://doi.org/10.1016/0005-2736(80)90205-9

Van der Doef, H. P., Kokke, F. T., van der Ent, C. K., & Houwen, R. H. (2011). Intestinal obstruction syndromes in cystic fibrosis: meconium ileus, distal intestinal obstruction syndrome, and constipation. *Current gastroenterology reports, 13*, 265-270. https://doi.org/10.1007/s11894-011-0185-9

VetTech Solutions Ltd (n.d.). Wall/Bench Anaesthetic Bracket Unit – Single Gas-Concentrator Option, Cat. No. AN009CO. [Apparatus]. https://www.vet-tech.co.uk/product/wall-bench-anaesthetic-bracket-unit-single-gas-concentrator-option/

Voipio, J., Pasternack, M., & MacLeod, K. (1994). Ion-sensitive microelectrodes. *In Microelectrode Techniques The Plymouth Workshop Handbook. The Company of Biologists, Ltd (pp. 275-316).*

Wang, H., Zeuschner, J., Eremets, M., Troyan, I., & Willams, J. (2016). Stable solid and aqueous H2CO3 from CO2 and H2O at high pressure and high temperature. *Scientific Reports*, *6*(1), 19902. https://doi.org/10.1038/srep19902

Wang, Y., Wrennall, J. A., Cai, Z., Li, H., & Sheppard, D. N. (2014). Understanding how cystic fibrosis mutations disrupt CFTR function: from single molecules to animal models. *The international journal of biochemistry & cell biology, 52*, 47-57. https://doi.org/10.1016/j.biocel.2014.04.001

Weiner, I. D., & Hamm, L. L. (1989). Use of fluorescent dye BCECF to measure intracellular pH in cortical collecting tubule. *American Journal of Physiology-Renal Physiology*, *256*(5), F957–F964. https://doi.org/10.1152/ajprenal.1989.256.5.F957

Williams, O. W., Sharafkhaneh, A., Kim, V., Dickey, B. F., & Evans, C. M. (2006). Airway mucus: from production to secretion. *American journal of respiratory cell and molecular biology, 34*(5), 527-536. https://doi.org/10.1165/rcmb.2005-0436SF

Wine, J. J. (2010). The development of lung disease in cystic fibrosis pigs. *Science translational medicine, 2*(29), 29ps20-29ps20. https://doi.org/10.1126/scitranslmed.3001130

Woodley Equipment Company Ltd. (n.d.). Pulse CO-Oximeter, Cat. No. 504. [Apparatus]. https://www.woodleyequipment.com/product/504

World Precision Instruments. (n.d.). Dual Channel Differential Electrometer, Cat. No. FD223a. [Apparatus]. https://www.wpiinc.com/media/wysiwyg/pdf/FD223a_IMs.pdf?srsltid=AfmBOortf5UgRxelbBWPXcfVumwKAf7lsHhs8ShfGvmLIkTG-J_T2VM8

World Precision Instruments. (n.d.). Microelectrode Holder, Cat. No. MEH2SFW. [Apparatus]. https://www.wpiinc.com/var-3793-microelectrode-holder-meh2sfw.html?srsltid=AfmBOooYINbnmJ3R8qvI7JoKbBcJqn5Wm7Mg8_cQbN_hEIbU0kWirRTd

World Precision Instruments. (n.d.). Microelectrode Holder STR M W Ag wire, Cat. No. EBH1. [Apparatus]. https://www.wpiinc.com/ehb1-microelectrode-holder-straight-male-connector.html

Xu, J., Livraghi-Butrico, A., Hou, X., Rajagopalan, C., Zhang, J., Song, J., Jiang, H., Wei, H.-G., Wang, H., Bouhamdan, M., Ruan, J., Yang, D., Qiu, Y., Xie, Y., Barrett, R., McClellan, S., Mou, H., Wu, Q., Chen, X., … Sun, F. (2021). Phenotypes of CF rabbits generated by CRISPR/Cas9-mediated disruption of the CFTR gene. *JCI Insight*, *6*(1). https://doi.org/10.1172/jci.insight.139813

Yoshida Welding. (n.d.). Solder Wire 0.6mm 500g Sn55 Tin Lead Rosin Core Soldering, Cat. No. 55. [Apparatus]. https://yoshida-welding.en.made-in-china.com/product/emAYMrQyhSVC/China-China-Factory-Solder-Wire-0-6mm-500g-Sn55-Tin-Lead-Rosin-Core-Soldering.html

Zajac, M., Dreano, E., Edwards, A., Planelles, G., & Sermet-Gaudelus, I. (2021). Airway surface liquid pH regulation in airway epithelium current understandings and gaps in knowledge. *International journal of molecular sciences, 22*(7), 3384. https://doi.org/10.3390/ijms22073384

Zeger, S. L., & Liang, K.-Y. (1986). Longitudinal data analysis for discrete and continuous outcomes. *Biometrics*, *42*(1), 121-130. https://doi.org/10.2307/2531248

Zuelzer, W. W., & Newton JR, W. A. (1949). The pathogenesis of fibrocystic disease of the pancreas: a study of 36 cases with special reference to the pulmonary lesions. *Pediatrics, 4*(1), 53-69. https://doi.org/10.1542/peds.4.1.53

APPENDIX A – SUPPLEMENTARY DATA

Table A.1. Nernstian slope, adjusted R^2, and response time derived from calibrations performed using 10 plastic H^+-selective electrodes in 4 consecutive days after their manufacture.

#	Day	Nernstian Slope (mV/[H+] decade)	Adjusted R^2	Response time (s)
1	1	50.00	0.9911	0.48
	2	49.50	0.9924	0.42
	3	53.15	0.9951	1.30
	4	49.40	0.9983	0.37
2	1	55.70	0.9971	1.18
	2	52.40	0.9988	1.52
	3	54.25	0.9996	2.10
	4	51.85	0.9999	2.80
3	1	55.30	0.9986	0.90
	2	51.40	0.9983	1.14
	3	54.25	0.9987	0.33
	4	49.55	0.9999	5.80
4	1	50.30	0.9829	1.20
	2	51.85	0.9932	1.50
	3	53.75	1	0.81
	4	53.50	0.9949	2.90
5	1	53.27	0.9995	0.25
	2	51.07	0.9942	0.18
	3	52.05	0.9944	0.83
	4	46.19	0.994	0.35
6	1	56.07	0.9999	0.83
	2	51.31	0.9964	1.45
	3	51.55	0.9973	2.09
	4	49.31	0.9945	2.41
7	1	57.25	0.9996	2.60
	2	54.10	1	3.10
	3	54.75	1	1.50
	4	54.85	0.9993	1.80
8	1	57.45	1	1.00
	2	53.30	0.9995	1.60
	3	50.80	0.998	2.20
	4	52.45	0.997	8.30
9	1	55.10	0.9959	1.50
	2	46.40	0.9962	3.20
	3	51.10	1	4.10
	4	51.45	0.9938	4.30
10	1	46.10	0.9962	2.00
	2	54.35	0.9999	3.10
	3	50.55	1	3.90
	4	50.70	0.9999	4.80

120

Table A.2. Noise amplitude (mV) observed in readings of 17 plastic H^+-selective electrodes at four different setups.

#	Shielded	Endoscope light off	Endoscope light on	Unshielded
1	0.084	0.084	0.144	1.836
2	0.123	0.102	0.153	1.899
3	0.101	0.108	0.068	2.253
4	0.119	0.088	0.082	1.965
5	0.111	0.115	0.088	1.628
6	0.154	0.092	0.130	2.159
11	0.200	0.095	0.096	2.500
12	0.087	0.135	0.181	1.640
13	0.090	0.087	0.153	2.522
14	0.109	0.096	0.088	2.230
15	0.085	0.087	0.110	1.771
16	0.096	0.087	0.070	2.318
17	0.133	0.079	0.100	3.705
18	0.086	0.123	0.078	0.562
19	0.078	0.063	0.068	1.652
20	0.064	0.074	0.128	3.145
21	0.086	0.105	0.078	2.848

Table A.3. Noise amplitude (mV) observed in readings of 10 shielded plastic H^+-selective electrodes performed during 4 consecutive days after their manufacture.

#	Day	Noise amplitude (mV)	#	Day	Noise amplitude (mV)
1	1	0.084	6	1	0.154
	2	0.078		2	0.135
	3	0.085		3	0.286
	4	0.065		4	0.121
2	1	0.123	7	1	0.108
	2	0.072		2	0.102
	3	0.167		3	0.091
	4	0.171		4	0.261
3	1	0.101	8	1	0.073
	2	0.133		2	0.169
	3	0.090		3	0.194
	4	0.178		4	0.157
4	1	0.119	9	1	0.268
	2	0.138		2	0.193
	3	0.259		3	0.112
	4	0.223		4	0.377
5	1	0.111	10	1	0.172
	2	0.098		2	0.171
	3	0.105		3	0.163
	4	0.112		4	0.321

Table A.4. Noise amplitude (mV) observed in readings of 12 shielded plastic H^+-selective electrodes performed at three different temperatures.

#	Temperature (°C)		
	22	27	32
1	0.084	0.124	0.123
2	0.123	0.112	0.076
3	0.101	0.162	0.157
4	0.119	0.084	0.104
5	0.111	0.268	0.333
6	0.154	0.143	0.12
11	0.2	0.26	0.182
13	0.09	0.153	0.18
18	0.086	0.082	0.176
19	0.078	0.144	0.213
20	0.064	0.084	0.114
21	0.086	0.11	0.161

Table A.5. Nernstian slope derived from calibrations performed using 12 plastic H^+-selective electrodes at three different temperatures.

#	Temperature (°C)		
	22	27	32
1	49.56	52.81	53.36
2	54.37	53.1	52.58
3	52.49	54.03	54.49
4	51.27	52.68	52.74
5	54.69	55.08	54.75
6	49.65	51.85	52.09
11	51.73	52.06	50.49
13	51.84	52.3	52.21
18	52.16	53.69	54.14
19	50.65	52.63	52.86
20	51.33	53.36	54.02
21	56.13	55.65	54.7

Table A.6. Calibration points, equation of the line, and voltages measured by 9 H^+-selective electrodes in a tracheostomized piglet.

Electrode #	pH 6	pH 7	pH 8	Calibration Curve Equation of the Line	Min. Voltage	Max. Voltage	ΔVoltage
1	55.7	-4.1	-61.8	y = 407.85 - 58.75*x	-39.95	-35.00	4.95
3	34.3	-27.1	-84.1	y = 388.77 - 59.2*x	-50.52	-44.64	5.88
4	35.9	-28	-77.7	y = 374.33 - 56.8*x	3.34	6.71	3.38
5	49.6	-14.3	-66	y = 394.37 - 57.8*x	13.33	14.70	1.37
6	45.3	-20.1	-74.3	y = 402.23 - 59.8*x	-30.31	-27.52	2.78
7	75	11	-43.5	y = 428.92 - 59.25*x	-11.12	-1.82	9.30
8	26.6	-38.1	-90.9	y = 377.12 - 58.75*x	-18.44	-14.84	3.60
9	65.3	2.1	-53.1	y = 419.17 - 59.2*x	-10.78	-8.82	1.95
10	65.7	2.2	-50.9	y = 413.77 - 58.3*x	-15.99	-14.07	1.92

Abbreviations: min, minimum; max, maximum.

APPENDIX B – LIST OF MATERIAL AND EQUIPMENT USED

Chapter 3 - Development And Characterization of a Long, Flexible Plastic H^+-Selective Electrode

Chemical products:

- Backfilling solution (BFS), 0.1 mol l-1 NaCl and 0.1 mol l-1 sodium citrate, adjusted to pH 6 (Thomas, 1978)
- Referencing solution (RS), 3M KCl (O'Donnel, 1992)
- Hydrogen ionophore I - cocktail B (Sigma Aldrich, Cat. No. 95293, St. Louis, MO, USA)
- Poly(vinyl chloride) (Sigma Aldrich, Cat. No. 81392, St. Louis, MO, USA)
- Tetrahydrofuran (Sigma Aldrich, Cat. No. 401757, St. Louis, MO, USA)
- Agar (Sigma Aldrich, Cat. No. A1296, St. Louis, MO, USA)
- Phosphate buffered saline (PBS) solution (Cytiva, Cat. No. SH30256.FS, Marlborough, MA, USA)

Consumables:

- PE tubing, 0.28 mm inner diameter and 0.61 mm outer diameter (BD Intramedic™, Cat. No. 14-170-12P, Waltham, MA, USA)
- 31-gauge blunt tip needle (Hamilton Company, Cat. No. 91031, Reno, NV, USA)
- 50 mL Falcon™ tubes (Thermo Fisher Scientific Inc., Cat. No. 14-432-22, Waltham, MA, USA)
- Stainless steel braid reinforced tubing, 0.057" inner diameter and 0.076" outer diameter (New England Tubing Technologies, Cat. No. NETT01218-C1, Lisbon, NH, USA)
- Silver conductive paint (MG Chemicals, Cat. No. 842AR-P, Burlington, ON, Canada)
- Copper conductive tape, 5 mm width (SparkFun Electronics, Cat. No. 13827, Niwot, CO, USA)
- Tin-lead solder stipe, 0.6 mm thick (Yoshida Welding, Cat. No. 55, Mito, Japan)

Equipment:

- Female Microelectrode Holder with Ag/AgCl wire (World Precision Instruments, Cat. No. MEH2SFW, Sarasota, FL, USA)
- Male Microelectrode Holder with Ag/AgCl wire, STR M W Ag wire (World Precision Instruments, Cat. No. EBH1, Sarasota, FL, USA)
- MM-3 Micromanipulators (Narishige, Cat. No. MM-3, London, UK)
- Faraday cage (Kinetic Systems, Inc, Pleasanton, CA, USA)
- (World Precision Instruments, Cat. No. FD223a, Sarasota, FL, USA)
- PowerLab 8/35 (ADInstruments, Sydney, Australia)
- Veterinary endoscope, Silver Scope (Karl Storz SE & Co., Cat. No. 13820 NKS, Tuttlingen, Germany)

Chapter 4 - Effectiveness of the Plastic H^+-Selective Electrode For In Vivo pH Measurements of Airway Surface Liquid

Pharmaceutical products:

- Lidodan® Endotracheal (Odan Laboratories Ltd., DIN 02231147, Pointe-Claire, QC, Canada)
- Isoflurane (Fresenius Kabi Canada Ltd., Cat. No. CP0406V2, Toronto, ON, Canada)
- Euthanyl (Bimeda-MTC Animal Health Inc., DIN 00141704, Cambridge, ON, Canada)

Equipment:

- Plastic H^+-selective electrodes and referencing electrodes made with PE tubing as described in 3.2.2
- Stainless steel braid reinforced tubing, 0.057" inner diameter and 0.076" outer diameter (New England Tubing Technologies, Cat. No. NETT01218-C1, Lisbon, NH, USA)
- Female Microelectrode Holder with Ag/AgCl wire (World Precision Instruments, Cat. No. MEH2SFW, Sarasota, FL, USA)
- Male Microelectrode Holder with Ag/AgCl wire, STR M W Ag wire (World Precision Instruments, Cat. No. EBH1, Sarasota, FL, USA)
- MM-3 Micromanipulators (Narishige, Cat. No. MM-3, London, UK)
- Custom-built Faraday cage
- Dual Channel Differential Electrometer, FD223a (World Precision Instruments)

- Veterinary Wall/Bench Anaesthetic Bracket Unit (VetTech Solutions Ltd., Cat. No. AN009CO, North-West England, UK)
- Pulse CO-Oximeter (Woodley Equipment Company Ltd., Cat. No. 504, Bolton, UK)
- Digital Thermometer, Age Precision™ (Braun, Cat. No. PRT2000CA, Taunus, Germany)
- Pulse Transducer (ADInstruments, Cat. No. MLT1010, Sydney, Australia)
- Dual Bio Amp (ADInstruments, Dual Bio Amp, Cat. No. FE232, Sydney, Australia)
- Respiratory Gas Analyzer (ADInstruments, Cat. No. ML206, Sydney, Australia)
- PowerLab 8/35 (ADInstruments, Sydney, Australia)